

# An introductory guide to effective operators in nuclei

P. J. Ellis\*

*School of Physics and Astronomy, University of Minnesota, Minneapolis, Minnesota 55455*

E. Osnes†

*Physics Department, State University of New York, Stony Brook, New York 11794 and Institute of Physics, University of Oslo, Oslo 3, Norway*

In this tutorial-style article we discuss the time-independent perturbation formalism of Brandow for effective interactions and operators in a nonrigorous, intuitive way. The simple example of a  $2 \times 2$  matrix is used to introduce the basic concepts, for instance the notion of folded diagrams. The same example is used subsequently in a discussion of the branch points arising from "level crossings" and the associated convergence difficulties with the perturbation series. Numerical calculations of the effective interaction and the effective charge are then reviewed, focussing, for the most part, on the  $(1s0d)$  shell. Whenever possible, simple physical models are used to illustrate the results. A fairly comprehensive summary of the calculations to date is given, and we attempt to synthesize and draw conclusions.

## CONTENTS

I. Introduction	777
II. Formal Perturbation Theory	779
A. Degenerate perturbation theory	780
B. A simple $2 \times 2$ matrix problem	781
1. Brillouin-Wigner perturbation theory (particle representation)	781
2. Brillouin-Wigner perturbation theory (hole representation)	782
3. Rayleigh-Schrödinger perturbation theory (hole representation)	782
4. Rayleigh-Schrödinger perturbation theory (particle representation)	783
5. The factorization theorem	783
6. Summation of the series	784
C. Shell-model effective interaction	785
D. Effective operators	790
E. Formal divergence problems	793
III. Results of Calculations	798
A. Brief reminder on the nucleon-nucleon interaction	798
B. The Brueckner-Bethe-Goldstone reaction matrix	799
C. Calculation of effective operators order by order in $G$	801
1. Effective interaction	802
2. Effective charge	807
D. Calculation of effective operators by infinite partial summations	809
1. Effective interaction	809
2. Effective charge	816
E. Calculations in a Hartree-Fock basis	818
F. Matrix diagonalization methods	820
G. Many-body effective operators	822
IV. Conclusions	823
V. Acknowledgments	824
Appendix A: Goldstone Diagrams versus Folded Diagrams	824

Appendix B: Nondegenerate Valence Energies	825
Appendix C: Diagram Rules	826
A. General structure of the diagrams	826
B. Evaluation of the diagrams	827
C. Further discussion and examples	827
Appendix D: Explicit Evaluation of the Core-Polarization Diagram	828
References	830

## I. INTRODUCTION

Although nuclear physics has been intensively studied for many years and reached a high level of sophistication, it still contains several unresolved fundamental problems. One very outstanding problem is the derivation of the effective interaction between nucleons bound in nuclei.

Indeed, the aim of nuclear theory is to describe the properties of atomic nuclei in terms of the interactions between the individual nucleons. This is a quantal many-body problem which cannot be solved exactly and therefore must be replaced by suitable approximations or models. These models have various degrees of resemblance to the original microscopic many-body problem to be solved. The most microscopic model is the shell model, which has been extremely successful in describing and predicting nuclear properties. We shall be concerned here with the fundamental justification of this model. One would then wish to go on and establish contact with more collective models, although the connection is known only in simple cases; this is, however, beyond the scope of the present article.

In the shell model the atomic nucleus is considered as a system of nucleons moving in a common potential well arising from their mutual interactions. Then, in the simplest version of the shell model, the extreme single-particle shell model first proposed by Mayer and Jensen in 1949 [for a review, see the monograph by Mayer and Jensen (1955)], all the properties of an odd-mass nucleus are assumed to be due to the last odd particle moving in this well, the remaining particles being paired to angular momentum zero. Not surprisingly this model is un-

\*Work supported in part by U.S.E.R.D.A. Contract No. AT(11-1) 1764.

†Work supported in part by U.S.E.R.D.A. Contract No. AT(11-1) 3001 and the Norwegian Research Council for Science and the Humanities.

‡Permanent address.

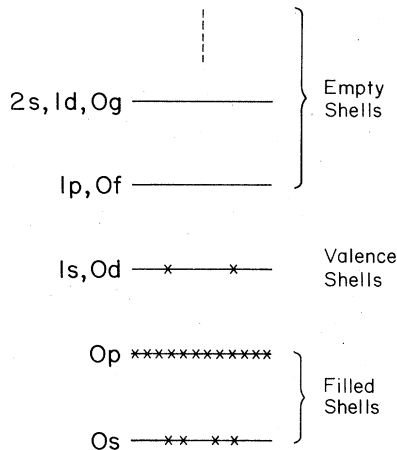


FIG. 1. Harmonic oscillator single-particle level scheme. The filling of orbitals appropriate to  $^{18}\text{O}$  is shown.

able to account for the wealth of nuclear data available, and nowadays it is usual to take into account all particles beyond a doubly magic core (i.e., the core has the "magic" number of 8, 20, 28, 50, 82, or 126 neutrons and protons) which shows exceptional stability (e.g., Elliott and Lane, 1957). Thus for  $^{18}\text{O}$ —the prototype nucleus for effective interactions—we could take  $^{16}\text{O}$  as a closed-shell core and consider configurations of two neutrons in the  $(1s0d)$  shell, as shown in Fig. 1. Energies are measured with respect to the  $^{16}\text{O}$  core and single-particle energies are taken from the known energies of the  $^{17}\text{O}$  levels, so that what is needed is a residual interaction between the two  $(1s0d)$  particles.

Now, the residual interaction that we need is an *effective* interaction which differs from the interaction between two free nucleons (to be referred to as the nucleon–nucleon interaction) in several respects. Firstly, a substantial part of the nucleon–nucleon interaction is absorbed in the common one-body potential which represents the average interaction between each individual nucleon and all the other nucleons. Secondly, the effective interaction differs from the nucleon–nucleon interaction because of the presence of other nucleons. Clearly the Pauli exclusion principle prevents two interacting nucleons within a nucleus from scattering to states which are already occupied by other nucleons. Thirdly, the shell-model eigenvalue problem must be solved in a finite basis, and hence the effective interaction must compensate for the excluded configurations. Similarly, effective operators are needed to compute other observable quantities from the truncated shell-model wave functions. For instance, by describing  $^{17}\text{O}$  in terms of a valence neutron outside a closed  $^{16}\text{O}$  core, we would obtain a vanishing electric quadrupole ( $E2$ ) moment, since the neutron carries no electric charge. However, the measured moment has the sign and the order of magnitude expected of a single-valence proton. Thus there must be contributions from other configurations—involving protons excited out of the core. A substantial part of these contributions may be taken into account by renormalizing the  $E2$  operator; this is generally done by associating a non-zero *effective charge* with the valence neutron. (Similar renormalization is needed for valence protons.) For con-

venience, we shall use *effective operator* as a common term for the effective interaction and other effective operators, when further specification is not needed.

In early shell-model calculations simple phenomenological potentials were used for the effective interaction. All these potentials contained parameters which were determined by fitting experimental level energies. Very interesting developments were made by Talmi and his school, who determined the matrix elements of the effective interaction in simple configurations directly from the experimental spectra. Both these approaches were very successful and provided useful interpretations of nuclear states. For further details, see for instance Elliott and Lane (1957), Talmi (1962), de-Shalit and Talmi (1963), and Schiffer and True (1976).

The early successes of the shell model prompted extensive efforts to understand its physical origin, and in particular to derive the one-body potential and the effective interaction from the nucleon–nucleon interaction. This program has encountered several obstacles. One difficulty is that the nucleon–nucleon interaction is not well known. Ultimately one expects to be able to derive the nucleon–nucleon interaction from meson theory. However, there are still many uncertainties associated with the potential models of meson theory (Brown and Jackson, 1975), and one rather employs potentials which are fitted to the nucleon–nucleon scattering data and the deuteron binding energy. Unfortunately, the nucleon–nucleon interaction cannot be uniquely determined this way. Potentials of different forms can be constructed which all fit the present two-nucleon data. One might hope that the properties of complex nuclei could be used to discriminate between different forms of the nucleon–nucleon interaction. Thus one is back to the original problem of deriving the shell-model potential and the effective interaction from a given nucleon–nucleon potential.

Powerful perturbation methods have been developed for the solution of the nuclear many-body problem in the last two decades, leaning heavily on techniques from quantum field theory and statistical mechanics. These very general methods are largely independent of the particular many-body system studied and have been found valuable in other areas of physics and chemistry. However, the nuclear many-body problem is more complicated than most other quantum many-body problems. This is partly because atomic nuclei contain too many particles to be treated exactly, but far too few particles to be treated statistically. Thus, one must resort to an approximate treatment where in principle all the nucleons contained in the nucleus are explicitly considered. Another complication with nuclei is that there is no natural center of force, as for instance in atoms where the nucleus generates the dominant electrostatic potential in which the electrons are bound. In nuclei one has in fact to derive the one-body, shell-model potential from the forces acting between the individual nucleons. The nuclear many-body problem is further complicated by the fact that the nucleon–nucleon interaction is very strong at short distances. Thus, as shown by Brueckner *et al.* (1954), one has to sum all terms involving pairs of interacting nucleons in order to obtain a well-behaved interaction, the so-called reaction matrix or  $G$  matrix, which can be used as

a starting point for perturbation expansions. However, the reaction matrix is by no means weak, so that questions of convergence become critical, as we shall see later on.

The nuclear many-body problem was first studied for infinite nuclear matter, which is a hypothetical nuclear system corresponding to the interior of a heavy nucleus, but being free of the complications introduced by the nuclear surface. These studies, which were pioneered by Brueckner, Bethe, and Goldstone (Brueckner *et al.*, 1954; Brueckner, 1955; Bethe, 1956; Bethe and Goldstone, 1957; Goldstone, 1957), appear to have developed a convergent expansion for the problem, namely the hole-line expansion (Bethe, 1965; Rajaraman and Bethe, 1967; see also Day, 1967).<sup>1</sup> As regards finite nuclei, the most ambitious application of these ideas is due to Zabolitzky (1974); we refer to Bethe (1971) for a review of earlier work. Now the hole-line expansion is intended for those parts of the nucleon-nucleon interaction, namely the tensor force and short-range repulsion, which excite nucleons to rather high energy. Here, by contrast, we shall primarily be interested in low-energy correlations, which could be characterized as surface effects.

Some ten years ago the basic perturbation-theoretic framework for effective operators in finite nuclei was laid down by Brandow (1966, 1967), and Kuo and Brown (1966) carried out their pioneering calculations.

The purpose of the present paper is to give a tutorial review of the basic formalism and the current status of calculations of effective operators needed for the nuclear shell model. Since nuclear many-body theory is just an application of general quantal many-body theory, it is often formulated in a language which may not be appreciated by the working nuclear physicist. On the other hand, as pointed out above, the nuclear many-body theory contains features which are peculiar to atomic nuclei, and thus its execution may be inaccessible to non-nuclear physicists. For both reasons an elementary review of the nuclear many-body theory of effective operators is in order. Furthermore, this will give us an opportunity to summarize the main features of the numerical results obtained in the field since the work of Kuo and Brown (1966).

There have been several reviews of the nuclear many-body theory during the last decade (e.g., Brandow, 1967; Baranger, 1969; Macfarlane, 1969; Brown, 1971a; Barrett and Kirson, 1973; Kuo, 1974; see also Brandow, 1975 for a critical assessment of the various formal approaches). The present review will be similar in spirit to the one by Brandow (1967), in the sense that the straightforward algebraic methods of time-independent perturbation theory are used. Time-dependent perturbation theory (Oberlechner *et al.*, 1970; Kuo *et al.*, 1971; Johnson and Baranger, 1971; Krenciglowa and Kuo, 1975) is probably more general and suitable for proving various essential theorems in the many-body theory than time-independent perturbation theory, but it is on the other hand more indirect, as most nuclear structure calculations are performed in a time-independent frame.

<sup>1</sup>Recent calculations by Pandharipande and Wiringa (1976) have raised doubts about the validity of the hole-line expansion.

We have thus followed Brandow in avoiding burdening the nonspecialist reader with the machinery of time-dependent perturbation theory. On the other hand, the present review is intended to be considerably more pedestrian and less general than Brandow's. Indeed, we shall not derive the theory rigorously, but rather illustrate it in terms of a simple, exactly solvable matrix model. Thus we expect that the non-specialist would be able to follow step by step the developments made and hope that thereby his possible phobia against many-body theory be overcome.

In Sec. II we discuss the structure of the formal diagrammatic perturbation theory which is needed in the theory of effective operators in the shell model. We shall be concerned primarily with the calculation of the effective residual shell-model interaction (and shall not discuss the derivation of the average one-body shell-model potential, which in principle can be calculated by similar methods). Furthermore, we shall discuss briefly the calculation of other effective operators, such as electromagnetic transition operators. Finally, some attention is paid to the formal convergence properties of the perturbation expansion for the effective interaction.

In Sec. III we review in a simple-minded way the main features of the numerical results obtained for the effective interaction and for the effective electromagnetic  $E2$  operator. Where convenient, we shall describe these results in terms of simple schematic models.

The final section, Sec. IV, contains brief concluding remarks. Various technical points relating to Sec. II are given in the Appendices A-D. At the end of each subsection we have placed a short summary of the salient points, which may be useful to the reader.

## II. FORMAL PERTURBATION THEORY

We wish to discuss in this section in a simple, intuitive way, without rigor, the formal diagrammatic perturbation theory structure which is needed in the theory of effective operators. The label perturbation theory does not imply that only corrections of, say, first and second order in the perturbation can be handled. Rather an exact formalism has been developed which treats the perturbation to arbitrary orders and therefore includes all possible physical processes. It is very helpful to associate diagrams with the various terms of the perturbation series. They give an immediate, precise picture of the process under discussion and are invaluable in trying to define the physically important processes for a given problem. Often a particular class of diagrams involving the perturbation to arbitrarily high order will be physically significant, so that it then becomes necessary to make a partial summation of this infinite series to obtain an approximate solution of the many-body problem.

This section is organized as follows. We start in Sec. II.A by deriving a general equation for the effective interaction (Bloch and Horowitz, 1958; Feshbach, 1962; Löwdin, 1962; Brandow, 1967). Applying this to a simple  $2 \times 2$  matrix problem in Sec. II.B, we are able to illustrate many of the features of diagrammatic perturbation theory needed subsequently. Then in Sec. II.C we show how the effective interaction of Sec. II.A can be cast into a form suitable for shell-model calcula-

tions. We follow here the time-independent approach of Brandow (1967) and refer to this work for general proofs. As well as using an effective interaction in the shell model, we need to replace all the other operators of interest, e.g., the electromagnetic transition operators, by effective operators. The necessary formalism is given in Sec. II.D; we restrict our attention to the case of a single particle beyond a nondegenerate core, since this results in great simplifications and since this is the case of most immediate interest. Finally in Sec. II.E we discuss formal divergence problems (Schucan and Weidenmüller, 1972, 1973) which arise in many cases of interest. Here we again lean on the  $2 \times 2$  matrix to illustrate both the divergence and suggested remedies.

### A. Degenerate perturbation theory

We wish to calculate the bound-state properties of a system of many interacting nucleons. We shall assume that they interact via two-body forces, although the introduction of many-body forces would cause no difficulty in principle. Since we cannot solve the Schrödinger equation

$$H\Psi = E\Psi \quad (2.1)$$

exactly, we seek approximate solutions using perturbation theory techniques. We split the Hamiltonian  $H$  into an unperturbed part  $H_0$ , for which we can obtain an exact solution, plus a perturbation  $V$ . Explicitly,

$$H = H_0 + V, \quad (2.2)$$

and

$$\begin{aligned} H_0 &= \sum_i (T_i + U_i), \\ V &= \sum_{i < j} V_{ij} - \sum_i U_i. \end{aligned} \quad (2.3)$$

Here  $T_i$  represents the kinetic energy of particle  $i$ , and  $V_{ij}$  gives the interaction between particles  $i$  and  $j$ . We have also added and subtracted a one-body potential  $U$ , which is therefore arbitrary in the sense that the results of an exact calculation will be independent of  $U$ . However, in an approximate calculation the results can be expected to depend on  $U$ , so that a reasonable physical choice should be made. It should also be convenient to work with—the harmonic oscillator potential is often used in practice; see Sec. III.

In Eq. (2.3)  $H_0$  is a sum of one-body Hamiltonians, so that we need to solve a one-body Schrödinger equation

$$(T + U)\phi_\nu = e_\nu \phi_\nu. \quad (2.4)$$

If, in some particular state  $i$  of the  $A$ -particle system, orbitals  $\alpha$  to  $\xi$  are filled, we have

$$H_0\Phi_i = \epsilon_i \Phi_i \quad (2.5)$$

with

$$\epsilon_i = \sum_{\nu=\alpha}^{\xi} e_\nu$$

and

$$\Phi_i = \frac{1}{\sqrt{A!}} \alpha \left( \prod_{\nu=\alpha}^{\xi} \phi_\nu \right) \equiv \left( \prod_{\nu=\alpha}^{\xi} \alpha_\nu^\dagger \right) | \rangle. \quad (2.6)$$

In the latter equation  $\alpha$  is the antisymmetrization operator needed in first quantization, and we have also written the equivalent expression using second quantization creation operators  $\alpha^\dagger$  acting on the vacuum  $| \rangle$ .

We can now expand the true wave function in the complete set of unperturbed states

$$\Psi = \sum_i a_i \Phi_i. \quad (2.7)$$

Inserting this in the Schrödinger equation (2.1) and taking the scalar product with  $\Phi_j$ , we obtain, using (2.5),

$$(E - \epsilon_j)a_j = \langle \Phi_j | V | \Psi \rangle. \quad (2.8)$$

Now we need to define the valence or model space (both terms are used). They refer to the set of states  $\Phi_i$  with  $i = 1, 2, \dots, d$  which we actually wish to work with explicitly in the shell model, i.e., we shall set up the energy matrix for this set of states and diagonalize it. An example of a valence space would be the case of two particles in the ( $sd$ ) shell beyond the filled  $0s$  and  $0p$  shells of the  $^{16}\text{O}$  core (see Fig. 1); this would be appropriate for the nuclei  $^{18}\text{O}$ ,  $^{18}\text{F}$ , and  $^{18}\text{Ne}$ . The remainder of the complete set of states we shall include implicitly by constructing effective operators, e.g., we shall construct an effective interaction  $\mathcal{U}$  which will be used in place of  $V$ . We can now split the summation in Eq. (2.7),

$$\begin{aligned} \Psi &= \sum_{i=1}^d a_i \Phi_i + \sum_{i=d+1}^{\infty} a_i \Phi_i \\ &= \Psi_D + \sum_{i=d+1}^{\infty} \frac{|\Phi_i\rangle \langle \Phi_i | V | \Psi \rangle}{E - \epsilon_i}. \end{aligned} \quad (2.9)$$

Here we have defined our valence wave function  $\Psi_D$  as that component of the true wave function which lies in the model space; we shall take it to be normalized to unity. This is the usual choice, although other definitions can be used (des Cloizeaux, 1960; Schucan and Weidenmüller, 1973). The second term in Eq. (2.9) has been transformed using Eq. (2.8).

It is useful and elegant to define projection operators  $P$  and  $Q$  which respectively project into and out of the valence space

$$\begin{aligned} P &= \sum_{i=1}^d |\Phi_i\rangle \langle \Phi_i|, \\ Q &= \sum_{i=d+1}^{\infty} |\Phi_i\rangle \langle \Phi_i|, \\ P + Q &= 1. \end{aligned} \quad (2.10)$$

It is easily verified that  $P$  and  $Q$  have the usual projection operator properties  $P^2 = P$ ,  $P^\dagger = P$ ,  $PQ = 0$ , etc. Then we can write Eq. (2.9) in operator notation

$$\Psi = \Psi_D + [Q/(E - H_0)]V\Psi \quad (2.11)$$

and

$$\Psi_D = P\Psi. \quad (2.12)$$

If we define a model or wave operator (Eden and Francis, 1955)  $\Omega$  by

$$\Psi = \Omega\Psi_D, \quad (2.13)$$

then clearly Eq. (2.11) gives

$$\Omega(E) = 1 + [Q/(E - H_0)]V\Omega(E). \quad (2.14)$$

Now, using Eq. (2.13) in Eq. (2.8), we obtain

$$\begin{aligned} (E - \epsilon_j)a_j &= \langle \Phi_j | V\Omega | \Psi_D \rangle \\ &= \sum_{k=1}^0 \langle \Phi_j | V\Omega | \Phi_k \rangle a_k \end{aligned} \quad (2.15)$$

or equivalently

$$[H_0 + \mathfrak{U}(E) - E]\Psi_D = 0, \quad (2.16)$$

where we have defined an effective interaction  $\mathfrak{U}$ , which depends on the energy  $E$  and acts within the model space, by

$$\mathfrak{U}(E) = V\Omega(E). \quad (2.17)$$

Using this relation and Eq. (2.14), we have an integral equation

$$\mathfrak{U}(E) = V + V[Q/(E - H_0)]\mathfrak{U}(E) \quad (2.18)$$

for the effective interaction, which shows its dependence on the energy  $E$ .

Now Eq. (2.16) looks something like a shell-model equation, but it is not quite of the right form. Firstly, the energy  $E$  is the total energy of the many-body system, rather than the energy relative to closed shells which we deal with in the shell model. Secondly, as we have remarked, the interaction  $\mathfrak{U}$  depends on the energy  $E$  which we wish to calculate, i.e., the energy denominator of Eq. (2.18) is of Brillouin-Wigner form. A related point is the occurrence of unlinked diagrams in the perturbation series for  $\mathfrak{U}$ . We indicate how this difficulty can be eliminated in the case of a simple example in the following Sec. II.B.

It is worth remarking that we have recast the Schrödinger equation in the form of Eqs. (2.16) and (2.18) which will yield  $d$  true eigenvalues. We have no guarantee, however, which eigenvalues will be obtained in an actual calculation. Only if the true wave function has no component in the model space,  $P\Psi = 0$ , are we in principle unable to obtain the corresponding eigenvalue.

Equation (2.18) for the effective interaction can be rewritten in a somewhat different form which is sometimes useful. Iterating this equation we have

$$\begin{aligned} \mathfrak{U} &= V + VQ \frac{1}{E - H_0} QV + VQ \frac{1}{E - H_0} QVQ \frac{1}{E - H_0} QV \\ &\quad + VQ \frac{1}{E - H_0} VQV \frac{1}{E - H_0} VQV \frac{1}{E - H_0} QV + \dots, \end{aligned} \quad (2.19)$$

where we have used the property  $Q^2 = Q$ . Now using the result

$$1 + x + x^2 + x^3 + \dots = (1 - x)^{-1}, \quad (2.20)$$

and noting that we are dealing with operators, we easily find

$$\begin{aligned} \mathfrak{U} &= V + VQ \frac{1}{E - H_0 - QVQ} QV \\ &= PVP + PVQ \frac{1}{E - QHQ} QVP. \end{aligned} \quad (2.21)$$

In the latter equation we have inserted  $P$  operators fore

and aft to remind ourselves that the effective interaction acts within the model space.

As well as using an effective interaction, we need to replace all the other operators of interest in the shell model, e.g., the electromagnetic transition operators, by effective operators. These are designed to take into account the  $Q$  space states which are not explicitly included in the calculations. Here we need to start with Eq. (2.13) for the true wave function, which involves the same undesirable features as outlined above for  $\mathfrak{U}(E)$ . This will be discussed further in Sec. II.D.

*Summary.* The Schrödinger equation has been rewritten as a secular equation (2.16) involving an effective interaction  $\mathfrak{U}$  [Eqs. (2.18) and (2.21)] acting within a model space of dimension  $d$ . Further manipulation will be required to put Eq. (2.16) into the desired form.

### B. A simple $2 \times 2$ matrix problem

We consider here by way of illustration the case of a simple  $2 \times 2$  matrix; discussions of this problem in various contexts have been given by Katz (1960), Ellis and Osnes (1973), and Schaefer (1974); see also Schucan and Weidenmüller (1973). We interpret this as an eigenvalue problem for a one-body system in which only two states,  $A$  and  $B$ , are available. The unperturbed solutions are

$$\begin{aligned} H_0\Phi_A &= \epsilon_A\Phi_A, \\ H_0\Phi_B &= \epsilon_B\Phi_B, \end{aligned} \quad (2.22)$$

and we specify that  $\epsilon_B > \epsilon_A$ . For the perturbation  $V$  we take, in second quantization,

$$V = X(a_A^\dagger a_B + a_B^\dagger a_A). \quad (2.23)$$

Thus  $V$  has only off-diagonal matrix elements; any diagonal terms could obviously be incorporated into  $H_0$ .

The exact solution to this problem is easily obtained by setting the secular determinant to zero:

$$\begin{vmatrix} \epsilon_A - E & X \\ X & \epsilon_B - E \end{vmatrix} = 0, \quad (2.24)$$

giving

$$(E - \epsilon_A)(E - \epsilon_B) = X^2 \quad (2.25)$$

and

$$E = \frac{1}{2}(\epsilon_A + \epsilon_B \pm [(\epsilon_B - \epsilon_A)^2 + 4X^2]^{1/2}). \quad (2.26)$$

If we make a power-series expansion in  $X^2$ , the lowest eigenvalue  $E_1$  is

$$E_1 = \epsilon_A + \frac{X^2}{\epsilon_A - \epsilon_B} - \frac{X^4}{(\epsilon_A - \epsilon_B)^3} + \dots \quad (2.27)$$

We now wish to apply perturbation theory to this problem, taking as our model space the single state  $A$  so that no diagonalization is necessary for Eq. (2.16), i.e., we are concerned with nondegenerate perturbation theory.

#### 1. Brillouin-Wigner perturbation theory (particle representation)

For our single model-space state Eqs. (2.16) and (2.18) become

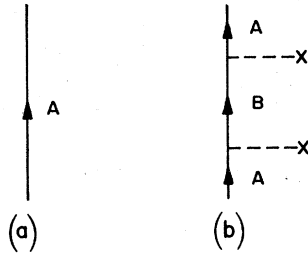


FIG. 2. Diagrams showing the unperturbed state (a), and the second-order perturbation contribution (b) in a particle representation.

$$E = \epsilon_A + \langle \Phi_A | V + V \frac{Q}{E - H_0} V + V \frac{Q}{E - H_0} V \frac{Q}{E - H_0} V + \dots | \Phi_A \rangle, \quad (2.28)$$

which is clearly standard Brillouin-Wigner perturbation theory. If we take a particle representation so that

$$| \Phi_A \rangle = a_A^\dagger | \rangle, \quad (2.29)$$

where  $| \rangle$  is the true vacuum, we can represent the unperturbed state as in Fig. 2(a). The second-order term

$$[X^2 / (E - \epsilon_B)] \langle | a_A a_A^\dagger a_B a_B^\dagger a_A a_A^\dagger | \rangle \quad (2.30)$$

is represented by the diagram in Fig. 2(b), where the perturbation  $V$  is represented by the cross. In fact, this is the only diagram which can occur, since the  $Q$  operator in Eq. (2.28) requires that the intermediate state be  $B$ . Our perturbation (2.23) can act on state  $A$  to excite  $B$ , and having excited  $B$  can only de-excite it to state  $A$  again. Thus we have

$$E = \epsilon_A + X^2 / (E - \epsilon_B), \quad (2.31)$$

which is the exact result of Eq. (2.25). Notice that this equation yields both eigenvalues of the problem (excepting the trivial case  $X = 0$ , when the upper state has no component of  $\Phi_A$ ).

2. Brillouin-Wigner perturbation theory (hole representation)

Now Eq. (2.28) still applies, but we choose the vacuum state to be  $| \Phi_A \rangle = a_A^\dagger | \rangle$  and discuss particle-hole excitations with respect to this vacuum. The analogue of Fig. 2(a) is now just a blank and is not shown. The analogue of Fig. 2(b) is Fig. 3(a), and the fourth-order diagrams which now occur are given in Figs. 3(b)-(e). [There are no diagrams of odd order in the perturbation because it is purely off-diagonal; see Eq. (2.23).] A little care is needed as regards energy denominators; we can write

$$E - H_0 \equiv \Delta E + \epsilon_A - H_0 = \Delta E + \Sigma \text{ (downgoing-upgoing) line energies} \quad (2.32)$$

since  $(\epsilon_A - H_0)$  gives minus the energy relative to the vacuum. The denominator in Fig. 3(a) is thus  $\Delta E + \epsilon_A - \epsilon_B$

$$E = \epsilon_A + \langle \Phi_A | V \frac{Q}{\epsilon_A - H_0} V + V \frac{Q}{\epsilon_A - H_0} V \frac{Q}{\epsilon_A - H_0} V \frac{Q}{\epsilon_A - H_0} V | \Phi_A \rangle - \langle \Phi_A | V \frac{Q}{(\epsilon_A - H_0)^2} V | \Phi_A \rangle \langle \Phi_A | V \frac{Q}{\epsilon_A - H_0} V | \Phi_A \rangle. \quad (2.34)$$

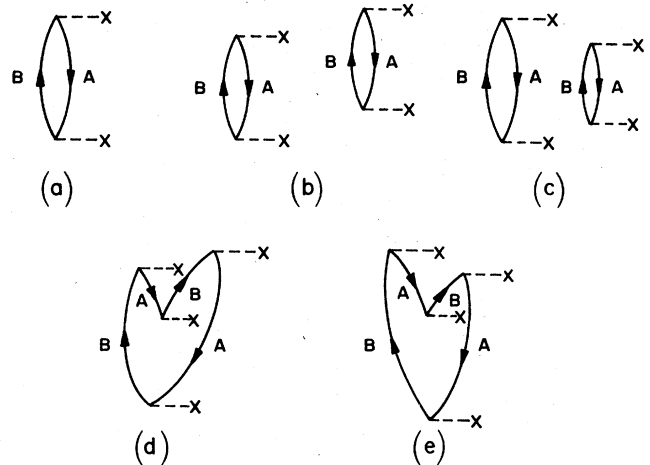


FIG. 3. Second- and fourth-order diagrams in a hole representation.

$= E - \epsilon_B$ , so that through second order we obtain the exact result of Eq. (2.31) above.

The remaining diagrams in Fig. 3 (and in higher orders) give zero contribution. This follows since the exclusion principle is violated in intermediate states; thus in Figs. 3(b)-(e) we have two particles in state  $B$  which can accommodate only one particle. Equivalently the exclusion principle can be ignored and the diagrams can be explicitly shown to cancel; thus diagrams 3(b) and (c) have the same magnitude and opposite sign to diagrams 3(d) and (e). Explicitly Fig. 3(b) involves the contraction

$$X^4 \langle \Phi_A | a_A^\dagger a_B a_A^\dagger a_B a_B^\dagger a_A a_A^\dagger a_B a_A^\dagger | \Phi_A \rangle,$$

and Fig. 3(d) involves the contraction

$$X^4 \langle \Phi_A | a_A^\dagger a_B a_A^\dagger a_B a_A^\dagger a_B a_A^\dagger a_B a_A^\dagger | \Phi_A \rangle,$$

and these clearly differ by a sign.

3. Rayleigh-Schrödinger perturbation theory (hole representation)

We now want to rewrite Eq. (2.28) in such a way that the energy denominators involve only the unperturbed energies, i.e., they are of Rayleigh-Schrödinger (RS) form. To do this we write the total energy  $E$  as the sum of the energy shift we wish to calculate,  $\Delta E$ , and the unperturbed energy,  $\epsilon_A$ , as in Eq. (2.32) and use the identity

$$\frac{1}{E - H_0} = \frac{1}{\epsilon_A - H_0} \left( 1 + \frac{\Delta E}{\epsilon_A - H_0} \right)^{-1} = \frac{1}{\epsilon_A - H_0} \left( 1 - \frac{\Delta E}{\epsilon_A - H_0} + \left( \frac{\Delta E}{\epsilon_A - H_0} \right)^2 - \dots \right) \quad (2.33)$$

in Eq. (2.28). Substituting the expression for  $\Delta E = E - \epsilon_A$  back into itself we obtain through fourth order, neglecting odd powers of  $V$ ,

The diagrams for the second quantity on the right-hand side will be just those indicated in Fig. 3, but now with RS denominators. Now a diagram is said to be unlinked if it consists of two or more pieces which are not connected together by any interactions. Thus the diagrams of Fig. 3(b) and (c) are both unlinked; further, the interaction matrix elements and the signs are obviously the same for both. The energy denominators are also the same, but let us be more general for the moment and take an excitation energy  $\alpha$  for just the left-hand piece of Fig. 3(b) or 3(c) and an energy  $\beta$  for just the right-hand piece. Then the sum of energy denominators for Figs. 3(b) and (c) reads

$$\frac{1}{\alpha(\alpha+\beta)\beta} + \frac{1}{\alpha(\alpha+\beta)\alpha} = \frac{\alpha+\beta}{\alpha^2\beta(\alpha+\beta)} = \frac{1}{\alpha^2\beta}. \tag{2.35}$$

This is a simple example of the factorization theorem, discussed further below, where a sum of energy denominators can be written more simply as a product of denominators referring to the left- and right-hand pieces separately. We thus have a contribution  $\langle \Phi_A | VQV | \Phi_A \rangle^2 / \alpha^2\beta$  [which in our case is just  $X^4 / (\epsilon_A - \epsilon_B)^3$ ] from the second term of Eq. (2.34), which is exactly canceled by the third term. Thus the unlinked diagrams are removed in this order. They are also removed in higher orders, so that one has a completely linked perturbation series; this general result was first proved in the famous paper by Goldstone (1957). The type of diagram discussed here is often referred to as a Goldstone or Feynman-Goldstone diagram. We are left with Figs. 3(a), (d), and (e) to calculate through fourth order. The latter two diagrams give the negative of the unlinked contribution derived above. We obtain

$$E = \epsilon_A + \frac{X^2}{\epsilon_A - \epsilon_B} - \frac{X^4}{(\epsilon_A - \epsilon_B)^3} \tag{2.36}$$

which, of course, is identical to Eq. (2.27) derived directly. Notice that it is now necessary to include the Pauli exclusion violating diagrams 3(d) and (e), since the cancelling diagrams, Figs. 3(b) and (c), have been removed.

#### 4. Rayleigh-Schrödinger perturbation theory (particle representation)

We now wish to obtain a perturbation series with RS denominators in a particle representation, i.e., using the true vacuum  $| \rangle$ . To do this we can again use Eq. (2.34), but now in the second term only the second-order contribution will be nonzero, and this gives the diagram of Fig. 2(b), with RS denominators. We are then left with the third term which we wish to represent diagrammatically. It looks something like Fig. 4(a), but this is not quite right since the upper energy denominator should be squared and since the initial state  $A$  appears at an intermediate level. We need a new form of diagram called a folded diagram (Brandow, 1967; see also Morita, 1963), and write this contribution as the sum of two folded diagrams, Figs. 4(b) and (c). Here we have folded the valence particle line  $A$  so that the arrow goes downwards, but it is not a hole line, and to indicate this a loop is put on the line. We associate a minus sign with each fold to obtain the signs of Eq. (2.33). Here this just

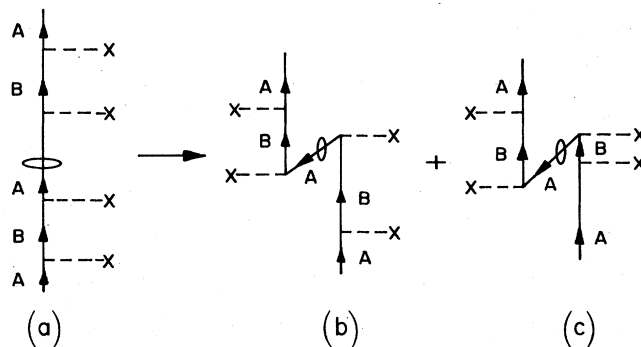


FIG. 4. Diagrams needed in Rayleigh-Schrödinger perturbation theory in a particle representation. The unfolded diagram (a) yields the two folded diagrams (b) and (c).

gives  $-1$  for a single fold, which is the correct sign for these diagrams, and the interactions obviously give  $X^4$  as desired. The energy denominators can be found by operating with  $\epsilon_A - H_0$  between the interactions, provided that the folded line is treated as a hole line for these purposes. For diagram 4(b) this gives

$$\frac{1}{(\epsilon_A - \epsilon_B)} \frac{1}{[\epsilon_A - (2\epsilon_B - \epsilon_A)]} \frac{1}{(\epsilon_A - \epsilon_B)} = \frac{1}{2(\epsilon_A - \epsilon_B)^3}$$

and the same result is obtained for Fig. 4(c). Thus the sum gives the desired  $(\epsilon_A - \epsilon_B)^{-3}$ . Actually this is again a simple application of the factorization theorem which has been used "backwards" in going from Figs. 4(a) to 4(b) and 4(c). We thus have a linked perturbation expansion through fourth order, consisting of Figs. 2(b), 4(b), and 4(c), which gives the same result, Eq. (2.36), as before. Again it can be shown (Brandow, 1967) that a linked series is obtained in general, using these folded diagrams.

We remark that Fig. 4(a) is called the unfolded form of Figs. 4(b) and (c). Further, in order to avoid double counting, we must specify that the topmost interaction of the folded diagram is the same as the topmost interaction of the unfolded diagram.

The reader may have noted that the folded diagrams of Fig. 4 could be produced by cutting an appropriate  $A$  hole line in the Goldstone diagrams of Fig. 3(d) and (e) and opening out the two pieces. Further, both forms of diagram yield the same result, so we simply have two different ways of representing a given contribution. This is a special feature of our simple example; in general for nondegenerate perturbation theory there is not a one-to-one correspondence between the folded diagrams and the Goldstone diagrams, although obviously the sums of such diagrams for a given order in the perturbation must be identical (we discuss this further for an explicit example in Appendix A).

#### 5. The factorization theorem

We have used the factorization theorem already and we shall need it in more generality later on, so it is well to give a simple algebraic proof of the general result. A somewhat different algebraic proof by induction has been given by Frantz and Mills (1960), while Bethe, Brandow, and Petschek (1963) have used a time-dependent method. Consider Fig. 5(a). The left-hand block is a schematic

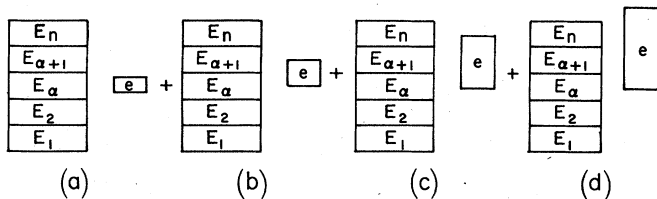


FIG. 5. Schematic representation of a set of diagrams which can be factorized.

representation of a diagram with the horizontal lines indicating the levels of the interactions. The energy denominators for this block considered alone are  $E_1, E_2, \dots, E_n$  and give a contribution to the diagram

$$\prod_{i=1}^n \frac{1}{E_i}.$$

We now insert a new right-hand block which may or may not be joined to the left-hand block. The right-hand block has two interactions and an energy denominator  $e$ ; it is inserted at level  $\alpha$ , actually  $\alpha=3$  in Fig. 5. If we allow

all orderings of the interactions of the left-hand block (above  $\alpha$ ) with respect to the topmost interaction of the right-hand block—Figs 5(a), (b), (c), and (d)—then the sum of these diagrams can be simplified. The interactions and signs of the diagrams are obviously the same in all cases, so it is only necessary to consider the energy denominators. We obtain for the sum of the diagrams

$$Z = \left( \prod_{i=1}^{\alpha} \frac{1}{E_i} \right) \left( \prod_{i=\alpha}^n \frac{1}{E_i} \right) \left[ \sum_{j=\alpha}^n \frac{1}{E_j} \left( \prod_{k=\alpha}^j \frac{E_k}{E_k+e} \right) + \frac{1}{e} \prod_{k=\alpha}^n \frac{E_k}{E_k+e} \right]. \quad (2.37)$$

The sum over  $j$  in the square brackets refers to the cases where the topmost interaction of the right-hand block is at level  $j$ , and the last term refers to the case in which the interaction is above the level  $n$ . Setting

$$\frac{1}{E_j} = \frac{E_j+e}{E_j e} - \frac{1}{e}$$

in Eq. (2.37) gives

$$Z = \left( \prod_{i=1}^{\alpha} \frac{1}{E_i} \right) \left( \prod_{i=\alpha}^n \frac{1}{E_i} \right) \left[ \frac{1}{e} + \sum_{j=\alpha+1}^n \frac{E_j+e}{E_j e} \left( \prod_{k=\alpha}^j \frac{E_k}{E_k+e} \right) - \frac{1}{e} \sum_{j=\alpha}^{n-1} \left( \prod_{k=\alpha}^j \frac{E_k}{E_k+e} \right) - \frac{1}{e} \prod_{k=\alpha}^n \frac{E_k}{E_k+e} + \frac{1}{e} \prod_{k=\alpha}^n \frac{E_k}{E_k+e} \right]. \quad (2.38)$$

Rewriting the second term in square brackets as

$$\frac{1}{e} \sum_{j=\alpha+1}^n \left( \prod_{k=\alpha}^{j-1} \frac{E_k}{E_k+e} \right) = \frac{1}{e} \sum_{l=\alpha}^{n-1} \left( \prod_{k=\alpha}^l \frac{E_k}{E_k+e} \right),$$

we observe that this cancels the third term of Eq. (2.38), and since the fourth and fifth terms cancel, we have

$$Z = \left( \prod_{i=1}^{\alpha} \frac{1}{E_i} \right) \left( \prod_{i=\alpha}^n \frac{1}{E_i} \right) \frac{1}{e} \equiv \left( \prod_{i=1}^n \frac{1}{E_i} \right) \frac{1}{E_\alpha e}. \quad (2.39)$$

This is the desired result, which shows the factorization into a product of energy denominators. [Note that if  $n=\alpha$ , the second and third terms of Eq. (2.38) are zero and we obtain Eq. (2.39) directly.] It should be obvious that this result can be generalized to the case where the right-hand block contains many interactions, by successive applications of the above argument. In this case  $e$  in Eq. (2.39) becomes the product of energy denominators for the right-hand block alone, and we shall have summed the diagrams with all possible orderings of the interactions in the left- and right-hand blocks, subject to the restriction that the lowest interaction of the right-hand block is fixed at level  $\alpha$ .

Notice that if we have a set of diagrams which take the form of Fig. 5 turned upside down, the same factorization arguments apply. The only difference is that the fixed interaction at level  $\alpha$  becomes the highest interaction of block  $e$ . Thus we may use the factorization theorem either upwards or downwards. Of course it is not possible to group all diagrams into classes such that the factorization theorem is applicable. Only those diagrams (or parts of a diagram) with a suitable topological structure can be treated in this manner.

## 6. Summation of the series

We have obtained a linked perturbation series with RS denominators using both the particle and hole representations for our  $2 \times 2$  matrix problem. Without explicitly retracing our steps it should be possible to sum the series and obtain the exact result. This we shall do here. This subsection is not essential to the subsequent development and may be skipped if the reader desires; it is, however, a useful illustration and, further, it is fun.

In the hole and particle representations the diagrams have different forms which suggest different ways of summing the series. Here we shall stay with the hole representation, leaving the particle case to a later section and a different context. The most straightforward way of summing the Goldstone diagrams of Fig. 3(a), (d), (e), and higher orders would be to obtain a general expression for the sum of all diagrams of a given order in the perturbation  $V$  and then sum over all orders. This has been carried out by Katz (1960), but it gets complicated.

An alternative procedure is suggested by considering the general structure of the diagrams. Consider the example illustrated in Fig. 6. The lowest interaction is labeled  $L_0$  and the next lowest interaction  $L_1$ . Now consider the left and right pieces above  $L_1$ ; we can of course take all possible orderings of the interactions and use the factorization theorem. Now the left-hand piece alone looks like a diagram of lower order,  $\Delta_L$  say, except that it is not closed off at the bottom by the equivalent of interaction  $L_0$ . Thus the left-hand piece gives a contribution  $\Delta_L/X$ , and similarly the right-hand piece gives  $\Delta_R/X$ . Thus the contribution of this set of diagrams of the type shown in Fig. 6 is

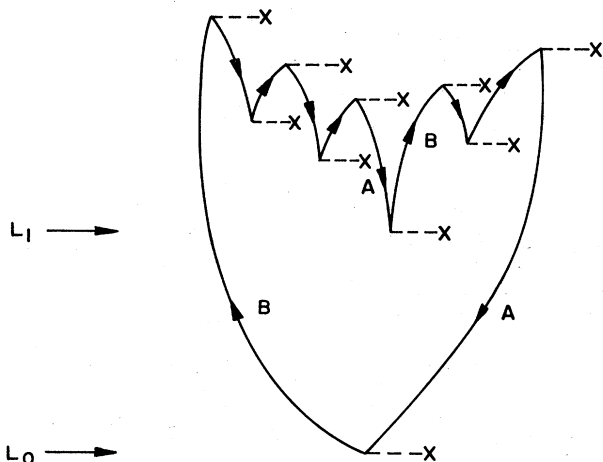


FIG. 6. General structure of a diagram for the  $2 \times 2$  matrix problem (hole representation).

$$-\frac{\Delta_L}{X} \frac{\Delta_R}{X} \frac{X^2}{(\epsilon_A - \epsilon_B)}. \tag{2.40}$$

(The reader may verify in detail that this is correct!) The minus sign in Eq. (2.40) follows as, using the subscripts 0 and 1 to indicate interactions  $L_0$  and  $L_1$ , the operators  $a_{B1}^\dagger a_{A1} a_{B0}^\dagger a_{A0}$  must be put in the form  $a_{B0}^\dagger a_{A1} a_{B1}^\dagger a_{A0}$  for our left and right argument to hold. This involves a sign change.

A little thought will convince one that, except for second order, every diagram takes the form in Fig. 6, i.e., interactions  $L_0$  and  $L_1$ , and above this left and right pieces of some lower order. Further, we can generate each diagram uniquely by taking all possibilities for  $\Delta_L$  and  $\Delta_R$ . Now if we call  $\Delta$  the sum of the infinite set of all Goldstone diagrams, we can generalize Eq. (2.40) to

$$\Delta = \frac{X^2}{\epsilon_A - \epsilon_B} - \frac{\Delta \Delta}{X X} \frac{X^2}{(\epsilon_A - \epsilon_B)}. \tag{2.41}$$

The first term here gives the second-order contribution. Taking this value for  $\Delta$  and substituting in the right-hand side, we get a new value of  $\Delta$ . Continuing this iterative process we shall generate all diagrams uniquely (although not in order-by-order sequence). To use this as a practical method of solving Eq. (2.41) we obviously need convergence. However, regardless of the convergence of this particular method of solution, Eq. (2.41) is clearly formally correct. If we add in the unperturbed energy and set  $E = \epsilon_A + \Delta$  as before, a little algebra leads to the result

$$(E - \epsilon_A)(E - \epsilon_B) = X^2. \tag{2.42}$$

This is the exact result of Eq. (2.25), as it should be, and consequently both eigenvalues are obtained.

Before leaving the  $2 \times 2$  problem, we feel it useful to demonstrate again the geometric series summation, discussed previously at the end of Sec. II. A, since it is so useful in practice. Let us add to the perturbation  $V$  of Eq. (2.23) a term diagonal in state  $B$ , i.e.,

$$V - V + X_B a_B^\dagger a_B. \tag{2.43}$$

Using for the sake of argument the hole representation, we shall now have, in addition to the diagram of Fig.

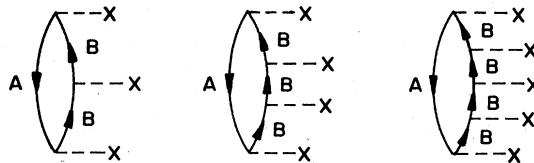


FIG. 7. Diagrams containing a sequence of diagonal  $X_B$  insertions. These are the lowest-order members of an infinite series which can be exactly summed.

3(a), those of Fig. 7. The sum of all these diagrams is

$$\frac{X^2}{(\epsilon_A - \epsilon_B)} \left[ 1 + \frac{X_B}{\epsilon_A - \epsilon_B} + \left( \frac{X_B}{\epsilon_A - \epsilon_B} \right)^2 + \dots \right], \tag{2.44}$$

and using Eq. (2.20) we easily obtain

$$\frac{X^2}{\epsilon_A - \epsilon_B} \left[ 1 - \frac{X_B}{\epsilon_A - \epsilon_B} \right]^{-1} = \frac{X^2}{\epsilon_A - \epsilon_B - X_B}. \tag{2.45}$$

Thus we have just replaced  $\epsilon_B$  by  $\epsilon_B + X_B$ . The same replacement is obtained in higher-order (in  $X$ ) diagrams, such as Figs. 3(d) and (e), when diagonal  $X_B$  insertions are allowed and the diagrams are summed using the factorization theorem [cf. the arguments leading to Eq. (2.41)]. Of course this simple result is to be expected, since we could equally well have incorporated the  $X_B$  term of Eq. (2.43) in the unperturbed Hamiltonian  $H_0$ . Then the replacement  $\epsilon_B - \epsilon_B + X_B$  for the unperturbed energies of Eq. (2.22) is trivial.

*Summary.* We have used a  $2 \times 2$  matrix problem to illustrate the transformation from Brillouin-Wigner (Sec. II.B.2) to Rayleigh-Schrödinger (Sec. II.B.3) perturbation theory, using the techniques of Brandow (1967). Folded diagrams were shown to arise in Sec. II.B.4 if the true vacuum was used and a completely linked expansion with RS denominators was desired. The factorization theorem, which plays a central role, was proved in Sec. II.B.5 [Eq. (2.39) referring to Fig. 5].

### C. Shell-model effective interaction

We now wish to indicate how the difficulties associated with Eq. (2.16) can be removed, bearing in mind the discussion of Sec. II.B. The formalism is completely general, but it is well to keep a definite example in mind, and we use the case of  $^{16}\text{O}$ . Here our unperturbed states consist of two particles in the  $(1s0d)$  shell outside a  $^{16}\text{O}$  core, which we take as the vacuum (see Fig. 1). It is convenient to take the valence states to have degenerate unperturbed energies  $e_{sd}$ . [This is not an essential restriction, since the degeneracy breaking terms can be incorporated in the perturbation, and later these may be summed as in the example at the end of Sec. II.B.6 so as to achieve nondegenerate energies (Brandow, 1967). We give an example of this in Appendix B.] We can then work with a model wave function  $\Psi_D$  which diagonalizes both  $(H_0 + \mathcal{U})$  and  $\mathcal{U}$ . Now taking Eqs. (2.16) and (2.18) in the form

$$E = \langle \Psi_D | H_0 + V + V[Q/(E - H_0)]V + \dots | \Psi_D \rangle, \tag{2.46}$$

we wish to represent the various contributions by means of diagrams, as in the previous Sec. II.B. Here we have a two-body interaction as well as a one-body interaction, and we write the perturbation in second quantization



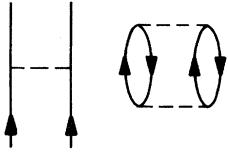


FIG. 9. A diagram which gives a contribution cancelling part of Figs. 8(a) and 8(b). See text.

throughout the first diagram of Fig. 8(b), i.e., in which the two upgoing lines represent initial, final, and intermediate states which are all  $\Psi_D$ . [Note: consider replacing the single lowest valence interaction in this diagram, which can give  $\langle \Psi'_D | V | \Psi_D \rangle$ , by multiple interactions corresponding to all the terms of Eq. (2.46). The sum of this infinite set of diagrams will be diagonal, so that we only need to consider the case  $\Psi'_D = \Psi_D$ .] This gives a contribution of the form

$$+ \frac{\mathfrak{M}_c}{(\epsilon_c - \epsilon'_c)^3} \mathfrak{M}_v^2, \tag{2.55}$$

where  $\mathfrak{M}_v$  is now  $\langle \Psi_D | V | \Psi_D \rangle$ . Further expanding  $\Delta_v$  out of Fig. 8(a) to second order gives

$$+ \frac{\mathfrak{M}_c}{(\epsilon_c - \epsilon'_c)^3} \Delta_v^2. \tag{2.56}$$

However, we must also expand out of the diagram of Fig. 9, which will give

$$-2 \frac{\mathfrak{M}_c}{(\epsilon_c - \epsilon'_c)^3} \mathfrak{M}_v \Delta_v. \tag{2.57}$$

The factor of two arises since there are two energy denominators in Fig. 9. Taking the appropriate part of  $\Delta_v$ , we observe that the contributions (2.55), (2.56), and (2.57) cancel.

Such arguments were generalized, using the full power of the factorization theorem, by Brandow (1967), who showed that all the mixed core-valence diagrams cancel. We are left with two types of diagrams. Firstly we have the pure core diagrams of the type indicated in Fig. 8(a) (denominators now independent of  $\Delta_c$  and  $\Delta_v$ ), which give the energy of the  $^{16}\text{O}$  ground state; the presence of the noninteracting valence lines is irrelevant. Secondly, we have pure valence diagrams [a sample occurs in Fig. 8(d)] with denominators involving  $\Delta_v$  but not  $\Delta_c$ ; these diagrams give the energy of  $^{18}\text{O}$  relative to  $^{16}\text{O}$ .

In the case of the core diagrams only, with  $\Delta_c$  expanded out of the denominators, Goldstone (1957) showed that all unlinked diagrams cancel, so that one obtains a purely linked expansion with Rayleigh-Schrödinger denominators. Brandow (1967) demonstrated the same result using the methods we have followed here. We refer to Day (1967) for an excellent introductory discussion of the nondegenerate problem and to Rajaraman and Bethe (1967) and Bethe (1971) for more advanced treatments.

Since the core energy is independent of the valence particle states, we can write

$$\mathfrak{U} = \Delta_c \mathbf{1} + \mathfrak{U}_v. \tag{2.58}$$

Then Eqs. (2.16) and (2.46) become the Bloch-Horowitz (1958) equations for the relative shell-model energies  $E_v$  in which we are interested, i.e.,

$$[H_{0v} + \mathfrak{U}_v(E_v) - E_v] \Psi_D = 0$$

with

$$\mathfrak{U}_v(E_v) = V + V \frac{Q}{E_v - H_0} V + \dots, \tag{2.59}$$

where only pure valence diagrams are allowed. In the first of Eqs. (2.59)  $H_{0v}$  operating on  $\Psi_D$  gives just the valence unperturbed energy, and in the second equation  $H_0$  operating on intermediate states gives the sum of particle minus hole energies. Equations (2.59) were independently derived by Day (1964).

It is worth commenting on the way exclusion principle effects have been treated to allow the separation of core and valence parts. Consider Fig. 10(a); this violates the exclusion principle, since the particle states in the core part of the diagram are the same as the valence particle states. The diagrams shown in Figs 10(b), (c), and (d) compensate for this violation, i.e., the sum of diagrams (a)-(d) is zero. Now we have included diagram (a) in the core energy  $E_c$ , whereas diagrams (b) and (c) are placed in the one-body part of the effective interaction  $\mathfrak{U}_v$ , and diagram (d) is included in the two-body part. Thus we have a whole series of diagrams in the effective interaction which arise from the Pauli blocking effect of the additional valence particles.

Now the Bloch-Horowitz equations (2.59) represent a giant step forward and could be used as they stand; they have, however, drawbacks. For instance, the interaction we need depends on the energy  $E_v$  that we wish to calculate. Further, we would have to include in the two-body interaction unlinked valence diagrams, such as Fig. 11(c), which look like "products of single particle energies." By now we should expect these undesirable effects to cancel when we expand out  $\Delta_v$  from the denominators, and from the discussion of Sec. II.B.4 we would expect folded diagrams to arise since we are using a particle representation. Things are just a little more complicated, as we will have several model space states in general, so that we will need matrix multiplications at the folds.

We need to expand out the energy shift in the manner of Eq. (2.33). This can be rewritten as a Taylor series, giving, for a single denominator,

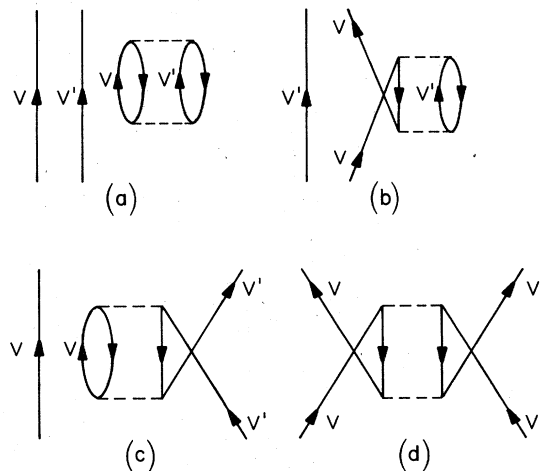


FIG. 10. A set of diagrams which compensate amongst themselves for violations of the Pauli exclusion principle, i.e., the sum of the four diagrams is zero.

$$\frac{1}{E_v - H_0} = \sum_{n=0}^{\infty} \frac{(-1)^n}{n!} \frac{d^n}{dE_v^n} \left( \frac{1}{E_v - H_0} \right) \Big|_{E_v = \epsilon_v} (-\Delta_v)^n = \sum_{n=0}^{\infty} \left( \frac{1}{E_v - H_0} \right)^{n+1} \Big|_{E_v = \epsilon_v} (-\Delta_v)^n. \quad (2.60)$$

Clearly we could equally well apply the Taylor series expansion to  $\mathcal{U}_v(E_v)$ , which contains many denominators. We get

$$\mathcal{U}_v(E_v) = \sum_{n=0}^{\infty} \frac{(-1)^n}{n!} \frac{d^n}{dE_v^n} \mathcal{U}_v(E_v) \Big|_{E_v = \epsilon_v} \sum_{i_1, i_2, \dots, i_n=1}^d |\Phi_{i_1}\rangle \langle \Phi_{i_1}| - \mathcal{U}_v(E_v) |\Phi_{i_2}\rangle \langle \Phi_{i_2}| - \mathcal{U}_v(E_v) |\Phi_{i_3}\rangle \langle \Phi_{i_3}| \cdots \langle \Phi_{i_n}| - \mathcal{U}_v(E_v). \quad (2.61)$$

It is easy to check that the matrix multiplication over the unperturbed valence states gives the correct result, by operating on  $\Psi_D$  and using  $\mathcal{U}_v(E_v)\Psi_D = \Delta_v\Psi_D$ . Now we can use this whole expression (2.61) for  $\mathcal{U}_v(E_v)$  and substitute repeatedly in the right-hand side at each point where  $\mathcal{U}_v(E_v)$  occurs, just as we did in Sec. II.B. The result may be written in the form due to des Cloizeaux (1960) and Brandow (1967):

$$\mathcal{U}_v = \sum_{n=0}^{\infty} \frac{(-1)^n}{n!} \frac{d^n}{dE_v^n} \mathcal{U}_v(E_v) \Big|_{E_v = \epsilon_v} (-\mathcal{U}_v)^n. \quad (2.62)$$

Here matrix multiplication over the unperturbed valence states is to be understood—this allows us to use just the unperturbed basis  $\Phi$  in setting up the matrix of the effective interaction, which can then be diagonalized to obtain  $\Psi_D$ . We have dropped the argument  $E_v$  from  $\mathcal{U}_v$  because the result is now formally independent of the shift  $\Delta_v$  we wish to calculate, i.e., only Rayleigh-Schrödinger denominators are involved. Further, Brandow (1967) shows that unlinked diagrams are eliminated. Let us verify this in a simple case and examine the structure of Eq. (2.62), which is less formidable than it appears.

Firstly the  $n=0$  terms of Eq. (2.62) have no folds and give the series

$$V + V \frac{Q}{\epsilon_v - H_0} V + V \frac{Q}{\epsilon_v - H_0} V \frac{Q}{\epsilon_v - H_0} V + \cdots \quad (2.63)$$

Typical diagrams are given in Fig. 11 for the two va-

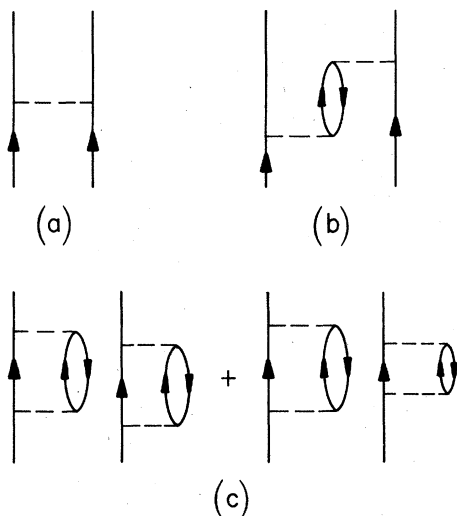


FIG. 11. Illustration of diagrams contributing to the two-body effective interaction, (a) and (b), and of unlinked diagrams (c), which do not contribute.

lence-particle case and, in particular, Fig. 11(c) shows two unlinked diagrams—the energy denominators can obviously be factorized. Now consider the  $n=1$  case in Eq. (2.62); we obtain [see also expression (2.66) below]

$$\left[ V \frac{Q}{(\epsilon_v - H_0)^2} V + V \frac{Q}{(\epsilon_v - H_0)^2} V \frac{Q}{(\epsilon_v - H_0)} V + V \frac{Q}{(\epsilon_v - H_0)} V \frac{Q}{(\epsilon_v - H_0)^2} V + \cdots \right] \times \left[ -V - V \frac{Q}{\epsilon_v - H_0} V - \cdots \right]. \quad (2.64)$$

The product of the second-order terms in the square brackets gives, among others, the diagrams of Fig. 12(a) and (b), which have one fold and are drawn in unfolded form. Remembering that we have a minus sign in Eq. (2.64) (a minus sign associated with each fold), it should be clear that Fig. 12(a) exactly cancels the two diagrams of Fig. 11(c). Thus these unlinked diagrams are removed and, as we have remarked, this is a general result. We do, of course, have new diagrams such as Fig. 12(b), which we have rewritten in folded form in Fig. 12(c)—

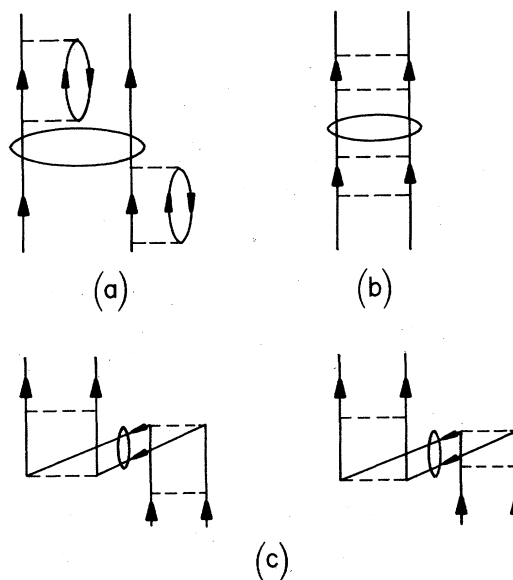


FIG. 12. Illustration of unlinked, folded diagram (a), which does not contribute to the two-body effective interaction, and linked, folded diagrams (c), which do contribute. Note that diagram (a) cancels with Fig. 11(c), and diagram (b) is the equivalent unfolded form of the folded diagrams (c).

two diagrams since the factorization theorem has been used "backwards." The loop around the downgoing lines reminds us that they are valence particle states and that we sum over all such states corresponding to the matrix multiplication explicitly shown in Eq. (2.61). Energy denominators may be evaluated in the standard way by operating with  $(\epsilon_v - H_0)^{-1}$  between the interactions, giving  $[\epsilon_v + \sum(\text{hole-particle energies})]^{-1}$ . It is essential that downgoing folded valence lines are treated as hole lines for this purpose, i.e., they give a contribution  $+\epsilon_v$  to the denominators (the reader may verify this for the example in Fig. 12!). We also need the rule that the topmost interaction in the folded diagram is the same as the topmost interaction in the unfolded diagram, so that we do not generate four folded diagrams from Fig. 12(b) instead of two. Finally we should point out that the removal of unlinked diagrams requires in general that each of the folded lines be summed over all the valence particle states regardless of the Pauli exclusion principle; the discussion of Appendix A illustrates this.

It is useful to study briefly the structure of twice-folded diagrams. The  $n=2$  term of Eq. (2.62) will give for instance a contribution

$$\left[ V \frac{Q}{(\epsilon_v - H_0)^2} V \right] \times \left[ -V \frac{Q}{(\epsilon_v - H_0)} V \right] \times [-V]. \quad (2.65)$$

Here we have folded twice out of the first denominator. A typical diagram drawn in unfolded form is shown in Fig. 13(a); the curly arrows are merely to indicate which denominator we have folded from. The resulting two folded diagrams are also given in Fig. 13(a). Now we will also have a twice-folded contribution from the  $n=1$  term of Eq. (2.62) because we fold out once the whole ef-

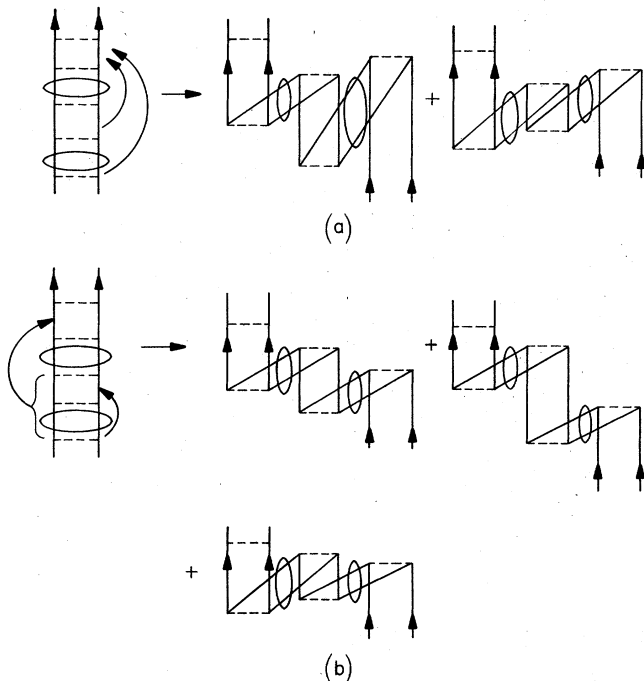


FIG. 13. Examples of twice-folded diagrams. In (a) both pieces are folded out of the upper denominator, while in (b) only a single piece is folded out, but this is, itself, folded.

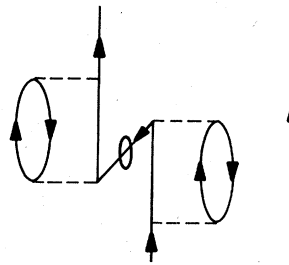


FIG. 14. A one-body component of the effective interaction, i.e., a contribution to the single-particle energy. Note that this diagram is to be considered linked.

fective interaction, which itself contains folded diagrams, i.e., in Eq. (2.64) the second term in square brackets will contain folded diagrams starting in third order. Thus we will have, for instance,

$$\left[ V \frac{Q}{(\epsilon_v - H_0)^2} V \right] \times \left[ -V \frac{Q}{(\epsilon_v - H_0)^2} V \right] \times [-V], \quad (2.66)$$

where we have folded out of the first denominator a diagram which is itself once folded. This yields diagrams such as Fig. 13(b), where we show the unfolded form and the resultant three folded diagrams. Clearly, in order to know what is being folded out of what, it is necessary to examine carefully the positioning of the topmost interaction of each folded block.

It is important to realize that in addition to the two-body components of the effective interaction we shall have one-body terms. An example is shown in Fig. 14—this diagram is to be considered linked. The essential difference from Fig. 11(c) is that one of the particles does not interact at all—one may, in fact, erase this noninteracting line. Clearly we shall have a whole series of diagrams where only one of the particles interacts, and this will lead to the single-particle energy for that particle. This is a quantity which can be deduced from experiment; for instance, the 0.871 MeV  $1/2^+$  state of  $^{17}\text{O}$  is thought to have a large component of the  $1s_{1/2}$  single-particle configuration beyond the  $^{16}\text{O}$  ground state, so we can take the single-particle energy as

$$E_{1s_{1/2}} = E(^{17}\text{O}, J^\pi = \frac{1}{2}^+) - E(^{16}\text{O}, J^\pi = 0^+) = -130.892 + 127.620 = -3.272 \text{ MeV}. \quad (2.67)$$

This procedure will be used in the calculations discussed in Sec. III, so that we can focus on just the two-body part of the interaction. (For a situation with  $n$  valence particles, one will have  $1, 2, 3, \dots n$ -body components in the folded, linked, effective interaction, in general. One hopes that, with a reasonable choice for the valence space, the one- and two-body components will dominate; phenomenological shell-model calculations seem to support this. Some further discussion of many-body effective operators is given in Sec. III. G.)

It should be noted that the expansion of Eq. (2.62) is asymmetric, as are the corresponding diagrams—for instance there is no analogue of Fig. 12(c), where the folded block is attached to the final valence lines instead of the initial ones. Thus the effective interaction depends on which valence state is the initial and which the final one, i.e.,  $\mathcal{U}_v$  is no longer Hermitian, so that the eigenvectors are not orthogonal. This is not unphysical, since they are simply the projection  $P\Psi$  of the true wave functions.

*Summary.* We have indicated how the difficulty, associated with Eq. (2.16) can be removed by expanding out of the energy denominators and using the factorization theorem. Firstly all reference to the core energy was removed, so that we obtained the Bloch–Horowitz equations (2.59) for the shell-model energies  $E_v$ , measured with respect to the exact energy of the closed-shell core. Only pure valence diagrams were needed. The energy dependence of the interaction was removed, leading to folded diagrams and in the process cancelling away all unlinked diagrams. We thus obtained a completely linked, folded, energy-independent, non-Hermitian effective interaction, given formally by Eq. (2.62). A summary of the diagram rules is given in Appendix C.

#### D. Effective operators

In the shell model we are interested not only in energies, but also in the matrix elements of observable operators. We shall discuss here the formalism needed for the calculation of effective operators. (This formalism could be used for the effective interaction, but would lead to unnecessary complications.) We shall have in mind the practical example of a calculation of the effective matrix elements of the electromagnetic  $E2$  operator for a single particle beyond the  $^{16}\text{O}$  core. In fact, we shall restrict our discussion here to the case of a single particle beyond a nondegenerate core. We further assume that, as for the  $(1s0d)$  shell, the model space contains only one single-particle state of a given angular momentum  $j$ —thus our model space is one-dimensional, since the core carries zero angular momentum. This circumvents the difficulty, associated with the development of effective operators, of needing to introduce orthogonal valence space eigenvectors in order to get a completely linked expansion (Brandow 1967)—clearly this is unnecessary for a one-dimensional case. Further, this is the case of most immediate practical interest.

First, following Brandow (1967), we discuss the perturbation expansion for the true wave function  $\Psi$ , using Eqs. (2.13) and (2.14) which we repeat:

$$\Psi = \Omega(E)\Psi_D; \quad \Omega(E) = 1 + \left( \frac{Q}{E - H_0} \right) V \Omega(E). \quad (2.68)$$

Iterating the model operator  $\Omega$  leads to a perturbation expansion, and we can associate wave function diagrams with the various terms—typical examples are shown in Fig. 15. All the terms in  $\Omega$ , apart from the unit operator (which leaves  $\Psi_D$  unchanged), contain a  $Q$  operator on the left, so that at the top of the diagram either the core particles or the valence particle or both must be excited. The analysis of these diagrams will be indicated rather briefly, since it follows closely the treatment of the effective interaction given in the previous subsection. Indeed, since the energy is  $\langle \Psi_D | V | \Psi \rangle$ , one can say, somewhat sloppily, that the only difference lies in the presence of an extra  $V$  for the effective interaction, which takes the true wave function back to the unperturbed state,  $\Psi_D$ , at the top of the diagram.

The diagrams of Fig. 15(a)–(d) are of similar structure to those discussed in Fig. 8(a)–(d); note that the label  $v$  in Fig. 15(b) indicates a valence state, so that we have a “closed valence piece” in the diagram, i.e., the single-

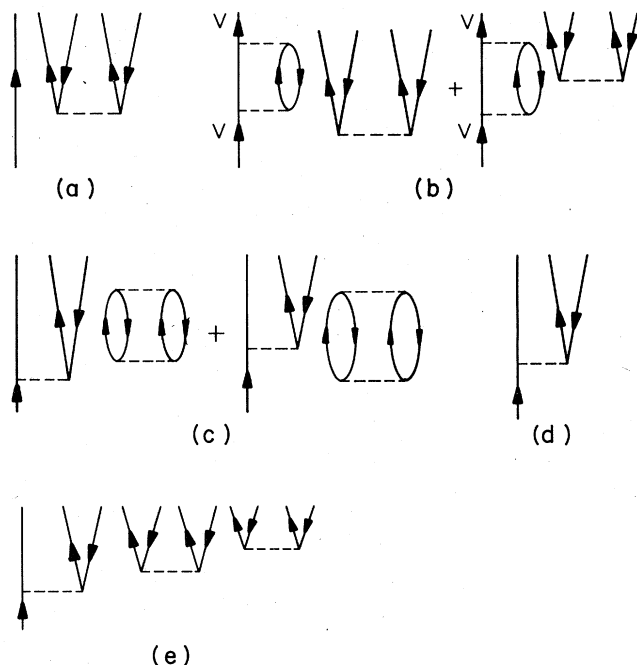


FIG. 15. Typical wave function diagrams. The general structure of diagrams (a)–(d) is similar to that of the effective interaction diagrams of Fig. 8(a)–(d).

particle line leaving the top of the diagram is not excited. Such “closed valence pieces” are simply diagrams which contribute to the single-particle energy shift  $\Delta_v$ . Now, as in Eq. (2.50), we split the total energy  $E$  into valence and core parts and expand out from the denominators the core energy shift  $\Delta_c$ . We also expand out the valence energy shift  $\Delta_v$  in cases where the intermediate state involves just a core excited part with the  $(sd)$  valence line undisturbed. For Fig. 15(c) we can write an expression of the same form as Eq. (2.51). ( $\mathcal{H}_c$  will now consist of a single matrix element and operators  $a^\dagger a^\dagger a$  creating a two-particle one-hole state.) Again this is canceled by expanding out  $\Delta_c$  from Fig. 15(d) as in Eq. (2.52). We can also use the arguments of Eqs. (2.53) and (2.54) to show that the diagrams of Fig. 15(b) are canceled by expanding  $\Delta_v$  out of Fig. 15(a). In general we have the result that all closed core pieces of the type encountered in  $\Delta_c$  are removed, and also “closed valence pieces” of the type encountered in  $\Delta_v$  are eliminated. We are left with core wave function diagrams [such as Fig. 15(a)], valence wave function diagrams [such as Fig. 15(d)] and products of these [such as Fig. 15(e)]. Note that Fig. 15(e) will not contribute to the effective interaction, since we cannot return to the single-particle valence state by operating at the top with a single  $V$  interaction. By virtue of the manipulations discussed above, diagrams such as Fig. 15(e) should be understood to have the core and valence parts factorized, so that we may write

$$\Psi = \Omega \Psi_D = \Omega_v \Omega_c \Psi_D$$

with

$$\Omega_v(E_v) = 1 + \left( \frac{Q}{E_v - H_0} \right) V \Omega_v(E_v). \quad (2.69)$$

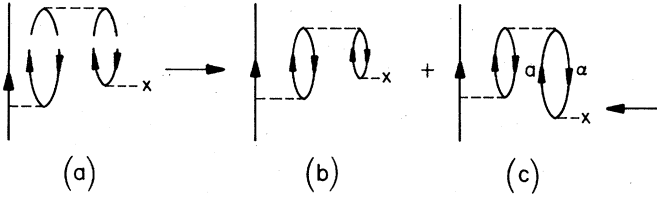


FIG. 16. Mixed wave function diagram which is linked together by a final interaction to give the contributions (b) and (c) to the one-body effective interaction. Note that the cross represents the one-body potential  $U$  of Eq. (2.3), and that diagram (a) is factorized, whereas (b) and (c) are not.

Here  $\Omega_c$  is the model operator which acts on the unperturbed core part of  $\Psi_D$  to give the true core wave function, e.g., for  $^{16}\text{O}$ , in the absence of valence particles. The additional valence diagrams (which will include terms compensating for exclusion principle violations) are included via  $\Omega_v$ , so that we obtain the true wave function of  $^{17}\text{O}$  in our example.

Equations (2.69) are clearly the analogues of the Bloch-Horowitz equations (2.59). Indeed, taking  $\langle \Psi_D | V | \Psi \rangle$ , we obtain simply  $\Delta_c + \Delta_v$ . Here we must include in  $\Delta_v$  cross terms where unlinked parts from  $\Omega_v$  and  $\Omega_c$  are joined together by the final  $V$  interaction so as to produce a valence diagram. An example is shown in Fig. 16(a), which yields the two unfactorized contributions to  $\Delta_v$  shown in Fig. 16(b) and (c). Notice, however, that the energy denominator in diagram (c) at the level indicated by the horizontal arrow is  $(e_\alpha - e_\alpha)$  rather than  $(\Delta_v + e_\alpha - e_\alpha)$  because we have expanded out  $\Delta_v$  and removed "closed valence pieces," i.e., the diagram of Fig. 17 does not occur. In the previous Sec. II.C we would include Fig. 17 in the Bloch-Horowitz expansion and observe that it is removed when we fold out  $\Delta_v$ . Clearly this is a general result for diagrams with this type of structure, which Brandow refers to as a downward projecting core excitation. We refer to Brandow (1967, 1975) for further details and discussion of the less obvious upward projecting core excitation case.

For the wave function the final step in the argument is to remove  $\Delta_v$  from Eq. (2.69) by expanding out the denominator via either Eq. (2.33) or the more complicated Eq. (2.60), thus generating folded diagrams. This is quite straightforward, since there are no unlinked diagrams or matrix multiplications to worry about in our one-particle case. We simply give examples of diagrams with 0, 1, and 2 folds in Fig. 18.

Now we are ready to discuss the matrix elements of an operator  $\mathcal{E}$

$$\begin{aligned} \langle f | \mathcal{E} | i \rangle &= \langle \Psi_f | \Psi_f \rangle^{-1/2} \langle \Psi_f | \mathcal{E} | \Psi_i \rangle \langle \Psi_i | \Psi_i \rangle^{-1/2} \\ &= \frac{\langle \Psi_{Df} | \Omega_{vf}^\dagger \mathcal{E} \Omega_{vi} | \Psi_{Di} \rangle}{\langle \Psi_{Df} | \Omega_{vf}^\dagger \Omega_{vf} | \Psi_{Df} \rangle^{1/2} \langle \Psi_{Di} | \Omega_{vi}^\dagger \Omega_{vi} | \Psi_{Di} \rangle^{1/2}} \\ &\quad + \delta_{if} \langle \mathcal{E} \rangle_{\text{core}}. \end{aligned} \tag{2.70}$$

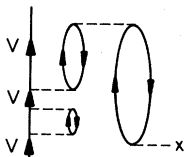


FIG. 17. A diagram containing a downward projecting core excitation which is discussed in the text.

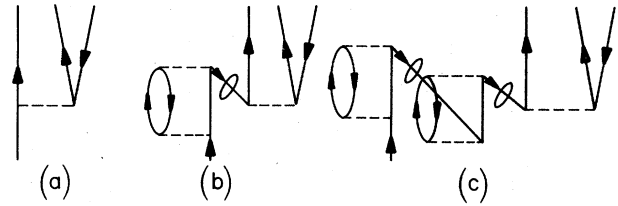


FIG. 18. Examples of wave function diagrams with 0, 1, and 2 folds.

Here  $\Psi_i$  and  $\Psi_f$  are the initial and final true wave functions, each of which can be written as a product of valence and core model operators acting on the model wavefunction, according to Eq. (2.69). We have then split the transition amplitude into a valence part, for which the core normalization cancels out, and a core part independent of the valence normalization. It should be understood that included in the valence contribution will be cross terms arising from pieces of  $\Omega_v$  and  $\Omega_c$  in the bra and ket which join together in such a way that a linked diagram is obtained (see the discussion above of Fig. 16). These cross terms cause no problem and occur naturally when one writes out the diagrams which can contribute.

As regards  $\langle \mathcal{E} \rangle_{\text{core}}$  we simply state that it is given by the sum of all linked Goldstone diagrams in which the operator  $\mathcal{E}$  occurs once (see e.g. Brandow, 1967). Since the core has angular momentum zero, it will only contribute if  $\mathcal{E}$  is a tensor of rank zero. As we shall be considering the electromagnetic  $E2$  operator, a tensor of rank two, in Sec. III, we need not concern ourselves further with the core term.

Now let us consider the valence contribution to Eq. (2.70) and try to represent it diagrammatically. The numerator just involves sandwiching the operator  $\mathcal{E}$  between our wave function expansion for the initial state and the Hermitian conjugate expansion for the final state, explicitly,

$$\begin{aligned} \langle \Psi_{Df} | \left\{ 1 + V \frac{Q}{e_{vf} - H_0} - \Delta_{vf} V \frac{Q}{(e_{vf} - H_0)^2} \dots \right\} \\ \times \mathcal{E} \left\{ 1 + \frac{Q}{e_{vi} - H_0} V - \Delta_{vi} \frac{Q}{(e_{vi} - H_0)^2} V \dots \right\} | \Psi_{Di} \rangle. \end{aligned} \tag{2.71}$$

Here  $e_{vi}$  and  $e_{vf}$  are the unperturbed energies of our initial and final valence particles, respectively. Taking the zeroth order terms 1 on the left and right, we obtain Fig. 19(a). Here our one-body operator,  $\mathcal{E}$ , is indicated by the dashed line and letter  $E$ . If we take the zeroth order term on the left with the first-order diagram of Fig. 18(a) on the right, we obtain Fig. 19(b). A second-order, nonfolded diagram is shown in Fig. 19(c). Taking the conjugate of the first-order Fig. 18(a) on the left, together with Fig. 18(b), we obtain Fig. 19(d). (We will also have another diagram with  $\mathcal{E}$  operating on an upgoing line—it does not matter which one if we use antisymmetrized matrix elements.) Using the diagram of Fig. 18(b) on both the left and right, we can generate Fig. 19(e). These are just a few examples of the series of nonfolded and folded diagrams which represent expression (2.71). Notice that the lower folds arising from expanding out  $\Delta_{vi}$  for the initial wave function must lie

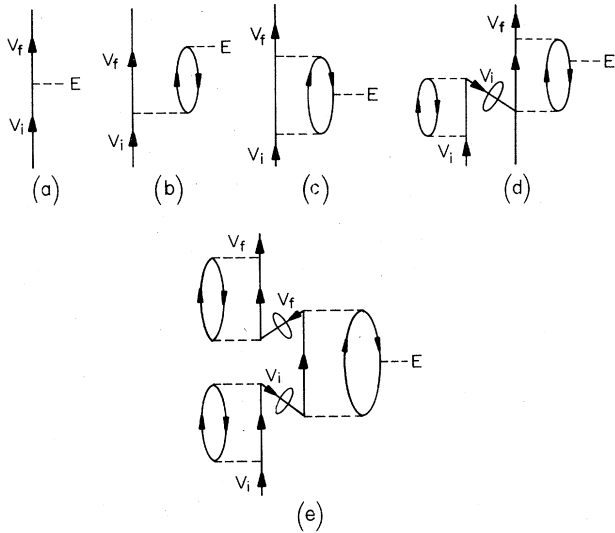


FIG. 19. Examples of nonfolded and folded diagrams which contribute to the matrix elements of an operator (denoted by the letter E). These contributions arise from the numerator of Eq. (2.70).

below the level of the operator  $\mathcal{E}$ . The upper folds arise from expanding out  $\Delta_{vf}$  and must lie above the operator  $\mathcal{E}$ ; they are folded upwards. Energy denominators are given by operating between the interactions (including  $\mathcal{E}$ ) with  $(e_{vi} - H_0)^{-1}$  up to the level of  $\mathcal{E}$  and with  $(e_{vf} - H_0)^{-1}$  above this level. Apart from these caveats we can use the rules of Appendix C.

To complete our analysis we need to discuss the normalization terms which arise in the denominator of Eq. (2.70). We can treat the normalization

$$N_v = \langle \Psi_D | \Omega_v^\dagger \Omega_v | \Psi_D \rangle \quad (2.72)$$

in just the same way as the numerator by replacing  $\mathcal{E}$  by the unit operator—this, of course, requires that initial and final states be the same. In this case Fig. 19(a) has the value 1, since our states are normalized to unity. Figure 19(b) does not arise, since the unit operator cannot connect particle and hole states. Figure 19(c) does occur, and we represent it as in Fig. 20(a); the horizontal line here represents the unit operator. As a practical matter this simply gives us an additional energy denominator. Figure 19(d) gives us Fig. 20(b). Proceeding thus with the horizontal line notation we can enumerate the diagrams.

A formal note in passing: Using the energy-dependent

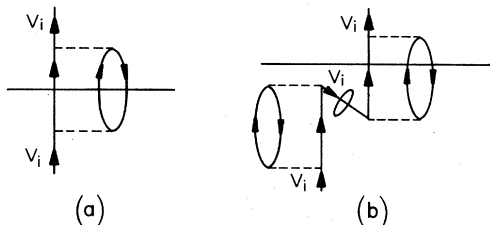


FIG. 20. Diagrams contributing to the wave function normalization. The horizontal bar indicates a squared energy denominator at that level.

form for  $\Omega_v$  in Eq. (2.69) we can write

$$N_v = \langle \Psi_D | 1 + V \left( \frac{Q}{E_v - H_0} \right)^2 V + V \left( \frac{Q}{E_v - H_0} \right)^2 V \frac{Q}{E_v - H_0} V + V \frac{Q}{E_v - H_0} V \left( \frac{Q}{E_v - H_0} \right)^2 V + \dots | \Psi_D \rangle = 1 - \langle \Psi_D | \frac{d^2 \mathcal{U}_v(E_v)}{dE_v^2} | \Psi_D \rangle. \quad (2.73)$$

Thus what is needed is the derivative of the effective interaction, since that has the effect of squaring each of the energy denominators in turn as required for the normalization. One could try to write the normalization diagrams in terms of the “downward folded” effective interaction expansion; however, it is neater to use the procedure of Fig. 20.

Now we have separate expansions for the numerator of Eq. (2.70) and for the norms  $N_{vi}$  and  $N_{vf}$  (which are raised to the power  $\frac{1}{2}$ ) of the denominator, and we could stop at this point. It is desirable, however, to obtain a diagram series for the whole valence term; indeed, for the many valence-particle case this is necessary if we are to eliminate unlinked terms. To this end we write

$$N_v^{-1/2} = (1 + \theta)^{-1/2} = 1 - \frac{1}{2}\theta + \frac{3}{8}\theta^2 \dots, \quad (2.74)$$

whereby  $\theta$  is defined, and a binomial expansion has been made (Brandow, 1967). Carrying out this expansion for the initial and final states, we can represent the  $\theta, \theta^2, \dots$  terms by diagrams folded once, twice, ... into the series of diagrams we have obtained for the numerator of Eq. (2.70). The signs follow correctly, but the factors of  $\frac{1}{2}, \frac{3}{8}, \dots$  are awkward and have to be put in explicitly so they will be shown on the diagram.

Let us see how this goes. The simplest diagrams are those of Fig. 21, which arise from the product of Fig. 19(a) with the normalization contribution to  $\theta$  of Fig. 20(a). Two diagrams arise, since we need to normalize both the initial and the final state. The horizontal bar is fixed at the level of the operator  $\mathcal{E}$  and can be erased. The energy denominators are given by the rule stated above, namely, for the first diagram

$$\left( \frac{1}{e_{vi} - (e_a + e_b - e_\alpha)} \right) \times \left( \frac{1}{e_{vf} - (e_{vf} + e_a + e_b - e_\alpha - e_{vi})} \right) = \frac{1}{(e_{vi} + e_\alpha - e_a - e_b)^2}, \quad (2.75)$$

which is what is needed for Fig. 20(a).

Some more complicated illustrations of the diagram series for the whole valence part of Eq. (2.70) are shown in Fig. 22. The diagrams of Fig. 22(a) correspond to

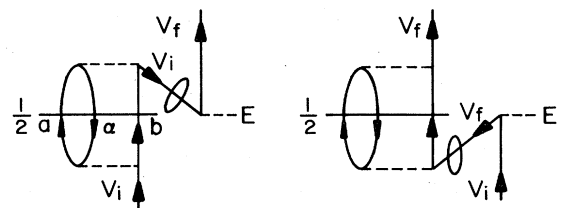


FIG. 21. Lowest-order contributions to the matrix element of an operator which arise from the normalization of the initial or final wave function.

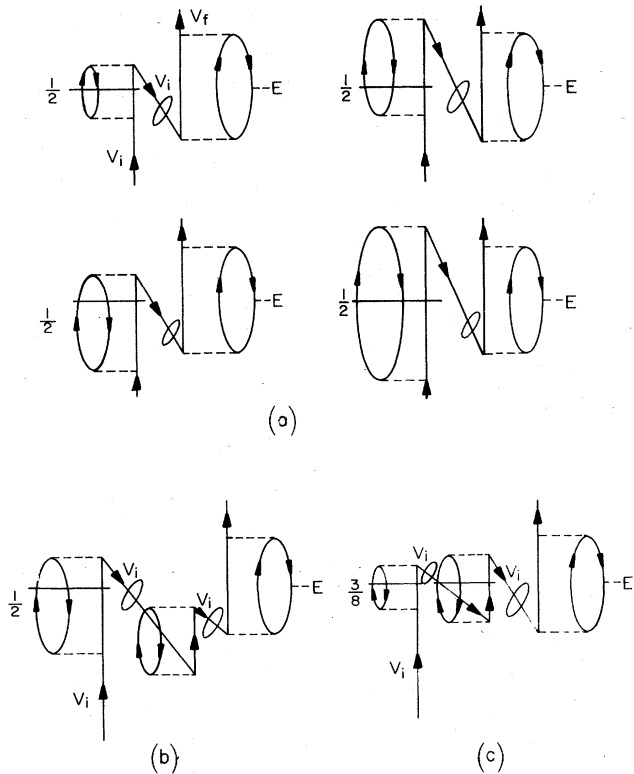


FIG. 22. Some diagrams which contribute to the matrix element of an operator due to the normalization of the initial wave function.

folding the normalization diagram of Fig. 20(a) with Fig. 19(c). As remarked above, the horizontal bar is to be considered fixed at the level of  $E$ . We then factorize both upwards and downwards—all the necessary diagrams are shown. In Fig. 22(b) we show one member of the “factorized set” obtained by combining the diagram of Fig. 19(d) with, again, the normalization diagram of Fig. 20(a). Similarly in Fig. 22(c) we show just one member of the set obtained by folding Fig. 20(a) twice out of Fig. 19(c), i.e., this is a  $\theta^2$  term. Note the different positioning of the folded blocks in diagrams (b) and (c). The reader will find it instructive to check the values of some of these diagrams using the rules above and in Appendix C.

**Summary.** We have indicated how a folded valence-diagram expansion with Rayleigh–Schrödinger denominators may be obtained for the transition amplitude of an operator; the series is trivially linked in the one-particle case considered. In addition, for expectation values a pure core term is present, Eq. (2.70). This result was achieved by first writing the wave function as a product of valence and core parts, Eq. (2.69). Then, for the valence part, expanding out the energy shifts  $\Delta_v$  and taking the matrix element of the operator, the folded series of Eq. (2.71) was obtained. The final step was to take the product of this series with a binomial expansion of the normalization factors [Eqs. (2.73) and (2.74)] in the denominator, thus producing additional folded diagrams.

### E. Formal divergence problems

It is most natural to begin to study the perturbation series for effective operators established in the previous Sec. II.C and D order by order in the perturbation  $V$ . However, Schucan and Weidenmüller (1972, 1973) have shown that in many cases of practical interest the perturbation series must diverge. They commented on a  $2 \times 2$  matrix example, which was studied further by Ellis and Osnes (1973) and Schaefer (1974). We will use this example here in discussing the divergence problem in simple terms; for a more general mathematical treatment the reader is referred to the original papers. We shall confine our remarks, for the most part, to the effective interaction.

We write our Hamiltonian

$$H = H_0 + zV, \tag{2.76}$$

where the perturbation is scaled by a parameter  $z$ . The variation of  $z$  from 0 to 1 thus takes us from the unperturbed to the perturbed Hamiltonian (although we shall not restrict  $z$  to this range in the simple  $2 \times 2$  model). We can thus study the effective interaction as a function of  $z$ . We then take our  $2 \times 2$  matrix in the form

$$\begin{pmatrix} \epsilon_A + X_A z & Xz \\ Xz & \epsilon_B + X_B z \end{pmatrix}. \tag{2.77}$$

The notation here is similar to that used in the discussions of Sec. II.B; we also include diagonal matrix elements of the perturbation  $X_B z$  for state  $B$  [as in Eq. (2.43)] and similarly for state  $A$ . We shall be interested in the case where  $\epsilon_A < \epsilon_B$  and  $X_B < X_A$  so that the perturbation pushes state  $B$  below state  $A$  as  $z$  increases.

The eigenvalues of the matrix (2.77) are given by

$$(E - \epsilon_A - X_A z)(E - \epsilon_B - X_B z) = X^2 z^2 \tag{2.78}$$

which leads to

$$E = \frac{1}{2} \{ \epsilon_A + \epsilon_B + X_A z + X_B z \pm (\epsilon_B - \epsilon_A + X_B z - X_A z) \times [1 + 4X^2 z^2 (\epsilon_B - \epsilon_A + X_B z - X_A z)^{-2}]^{1/2} \}. \tag{2.79}$$

We have written the expression in this form so that a power-series expansion in  $z$  (i.e., in orders of the perturbation) can be made. The lower sign will be taken while noting that the quantity  $(\epsilon_B - \epsilon_A + X_B z - X_A z)$ , which gives the difference between the diagonal elements of the matrix (2.77), changes sign at  $z_F = (\epsilon_B - \epsilon_A) / (X_A - X_B)$ . Thus we have an expression which gives the lower eigenvalue for  $z < z_F$  and the upper one for  $z > z_F$ . This discontinuity at  $z = z_F$  is a good hint of trouble to come. The power-series expansion reads

$$E_1 = \epsilon_A + X_A z + \frac{X^2 z^2}{\epsilon_A - \epsilon_B} + \frac{X^2}{(\epsilon_A - \epsilon_B)^2} (X_B - X_A) z^3 + \frac{X^2}{(\epsilon_A - \epsilon_B)^3} [(X_B - X_A)^2 - X^2] z^4 + \dots \tag{2.80}$$

[In the special case  $X_A = X_B = 0$  and  $z = 1$ , we regain Eq. (2.27) of Sec. II.B.] We can view this as an effective interaction for state  $A$  in which state  $B$  is taken into account by successive orders of the perturbation. Since

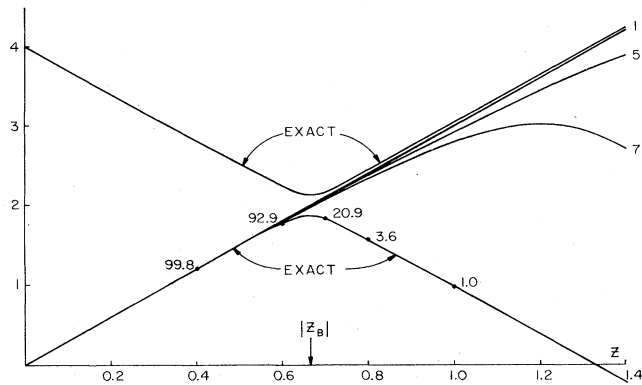


FIG. 23. Comparison of the exact eigenvalues of a  $2 \times 2$  matrix with the results of a power-series expansion taken through first, fifth, and seventh order. For the lower level we show, at various points, the percentage of the unperturbed state  $\Phi_A$  in the exact eigenvector.

our valence space is one dimensional here, the effective interaction just gives the eigenvalue directly. We leave it to the reader to write out the corresponding diagrams through fourth order. Now choosing parameters  $\epsilon_A = 0$ ,  $\epsilon_B = 4$ ,  $X_A = 3$ ,  $X_B = -3$ , and  $X = 0.2$ , we compare in Fig. 23 the exact eigenvalues as a function of the parameter  $z$ , with the power-series expansion (2.80) taken through first, fifth, and seventh order. For small  $z$  we obtain rapid convergence to the lower eigenvalue. For large  $z$ , however, first order provides a good approximation to the upper eigenvalue, but as we add higher-order terms the series starts to diverge. The reason for this divergence is easily seen if we allow  $z$  to become a complex variable. The square root of Eq. (2.79) generates a pair of branch points at  $z_B$  and  $z_B^*$  in the complex plane, which limit the radius of convergence of the power-series expansion to be  $|z_B|$ . It is easy to show that

$$|z_B| = |\epsilon_B - \epsilon_A| [(X_B - X_A)^2 + 4X^2]^{-1/2},$$

and the numerical value of  $|z_B|$  for our chosen parameters is indicated in Fig. 23. [Note that the discontinuity in Eq. (2.79) mentioned above requires that the branch cut joining  $z_B$  and  $z_B^*$  go through  $z_P$ .]

In more physical terms we can study the behavior of the eigenvectors as a function of  $z$ . At  $z = 0$ , the eigenvector of the lower level is just the unperturbed state  $\Phi_A$ . As  $z$  increases,  $\Phi_A$  and  $\Phi_B$  begin to mix, and we indicate in Fig. 23 the intensity of  $\Phi_A$  in the lower state at various points. The intensity remains large until  $z$  is in the region of  $|z_B|$ , when it decreases rapidly, becoming very small for large  $z$ . Thus for large  $z$  the lower state is dominantly  $\Phi_B$ , whereas the upper state is mainly  $\Phi_A$ . The character of the eigenvectors of the two states has therefore been exchanged in passing through  $|z_B|$ ; in this sense a level "crossing" has taken place. We are not able to follow the system through such a "crossing" using order-by-order perturbation theory. The strong mixing of the two states between  $|z_B|$  and the equal admixture point  $z_P$  and then the jump to the upper eigenvalue curve are simply too much for the perturbation series to handle.

Although we have used the term "crossing," we should emphasize that the eigenvalues can actually cross, i.e.,

be exactly degenerate, only for  $z$  complex. Obviously this actual crossing occurs at  $z_B$  and  $z_B^*$ , and it is only in the no-mixing case, where the off-diagonal matrix element  $X$  is zero, that  $\text{Im}z_B = 0$ .

Schucan and Weidenmüller (1972, 1973) have shown that similar ideas carry through in the general case. Here, as we have discussed, we pick a set of approximately degenerate valence states ( $P$  space), which we treat explicitly, and the remaining states ( $Q$  space) we take into account via an effective interaction. Clearly to avoid very small energy denominators in the perturbation series, the unperturbed energies of the  $P$  space should lie well below those of the  $Q$  space. Now as we increase  $z$  of Eq. (2.76) from 0 to 1 the exact eigenvalues will evolve from the unperturbed states. The situation is illustrated in Fig. 24 (taken from Weidenmüller, 1974) where we show a three-dimensional  $P$  space and assume only a single  $Q$  space state is relevant for the present discussion. Now if we find that a state originating from the  $Q$  space "crosses" (in the above sense) a state originating from the  $P$  space, a pair of branch points is obtained for complex  $z$ . These branch points are termed biexceptional points by Schucan and Weidenmüller. Each "crossing" that takes place will generate a pair of biexceptional points—two pairs for Fig. 24. The radius of convergence of the order-by-order series for the effective interaction is given by the distance  $|z_B|$  of the closest biexceptional point to the origin. Thus for Fig. 24 the "crossing" at  $z \approx 0.5$  will determine the radius of convergence. We remark in passing that the position of the biexceptional points depends on the choice of the unperturbed Hamiltonian  $H_0$ ; some model studies have compared different choices of  $H_0$  (Anastasio *et al.*, 1976; Leinaas and Kuo, 1976a).

Now the determination of the branch point positions would require that we solve the problem exactly, which we cannot do. However, we can diagonalize our approximate effective interaction and compare to the experimental spectrum. If one (or more) of the known levels is not given by the calculation, and this missing level lies between the predicted states, we have a clear indication that a level "crossing" has taken place. For example, in Fig. 24 the dashed level would not be reproduced by the calculation. Naturally it is necessary to appeal to phenomenological considerations to check that the missing state, often called an intruder state, is predominantly of a different structure from the valence space states, so that its absence is not merely due to a poor choice of the effective interaction. Such intruder states, unfortunately, are often found to be present in

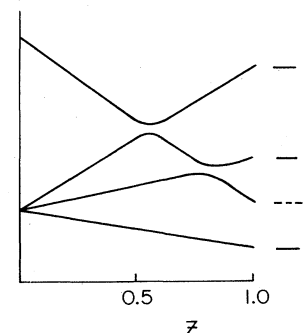


FIG. 24. Schematic evolution of a spectrum as the interaction is switched on, i.e., as  $z$  increases from 0 to 1. The dashed line in the level scheme, shown for  $z = 1$ , indicates an intruder state whose wave function has small components within the valence space.

nature, as for instance in the case of  $^{18}\text{O}$  to be discussed in Sec. III, so that the order-by-order perturbation expansion must diverge. [Note that any level "crossings" that take place as we vary  $z$  in the "unphysical" range 0 to  $-1$  will also limit the radius of convergence of the power-series expansion. The presence of intruder states for negative  $z$ , often called backdoor intruders, cannot be inferred from the experimental spectrum which corresponds to  $z=+1$  (Pittel *et al.*, 1976).]

Now we have pointed out that any level "crossings" cause the perturbation series to diverge. However, as a practical matter we see from Fig. 23 that the divergence for  $z > |z_B|$  does not set in until we go to quite high orders of perturbation theory, so that, say, third-order perturbation theory would provide a reasonable approximation here. The possibility that this might carry over to more realistic cases has been studied by Vincent and Pittel (1973; see also Vincent, 1976) in model calculations for  $^{18}\text{O}$ . They find that the influence of the formal divergence of the series on low-order perturbation theory is very small. This is due to the weakness of the coupling between the intruder state and the valence-space states, a condition which is met in the example of Fig. 23. Pittel (1976) has recently estimated the errors involved in low-order perturbation theory for  $^{18}\text{O}$  when branch point singularities are present. Unfortunately they are found to be quite sizeable in some cases, so that low-order perturbation theory may be a poor approximation in realistic cases.

We should not lose sight of the fact that we started with a perturbation series which is exact if considered to all orders. It may be that the presence of intruder states renders it inappropriate to carry out order-by-order calculations in powers of  $z$ . This does not invalidate the formalism; rather it implies that we should direct our efforts to reordering the series into sets of diagrams which we can sum to all orders. Hopefully we can do this in such a way that the series becomes convergent with respect to the sets that we have defined, i.e., we shall have analytically continued the effective interaction.

We illustrate this by means of our  $2 \times 2$  matrix example, interpreting the states  $\Phi_A$  and  $\Phi_B$  as two-particle states for present purposes. As before we take the single state  $\Phi_A$  for the valence space and wish to take the effect of  $\Phi_B$  into account via perturbation theory, but here we are looking for a sequence of partial summations rather than an order-by-order treatment. As the first partial summation we shall take the sequence of ladder diagrams shown in Fig. 25(a). Including also the unperturbed energy  $\epsilon_A$ , this gives

$$\lambda_2 = \epsilon_A + X_A z + \frac{X^2 z^2}{\epsilon_A - \epsilon_B - X_B z} - \frac{X^2 z^2 (\lambda_1 - \epsilon_A)}{(\epsilon_A - \epsilon_B - X_B z)^2} + \frac{X^2 z^2 (\lambda_1 - \epsilon_A)^2}{(\epsilon_A - \epsilon_B - X_B z)^3} - \dots = \epsilon_A + X_A z + \frac{X^2 z^2}{\lambda_1 - \epsilon_B - X_B z} \quad (2.82)$$

For the next approximation we shall fold out of the main ladder skeleton not only the diagrams of Fig. 25(a), but also those of Fig. 25(b). In other words, we take all the diagrams of Fig. 25 and fold them any number of times out of the main ladder skeleton. We then have cases where the diagram folded out of the main skeleton is

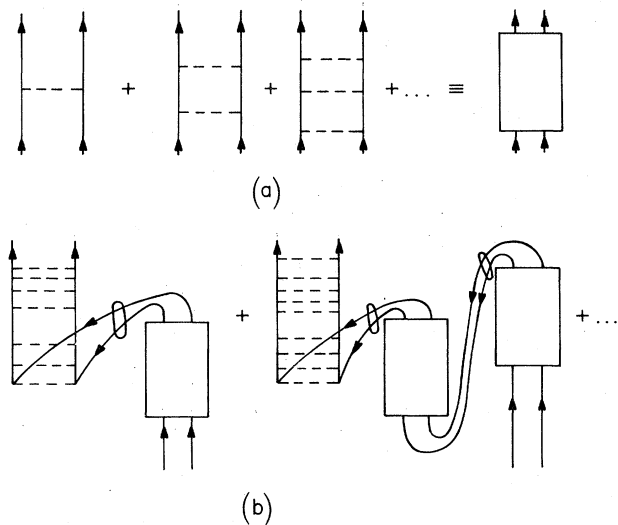


FIG. 25. Illustration of the rearrangement of the perturbation series into a convergent sequence of partial summations. First the ladder series (a), represented by a box, is summed and in the next approximation, (b), any number of boxes are folded out of the main ladder part.

$$\lambda_1 = \epsilon_A + X_A z + \frac{X^2 z^2}{\epsilon_A - \epsilon_B} + \frac{X^2 X_B z^3}{(\epsilon_A - \epsilon_B)^2} + \frac{X^2 X_B^2 z^4}{(\epsilon_A - \epsilon_B)^3} + \dots = \epsilon_A + X_A z + \frac{X^2 z^2}{\epsilon_A - \epsilon_B - X_B z} \quad (2.81)$$

In the latter equation we have summed the geometric series just as in Eqs. (2.44) and (2.45) of Sec. II.B.6. These ladder diagrams are the only nonfolded diagrams which occur, and their sum is represented in Fig. 25(a) by a box. The remaining folded diagrams will all take the form of a main ladder part, out of which will be folded any number of boxes which may themselves have boxes folded out of them, which may themselves have boxes folded out of them, . . . . We enumerate these in a systematic way starting with the case of any number of boxes folded out of the main ladder part. The one- and two-box cases are illustrated in Fig. 25(b). It is understood here that all orderings of the interactions are to be taken so that the factorization theorem can be used. Further, any number of interactions are allowed in the main skeleton, and we shall fold out of all the energy denominators in turn. Then we can write for the sum of the unperturbed energy, the ladder series of Fig. 25(a), and the folded series of Fig. 25(b)

itself, folded ("second generation folds"). It is a useful exercise to convince oneself that the simple result

$$\lambda_3 = \epsilon_A + X_A z + \frac{X^2 z^2}{\lambda_2 - \epsilon_B - X_B z} \quad (2.83)$$

is obtained. Clearly this process can be continued, and

defines a sequence of successive approximations. If this process converges to a value  $\lambda$ , we shall have solved by iteration the equation

$$\lambda = \epsilon_A + X_A z + \frac{X^2 z^2}{\lambda - \epsilon_B - X_B z}. \quad (2.84)$$

This can be rewritten as

$$(\lambda - \epsilon_A - X_A z)(\lambda - \epsilon_B - X_B z) = X^2 z^2, \quad (2.85)$$

which is the exact eigenvalue equation (2.78), so that we have obtained one of the true eigenvalues. Now recall that we defined  $z_F = (\epsilon_B - \epsilon_A)/(X_A - X_B)$ ; this is the point where equal admixtures of  $\Phi_A$  and  $\Phi_B$  occur in the true eigenvectors. Then one can show (Ellis and Osnes, 1973; Schaefer, 1974), subject to one proviso, that the sequence of approximations converges to the lower eigenvalue for  $z < z_F$  and the upper eigenvalue for  $z > z_F$  (at  $z = z_F$  successive iterations oscillate and there is no convergence). The situation is illustrated in Fig. 26. The aforementioned proviso is that if our initial value of  $\lambda$  is an exact eigenvalue, subsequent iterations will not change this value. This case actually occurs, since the denominator  $(\epsilon_A - \epsilon_B - X_B z)$  goes to zero at  $z = \frac{4}{3}$ , so that  $\lambda_1$  goes to  $-\infty$ . At one point in this region  $\lambda_1$  must therefore coincide with the exact lower eigenvalue which traps the value of  $\lambda$  as indicated in Fig. 26. Elsewhere in this region the upper eigenvalue is obtained. Notice that while the order-by-order approach yields the lowest eigenvalue for a restricted range of  $z$ , here we obtain either the upper or lower eigenvalue (in this particular approach we converge to the state which is mostly  $\Phi_A$ , apart from the "trapped point").

Now the simple  $2 \times 2$  problem is essentially solved, and we would like to turn briefly to the general case. Principally two different methods have been proposed for obtaining the effective interaction when intruder states are present, and interestingly they both give the

same result for the  $2 \times 2$  case—just the procedure we have been discussing! The method which generalizes the approach of Eqs. (2.81)–(2.84) in the most natural way is due to Krenciglowa and Kuo (1974)—we refer to this as the  $\hat{Q}$ -box method. They observe that Eq. (2.82) and (2.83) can be written

$$\begin{aligned} \lambda_2 &= \lambda_1 + \sum_{n=1}^{\infty} \frac{(-1)^n}{n!} \frac{d^n \lambda_1}{d\epsilon_A^n} [-(\lambda_1 - \epsilon_A)]^n, \\ \lambda_3 &= \lambda_1 + \sum_{n=1}^{\infty} \frac{(-1)^n}{n!} \frac{d^n \lambda_1}{d\epsilon_A^n} [-(\lambda_2 - \epsilon_A)]^n, \end{aligned} \quad (2.86)$$

and in general

$$\lambda_n = \lambda_1 + \sum_{n=1}^{\infty} \frac{(-1)^n}{n!} \frac{d^n \lambda_1}{d\epsilon_A^n} [-(\lambda_{n-1} - \epsilon_A)]^n. \quad (2.87)$$

If we have several states in the valence space,  $\lambda$  becomes a matrix and, as we assume degenerate unperturbed energies,  $\epsilon_A$  becomes  $\epsilon_A \mathbf{1}$ . Comparing the above with Eq. (2.62) of Sec. II.C, we see that this provides an iterative method of solution of the general problem if we identify the matrix of the effective interaction  $\mathcal{V}_v$  with the matrix  $(\lambda - \epsilon_A \mathbf{1})$ . (Note that for two-valence particles both one- and two-body diagrams must be included in  $\lambda_1$  so they will both be present in  $\mathcal{V}_v$  also.) The sequence of approximations to  $\mathcal{V}_v$  is clear from our previous remarks. In the first approximation,  $\lambda_1$ , we take the sum of all diagrams without any folds; Kuo (1974) and co-workers refer to  $\lambda_1$  as the  $\hat{Q}$ -box. In the second approximation,  $\lambda_2$ , we also allow diagrams obtained by folding out of the diagrams of  $\lambda_1$  the nonfolded diagrams (i.e.,  $\lambda_1$ ). In the next approximation,  $\lambda_3$ , we also fold out of the diagrams of  $\lambda_1$  some diagrams which are themselves folded (from the  $\lambda_2$  approximation). And so on. The method has been tested in model calculations where intruder states are present (Krenciglowa and Kuo, 1974; Anastasio and Kuo, 1975). In the case of a one-dimen-

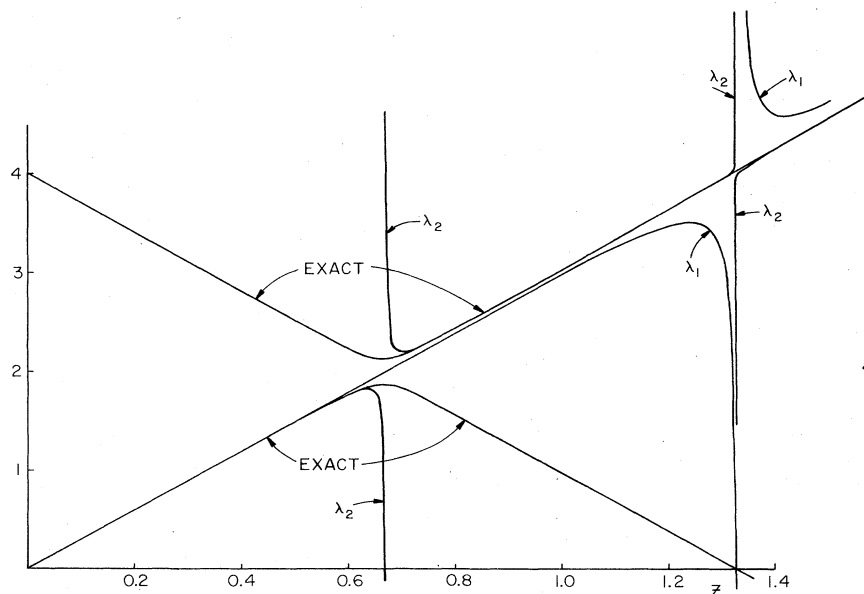


FIG. 26. Comparison of the exact eigenvalues of a  $2 \times 2$  matrix with the approximations  $\lambda_1$  and  $\lambda_2$  of Eqs. (2.81) and (2.82), which involve partial summations of the perturbation series.

sional valence space there is a simple criterion for convergence. If one of the exact solutions has an eigenstate which contains more than 50% by intensity of the valence state, the iteration procedure converges to that solution, as we found for the  $2 \times 2$  matrix. An improved method of iteration—the AHK algorithm—has been put forward by Anastasio, Hockert, and Kuo (1974). In the model calculations carried out thus far (Anastasio *et al.*, 1974, 1975) convergence has always been obtained. Further, for a  $d$ -dimensional valence space, different sets of  $d$  eigenvalues were often obtained by starting the iteration procedure differently. A major difficulty with the  $\hat{Q}$ -box approach in practical calculations of, say,  $^{18}\text{O}$  is that we start by requiring the sum of all diagrams with no folds ( $\lambda_1$ ). For this some approximation technique is required, for instance Padé approximants, which brings us to the second method of generalizing the  $2 \times 2$  approach.

The  $[n, m]$  Padé approximant to a function

$$\lambda(z) = \sum_{n=0}^{\infty} a_n z^n \tag{2.88}$$

is defined by

$$[n, m]\lambda(z) = \frac{R_n(z)}{S_m(z)} = \frac{\sum_{i=0}^n r_i z^i}{\sum_{i=0}^m s_i z^i} = \lambda(z) + O(z^{n+m+1}). \tag{2.89}$$

The Padé approximant is thus the ratio of two polynomials of degree  $n$  and  $m$ . The coefficients of the polynomials are obtained uniquely by taking  $s_0 = 1$  and by requiring that the Padé approximant reproduce the series  $\lambda(z)$  up to and including the power  $z^{n+m}$ . The Padé approximant then differs from  $\lambda(z)$  by terms of order  $z^{n+m+1}$  and higher powers as indicated in Eq. (2.89). To make contact with the  $2 \times 2$  problem, consider the iterated solution of Eq. (2.84). This can be written in the form of a continued fraction

$$\lambda = \epsilon_A + X_A z + \left[ X^2 z^2 / \left( -\epsilon_B - X_B z + \epsilon_A + X_A z + \frac{X^2 z^2}{-\epsilon_B - X_B z + \epsilon_A + X_A z + \frac{X^2 z^2}{\vdots}} \right) \right]. \tag{2.90}$$

Now it can be shown that if this continued fraction is terminated at the  $n$ th term, corresponding to the approximation  $\lambda_n$ , the result is just the  $[n+1, n]\lambda(z)$  Padé approximant. In view of our previous discussion, it is clear that the convergence properties of the Padé approximant are much better than those of the original power series, Eq. (2.88). For more general situations little is available by way of mathematical proofs (see Schucan, 1975), so a number of model calculations have been carried out to test the properties of Padé approximants. The procedure is to obtain the coefficients  $a_0, a_1, \dots, a_n$  of Eq. (2.88) by computing the perturbation expansion for the effective interaction through  $n$ th order (the unperturbed Hamiltonian  $H_0$  is usually not included, so  $a_0 = 0$ ). Various Padé approximants can then be obtained and used to compute approximate eigenvalues for comparison with the exact answers. Note that in this discussion we are concerned with, say, the two-body effective interaction, so that all folded and unfolded two-body diagrams are to be included. Now in general the valence space will have more than one state, and it is usual to approximate the whole effective interaction matrix at once. Thus  $\lambda$  becomes a matrix (more correctly referred to as an operator-valued function) and the coefficients  $r_i$  and  $s_i$  also become matrices. The  $[n+1, n]$  Padé approximants have generally been selected for study, since for large  $z$  they yield an interaction linear in  $z$  which is the correct behavior for the Hamiltonian of Eq. (2.76).

Calculations with small matrices (Hofmann *et al.*, 1973, 1974a, 1974b; Richert *et al.*, 1976) have shown encouraging results. The  $[2, 1]$  Padé approximant generally gives a good approximation to those eigenvalues whose associated eigenfunctions have maximum overlap

with the valence space—this remains true when the order-by-order series diverges. Singularities which are obtained in the approximant for some values of  $z$  usually indicate branch points associated with “level crossings”—this, however, is not always the case. As a practical matter a singularity means that one of the eigenvalues is not reproduced; away from these points a rather weak dependence on  $z$  seems to indicate reliable results.

Turning to the large matrix calculations (Hofmann *et al.*, 1976; Pittel *et al.*, 1976), which should be more realistic, we find the results disappointing. Firstly the pole structure is an unreliable indicator of “level crossings.” More importantly, it is found that to obtain accurate results it is necessary to go to the  $[3, 2]$  or  $[4, 3]$  approximants, which require fifth- and seventh-order perturbation theory, respectively. This is unfortunate, since in actual calculations of nuclei it has only been possible to go to third order, thus restricting one to the  $[2, 1]$  approximant. The model calculations indicate that this does not represent any improvement over just third-order perturbation theory. Rather similar results are obtained if one opts for the alternative approach of taking Padé approximants to each matrix element of the effective interaction separately or if one uses a variant of this approach suggested by Lee and Pittel (1975).

As regards effective operators (other than the interaction), it is known that the radius of convergence is the same as for the effective interaction (Schucan and Weidenmüller, 1973). Fewer model studies have been carried out, but it is found that  $[1, 1]$  Padé approximants give poor results, although a scheme based on Brillouin-Wigner perturbation theory shows some promise (Richert *et al.*, 1976; Leinaas and Kuo, 1976b).

*Summary.* We have pointed out that if, as the perturbation is switched on, a level originating from the valence space "crosses" (in the sense of exchanging the character of the eigenvectors) a level originating from outside the valence space, a pair of branch points is obtained in the complex plane. This limits the radius of convergence of the order-by-order perturbation series. The point was illustrated by a  $2 \times 2$  matrix example, for which it was shown that, even where the order-by-order results diverged, a reordering of the perturbation series gave convergent results. Generalizations of this approach—the  $\hat{Q}$ -box method and Padé approximants—worked well in simple models, but the results obtained in more realistic situations were less encouraging.

### III. RESULTS OF CALCULATIONS

A vast number of calculations of effective operators in finite nuclei have been performed over the last decade. Researchers have calculated essentially all contributions to the effective interaction and other effective operators that could conveniently be calculated within existing budgetary and computational limits. Thus it is appropriate to pause and see what has been achieved, and try to put the bits and pieces together into a coherent picture of the present state of the art.

Since, as will become evident, no clear-cut theory of effective operators has yet emerged, we shall emphasize the qualitative rather than the quantitative features of the results. Furthermore, we shall be more concerned with the physical interpretation of the results than with their detailed derivation. Where convenient, we shall illustrate and interpret the results in terms of simple approximations and models. It is, in fact, amusing that several elaborate calculations of effective operators can be well represented by very naive models. Finally, a main objective of our discussion will be to attempt to assess the convergence properties of the perturbation expansion for effective operators from the relative magnitude of the various terms that have been calculated.

Since the starting point of any microscopic description of the effective interaction and other effective operators is the free nucleon–nucleon interaction, we shall begin with a brief reminder of the main features of this interaction. As pointed out in Sec. I, the nucleon–nucleon interaction determined from a phase-shift analysis of the scattering data is not unique. We shall therefore not enter into a detailed discussion of the different available forms of the nucleon–nucleon interaction, but only discuss the features necessary for an understanding of the physical basis for the calculation of effective operators. This is done in Sec. III.A.

As the nucleon–nucleon interaction  $V_{12}$  is very strong at short distances, thus producing very large two-particle matrix elements in a shell-model basis, the perturbation expansion of the effective interaction and other effective operators will diverge if summed order by order in  $V_{12}$ . However, as shown in Sec. III.B, the strong two-body correlations can be summed to infinite order to give a well-behaved reaction matrix interaction  $G$ , in terms of which the perturbation expansion can be expressed. This reaction matrix, which was first introduced by Brueckner *et al.* (1954) to handle short-range

correlations in nuclear matter, is a central concept in the many-body theory of finite nuclei. Several methods exist to calculate  $G$ . However, in the present review we shall not be concerned with the technical details of the calculation of  $G$ , but rather consider  $G$  as given to us and serving as a starting point for the evaluation of higher-order terms in the perturbation expansion of effective operators.

This expansion can either be evaluated order by order in  $G$ , as discussed in Sec. III.C, or by performing partial summations of infinite subsets of terms, as discussed in Sec. III.D. In these discussions we shall attempt to emphasize the main physical processes at work.

Most calculations of effective operators to date have been performed in a harmonic oscillator single-particle basis. There are, however, indications that the self-consistency corrections are large, as shown in Sec. III.E. Then, in Sec. III.F we describe attempts to assess the convergence properties of the effective interaction from model calculations where an "exact" effective interaction is obtained by diagonalization of large matrices. Although the present paper is concerned mainly with effective operators of one- and two-body character, we discuss in the final Sec. III.G many-body effective operators which will, in general, arise in systems of several particles.

#### A. Brief reminder on the nucleon–nucleon interaction

The perturbation expansion for effective operators in nuclei discussed in Sec. II [see Eqs. (2.62) and (2.71)] is expressed in terms of matrix elements of the free nucleon–nucleon interaction<sup>2</sup>  $V_{12}$  in the unperturbed shell-model basis (generated by  $H_0$ ). In order to evaluate these matrix elements we need to know the decomposition of  $V$  into partial waves of given orbital and spin angular momenta. We shall not discuss here the detailed properties of  $V$  in the various partial-wave channels. Neither shall we discuss the various alternate forms of  $V$  which have been derived by phase-shift analyses of nucleon–nucleon scattering data. A survey of representative phase-shift determined potentials is given in Appendix A to Chapter X of the monograph on the nucleon–nucleon interaction by Brown and Jackson (1975). For the present discussion it will suffice to have qualitative knowledge of a few basic features of  $V$ , which are illustrated by the schematic picture of the spin-singlet (i.e.,  $S=0$ )  $s$ -wave (i.e.,  $l=0$ ) component of  $V$  shown in Fig. 27. At short distance ( $r \lesssim 0.4$  fm, where  $1 \text{ fm} = 10^{-15} \text{ m}$ ) the potential has a strong repulsive core which is currently believed to be due to the exchange of vector mesons. Then comes a moderately strong, intermediate-range attractive part with maximum strength at  $\approx 0.7$  fm. This part is believed to arise from the exchange of two pions. However, these are mainly coupled together to total angular momentum zero, and may thus for simplicity be thought of as a "scalar meson" (although no scalar meson has yet been found in nature). The tail of the potential is due to one-pion (pseudoscalar) ex-

<sup>2</sup>In the following we shall omit the subscripts from  $V_{12}$ , except where it is necessary to distinguish it from the total perturbing potential  $V = \sum V_{ij} - \sum U_i$  of Eqs. (2.2) and (2.3).

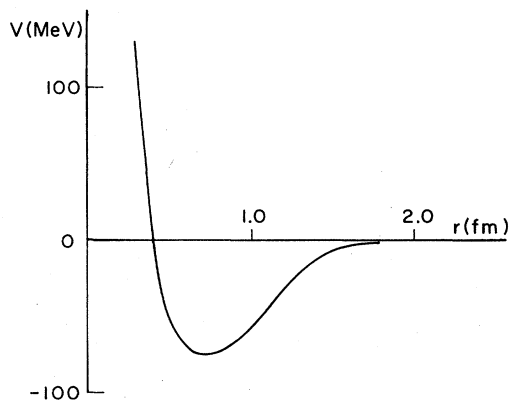


FIG. 27. Schematic representation of the spin-singlet  $s$ -wave component of the nucleon-nucleon interaction as a function of the internucleon distance  $r$ .

change and has a range of  $\approx 1.4$  fm. The one-pion tail is considered a well-established result of meson theory and is generally built into phase-shift determined phenomenological potentials. By the uncertainty principle, the range of a given meson-exchange component of the nucleon-nucleon interaction is inversely proportional to the mass of the appropriate meson. We refer the reader to the monograph by Brown and Jackson (1975) for a complete discussion and additional references.

The most simple meson-exchange potential is the well-known potential of Yukawa (1935),

$$V(r) = -g^2(e^{-\mu r}/r), \quad (3.1)$$

which is mediated by scalar mesons. In Eq. (3.1)  $g$  is the coupling constant measuring the strength of the interaction between the nucleon and the mesonic field. Furthermore, we have  $\mu = mc/\hbar$ , where  $m$  is the mass of the meson. Thus the range of the potential is inversely proportional to  $m$ , as stated above. We note in passing that the phenomenological Reid (1968) soft-core potential is essentially just a superposition of Yukawa potentials of different ranges and strengths.

It is worth pointing out that the spin-singlet  $s$ -wave potential shown in Fig. 27 is quite similar to the Van der Waals potential between molecules. However, unlike the Van der Waals force, the nucleon-nucleon interaction is spin dependent, having strong spin-orbit and tensor components in the appropriate spin-triplet channels.

The potential shown in Fig. 27 can be further schematized to a potential with an infinite hard core and a sharp core radius, as shown in Fig. 28. This is the form assumed for the much used potential of Hamada and Johnson (1962). It is obvious from Fig. 28 that the unperturbed matrix elements of  $V$  must be infinite, since the unperturbed wave function,  $\phi$ , shown by the dotted curve is finite inside the core radius where the potential is infinite. Even for potentials with finite repulsive cores, the unperturbed matrix elements will be very large and thus make the perturbation expansion in terms of  $V$  divergent.

This difficulty is however purely mathematical because unperturbed wave functions are used which totally disregard the correlations induced between the nucleons

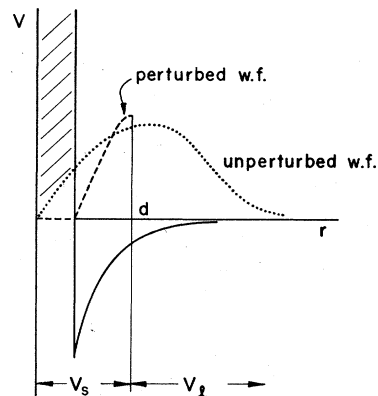


FIG. 28. Nucleon-nucleon potential (solid curve) with infinite hard core. The unperturbed wave function,  $\phi$ , of relative motion is represented by the dotted curve, whereas the perturbed wave function,  $\psi$ , is represented by the dashed curve. The two wave functions have equal logarithmic derivatives at the separation distance  $d$  which divides the potential into a short-range part  $V_s$  and a long-range part  $V_l$ . Beyond  $d$  the perturbed wave function approaches the unperturbed one in an oscillatory manner.

by the interaction. Physically, there is a subtle balance between the repulsive and attractive parts of the interaction. The strong repulsive core serves to keep the nucleons apart from each other, while the attractive part is responsible for binding the nucleons together. Indeed, the attractive part is just strong enough to hold a proton and a neutron together with a few MeV binding energy in the deuteron. Thus the corresponding energy shift

$$\Delta E \equiv E - E_0 = \langle \phi | H - H_0 | \psi \rangle = \langle \phi | V_{12} - U_1 - U_2 | \psi \rangle \quad (3.2)$$

obtained from Eq. (2.8), using the normalization  $\langle \phi | \psi \rangle = 1$ , is a very finite quantity. This may be understood from Fig. 28, where the exact two-nucleon wave function  $\psi$  shown by the dashed curve is zero inside the infinite hard core, and thus the product  $V\psi$  is finite. We shall use this property in the following Sec. III.B to construct a finite reaction matrix interaction to replace  $V$  in perturbation expansions for effective operators.

*Summary.* We have discussed the main characteristics of the nucleon-nucleon interaction  $V$  as derived from meson theory and phase-shift analysis of nucleon-nucleon scattering. The important point to keep in mind is that the unperturbed matrix elements of  $V$  are either very large or infinite due to the strong short-range repulsion in  $V$ . Thus perturbation expansions of effective operators would be meaningless if evaluated in terms of individual matrix elements of  $V$ .

## B. The Brueckner-Bethe-Goldstone reaction matrix

We remarked in the previous subsection that although the unperturbed matrix elements  $\langle \phi | V | \phi \rangle$  of the nucleon-nucleon interaction  $V$  are very large or infinite, the interaction energy  $\langle \phi | V | \psi \rangle$  of two nucleons bound in the deuteron is finite. Now, consider two interacting nucleons bound inside the nucleus. It is convenient to rewrite the analogue of Eq. (3.2) using the wave operator of Eqs. (2.13)–(2.14); hence

$$\Delta\omega \equiv \langle \phi | V | \phi \rangle = \langle \phi | V \Omega | \phi \rangle, \tag{3.3}$$

$$\Omega = 1 + [Q/(\omega - H_0)]V\Omega. \tag{3.4}$$

Here  $\omega$  is the total energy of the two interacting nucleons, and  $Q$  is the Pauli exclusion operator which prevents the nucleons from being excited to intermediate states which are occupied by other nucleons. Thus the interaction between the two nucleons in question is modified by the presence of the surrounding nucleons. In more technical language we say that many-body effects arise from the exclusion operator  $Q$ .

Now, because of the short-range nature of the strong repulsion in  $V$ , the intermediate-state excitations  $Q$  are dominated by two-particle excitations  $Q_{2p}$  of rather high energy. Thus, if we replace  $Q$  by  $Q_{2p}$  in Eq. (3.4), the corresponding matrix element (3.3) would still be finite. Then, defining in analogy with Eq. (2.17) an operator  $G$  by

$$G(\omega) \equiv V\Omega_{2p} = V + V \frac{Q_{2p}}{\omega - H_0} G(\omega) \tag{3.5a}$$

$$= V + V \frac{Q_{2p}}{\omega - H_0} V + V \frac{Q_{2p}}{\omega - H_0} V \frac{Q_{2p}}{\omega - H_0} V + \dots, \tag{3.5b}$$

we have by Eq. (3.3)

$$\langle \phi | G(\omega) | \phi \rangle = \langle \phi | V \Omega_{2p} | \phi \rangle = \Delta\omega_{2p}. \tag{3.6}$$

Thus the matrix elements of  $G$  in the unperturbed basis are finite, although the individual terms in the perturbation expansion (3.5b) are essentially infinite, as discussed above.

The operator  $G$  is generally referred to as the *reaction matrix*. It was introduced by Brueckner *et al.* (1954) to handle singular potentials in nuclear matter, and subsequently refined by Bethe and Goldstone (Bethe, 1956; Bethe and Goldstone, 1957). The concept of the  $G$  matrix originates from Watson's (1953) theory of multiple scattering, but it is important to note that we are here dealing with *bound* states rather than scattering states. Furthermore, the  $G$  matrix differs from the scattering matrix in containing the Pauli exclusion operator  $Q$ , which prevents particles from being excited to states which are already occupied by other particles in the surrounding nuclear medium. Also,  $G$  is a function of the energy variable  $\omega$ , the so-called starting energy, which depends on the energy of the interacting pair of particles as well as on the energy of other interacting particles present. Thus, as we shall see later on, the starting energy  $\omega$  will depend on the position of  $G$  in a particular diagram.

The perturbation expansion (3.5b) for  $G$  can be represented diagrammatically by the series of "ladder" diagrams shown in Fig. 25(a). The physical interpretation of this diagrammatic expansion is intuitively clear. Since  $V$  is very strong in the unperturbed basis, the particles must interact virtually with each other an arbitrary number of times in order to produce a finite interaction matrix element.

We shall now take advantage of the finiteness of  $G$  to rewrite the perturbation expansion for effective operators in terms of  $G$ . This can be done by grouping together diagrams which differ from each other only in the

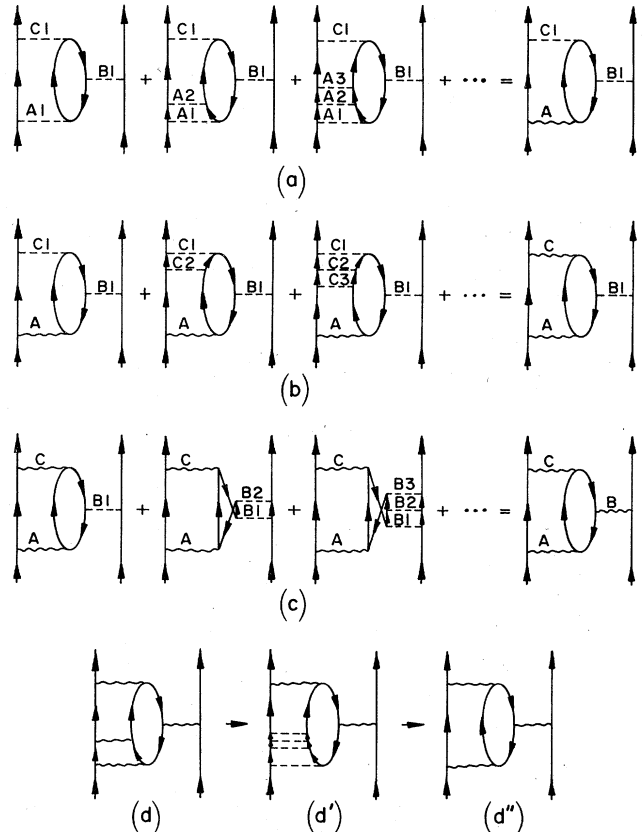


FIG. 29. Illustration of partial summation procedure used to replace  $V$  vertices (dashed lines) by  $G$  vertices (wavy lines). Note that two-particle intermediate states between successive  $G$  vertices (d) are not allowed, since they are already included in the appropriate  $G$  (d').

number of successive  $V$  interactions between two particle lines. The infinite sum of such ladders of  $V$  can then be replaced by a single  $G$  interaction. Various examples are shown in Fig. 29. In Fig. 29(a) the sequence of  $V$  vertices  $A_1, A_2, A_3, \dots$  gives rise to the  $G$  vertex denoted by  $A$ . We have here represented  $G$  by a wavy line to distinguish it from  $V$  which is denoted by a dashed line. Clearly, the top vertex  $C_1$  does not contribute to this  $G$ , since the vertex  $B_1$  comes in between the sequence  $A_1, A_2, A_3, \dots$  and  $C_1$ . In fact, the vertex  $C_1$  belongs to the sequence  $C_1, C_2, C_3, \dots$  producing the  $G$  vertex  $C$ , as shown in Fig. 29(b). Note that each diagram in Fig. 29(b) represents an infinite set of diagrams of the type shown in Fig. 29(a), which are needed to build up the  $G$  vertex  $A$ . The remaining  $V$  vertex  $B_1$  can also be replaced by  $G$ , by summing the diagrams shown in Fig. 29(c). Here it is worth noting that only ladders of  $V$  between *particle* lines are included in  $G$ . By systematically carrying through this procedure of partial summation of ladders of  $V$ , one can clearly rewrite the perturbation expansion in terms of diagrams with  $G$  vertices only. As a general rule, one may simply replace  $V$  by  $G$  in all diagrams except the ones with successive  $V$  vertices between particle lines, which are included in the corresponding diagram with a single  $G$ . Thus in the new series there are no diagrams with ladders of  $G$

between particle lines. For example, diagram (d) in Fig. 29 is a sum of diagrams of the form (d') which are obviously included in the corresponding diagram (d'') with a single  $G$  vertex.

The calculation of  $G$  from the nucleon-nucleon interaction is both cumbersome and subtle, and has a long history of evolution. This is not the place to go into a detailed discussion of the techniques used for calculating  $G$ . For the present purpose it is more important to have a physical understanding of the concept of the reaction matrix  $G$  than to know in detail how it is evaluated. It may, however, be instructive to consider briefly the separation method of Moszkowski and Scott (1960), which is probably the physically most intuitive method for calculating the  $G$  matrix. The essence of this method is illustrated in Fig. 28. It consists of dividing the potential  $V$  into a short-range part  $V_s$  and a long-range part  $V_l$ . This division is made at the so-called separation distance  $d$ , which is chosen so that the free-space (i.e.,  $Q = 1$ ) reaction matrix due to  $V_s$  is zero, or equivalently, the logarithmic derivatives of the unperturbed and perturbed wave functions are equal. Now, since short distances correspond mostly to highly excited states where  $Q$  is unity, the reaction matrix is to a good approximation due to the long-range potential  $V_l$  alone, which is well behaved and relatively weak. The separation distance  $d$ , which is in principle state dependent, is generally found to be about 1 fm. For further details on this and other methods, the reader is referred to the nuclear physics textbook by Brown (1971a) and review papers by Day (1967), Baranger (1969), Dahll *et al.* (1969), and Kuo (1974) and references therein.

In the following Secs. III.C–Sec. III.G., we shall go on to discuss the numerical results obtained for perturbation calculations of effective operators, starting from a given reaction matrix  $G$ . Most of our discussion will be based on the results obtained using the  $G$  matrix elements calculated by Kuo and Brown (1966, 1968) and Kuo (1967) from the potential of Hamada and Johnston (1962). More recent and accurate calculations of the  $G$  matrix (Sauer, 1970; Tsai, 1973; and Krenciglowa *et al.*, 1976b) from an updated potential (Reid, 1968) have shown surprisingly good agreement with the early Kuo–Brown calculations. In these calculations the Pauli exclusion operator  $Q_{2p}$  was constructed in a plane-wave basis. This choice of intermediate-state spectrum rests on the assumption that the hole-line expansion of nuclear matter theory is valid for finite nuclei (Krenciglowa *et al.*, 1976a, 1976b). It is interesting to note that very similar results may be obtained using harmonic oscillator intermediate states, provided that the intermediate-state spectrum be given an upward shift with respect to the occupied states (Barrett, 1974; Barrett and Kirson, 1975; Sandel *et al.*, 1977).

In conclusion it should be pointed out that several methods exist for calculating the reaction matrix, and several nucleon-nucleon potentials may be used as a starting point. On the whole, different calculations appear to have given qualitatively similar results for the reaction matrix, and, accordingly, perturbation calculations of effective operators have shown little sensitivity to the particular reaction matrix chosen as input.

*Summary.* The concept of the reaction matrix  $G$  is introduced via Eq. (3.5). The unperturbed matrix elements of  $G$  are finite, and thus  $G$  may be used to replace the singular nucleon-nucleon interaction  $V$  in perturbation expansions of effective operators, as shown diagrammatically in Fig. 29. The physical significance of  $G$  is most readily seen in the separation method of Moszkowski and Scott (1960), as discussed briefly.

### C. Calculation of effective operators order by order in $G$

We shall now discuss the results obtained for the effective interaction and electric quadrupole ( $E2$ ) operator by summing the appropriate perturbation expansions to successive orders in the reaction matrix  $G$ . As the purpose of the present review is to discuss the physical properties and relative sizes of the various terms in the perturbation expansions in question, we shall restrict ourselves to nuclei for which enough terms have been calculated to enable us to draw conclusions about the convergence properties. More specifically, we shall consider the effective interaction for two nucleons in the ( $1s0d$ ) shell outside a closed  $^{16}\text{O}$  core—restricting our attention mainly to the case of  $^{18}\text{O}$  with two valence neutrons. Similarly, we shall discuss calculations of the effective  $E2$  operator for nuclei with a single nucleon in the ( $1s0d$ ) shell outside the  $^{16}\text{O}$  core. However, to further illustrate and amplify our discussion we shall make occasional reference to the corresponding calculations for valence nucleons in the ( $1p0f$ ) shell outside a closed  $^{40}\text{Ca}$  core.

Unless otherwise stated, the input  $G$  matrix elements were taken from Kuo (1967) for the ( $1s0d$ ) shell calculations and from Kuo and Brown (1968) for the ( $1p0f$ ) shell

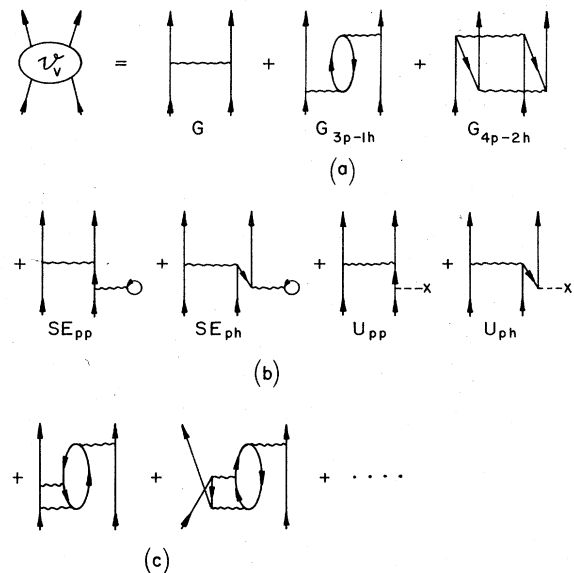


FIG. 30. Low-order contributions to the effective interaction between two valence nucleons. Antisymmetrized  $G$  vertices (wavy lines) are employed and exchange of external lines is implied, except where it is implicitly taken into account by the use of antisymmetrized vertices (see Appendix C). Further, a dashed line with a cross denotes a  $(-U)$  vertex. In (b) it is understood that the closed-loop and  $(-U)$  insertions are made in any one of the four valence lines.

calculations. Both sets were calculated from the nucleon-nucleon potential of Hamada and Johnston (1962) and expressed in a harmonic oscillator basis, using an oscillator energy  $\hbar\omega = 14$  MeV for the (1s0d) shell and  $\hbar\omega = 10.5$  MeV for the (1p0f) shell. Plane-wave intermediate states were employed in both cases, and the  $G$  matrices were taken to be independent of the starting energy.

1. Effective interaction

Following the prescription of Sec. III.B, we may rewrite the perturbation expansion for the effective inter-

$$\begin{array}{c}
 \begin{array}{ccccc}
 & 2p & 3p-1h & 4p-2h & 5p-3h & \dots \\
 2p & \boxed{\phantom{0}} & \boxed{\phantom{0}} & \boxed{\phantom{0}} & \boxed{\phantom{0}} & \\
 3p-1h & \boxed{\phantom{0}} & \boxed{\phantom{0}} & \boxed{\phantom{0}} & \boxed{\phantom{0}} & \\
 4p-2h & \boxed{\phantom{0}} & \boxed{\phantom{0}} & H=H_0+V & \boxed{\phantom{0}} & \\
 5p-3h & \boxed{\phantom{0}} & \boxed{\phantom{0}} & \boxed{\phantom{0}} & \boxed{\phantom{0}} & \\
 \vdots & \boxed{\phantom{0}} & \boxed{\phantom{0}} & \boxed{\phantom{0}} & \boxed{\phantom{0}} & \\
 \vdots & \boxed{\phantom{0}} & \boxed{\phantom{0}} & \boxed{\phantom{0}} & \boxed{\phantom{0}} & \\
 \end{array}
 \end{array}
 \rightarrow
 \begin{array}{c}
 2p_v \\
 \left[ \begin{array}{c} H_{eff} \\ H_0 + U_v \end{array} \right]
 \end{array}
 2p_v. \tag{3.7}$$

To lowest order the effective interaction is simply given by the  $G$  matrix itself. We shall refer to this as the *bare* interaction. This term is not sufficient to reproduce well the low-energy spectrum of  $^{18}\text{O}$ , as pointed out by Dawson *et al.* (1962) and Kuo and Brown (1966). As shown in Fig. 31, the spectrum calculated with the bare  $G$  of Kuo and Brown (column 2) is clearly too compressed compared to the experimental spectrum (column 1) and shows too little ground-state binding energy. (Note that the slightly revised  $G$  of Kuo (1967) was used in the calculations quoted in Fig. 31.) Thus Kuo and Brown (1966) went on to calculate the second-order diagrams shown in Fig. 30(a), including intermediate states of  $2\hbar\omega$  oscillator excitation energy (e.g., for  $G_{3p-1h}$  using

$p-h$  states of (1s0d)-0s and (1p0f)-0p). Among the second-order contributions, the core-polarization diagram  $G_{3p-1h}$ , which was first considered by Bertsch (1965), turned out to be the most important. As shown in column 3 of Fig. 31, the second-order corrections serve to open up the spectrum, thus improving the agreement with experiment. In this regard it is important that  $G_{3p-1h}$  corrections to the diagonal matrix elements can have either sign [see Eq. (D2) of Appendix D], unlike  $G_{4p-2h}$  which always yields a negative contribution (and mainly serves to push the  $0_1^+$  level down a little). It is seen from Fig. 31 (column 3) that negative (i.e., attractive) contributions are obtained for the lowest  $T=1, J=0$  and 2 states which have too little binding for the bare interaction, while positive (i.e., repulsive) contributions are obtained for the  $T=1, J=3$  and 4 states which are too strongly bound. This effect is the desired one, and quite good agreement with experiment is obtained.

The effect of the core-polarization term is still more transparent in  $^{42}\text{Ca}$ , where the average effective interaction lends itself to a simple parametrization. It is well known that the binding energies of the Ca isotopes with  $n$  neutrons beyond  $^{40}\text{Ca}$  can be well described in terms of pure  $(0f_{7/2})^n$  configurations using effective two-particle matrix elements which are taken as free parameters. For any two-body interaction we have (de-Shalit and Talmi, 1963)

$$\langle j^n | \sum_{i < j} V_{ij} | j^n \rangle_{g.s.} = \frac{n(n-1)}{2} \alpha + \left[ \frac{n}{2} \right] \beta, \tag{3.8}$$

where  $[n/2]$  is  $n/2$  if  $n$  is even, and  $(n-1)/2$  if  $n$  is odd, and  $\alpha$  and  $\beta$  can be expressed in terms of the two-particle matrix elements of  $V_{12}$  as follows

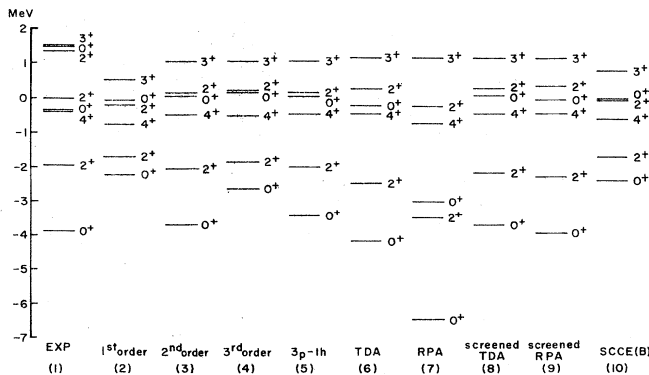


FIG. 31. Calculated spectra of  $^{18}\text{O}$  for various approximations to the effective interaction. The spectra are taken from the following references: (1) Ajzenberg-Selove, 1972; (2-4) Goode, 1974 and private communication; (5-9) Kuo and Osnes, 1974; and (10) Kirson, 1974.

$$\alpha = \frac{2(j+1)\bar{V}_2 - V_0}{2j+1},$$

$$\beta = \frac{2(j+1)}{2j+1}(V_0 - \bar{V}_2), \quad (3.9)$$

with

$$V_0 = \langle j^2 J=0 | V_{12} | j^2 J=0 \rangle,$$

$$\bar{V}_2 = \sum_{\substack{J>0 \\ \text{even}}} (2J+1) \langle j^2 J | V_{12} | j^2 J \rangle / \sum_{\substack{J>0 \\ \text{even}}} (2J+1). \quad (3.10)$$

In Eq. (3.8) it is understood that we are dealing with identical particles and that the ground state is given by the state with minimum seniority. It follows from Eq. (3.9) that  $\alpha$  is essentially the average two-particle interaction in the states with  $J>0$ , whereas  $\beta$  is the  $J=0$  interaction relative to the average  $J>0$  interaction. By a fit to experimental binding energies  $\alpha$  was found to be small and repulsive, and  $\beta$  large and attractive. In Table I the empirical values of  $\alpha$  and  $\beta$  are compared to the values calculated with  $G$  and  $G+G_{3p-1h}$  by Brown and Kuo (1967). It is seen that the bare interaction fails to give a repulsive  $\alpha$ ; i.e., the corresponding spectrum is too compressed. On the other hand,  $\beta$  has the correct sign, but is too small in magnitude, corresponding to underbinding of the ground state. The inclusion of the core-polarization term is seen to give desired, although quantitatively insufficient, corrections to  $\alpha$  and  $\beta$ .

Brown and Kuo (1967) have given a neat physical interpretation of the core-polarization term. As shown in Appendix D, the expression for the core-polarization diagram  $G_{3p-1h}$  involves the summation over intermediate particle-hole states coupled to different  $J''$  and  $T''$ . Each  $J''$  and  $T''$  excitation is mediated via the  $J''$  and  $T''$  multipole component of the interaction. Decomposition of  $G_{3p-1h}$  into individual  $J''$  and  $T''$  contributions (see Table IV) shows that the dominant contribution comes from the  $J''=2, T''=0$  particle-hole excitations. If we neglect the exchange matrix elements and possible spin dependence of the interaction, and adjust the radial dependence, the  $J''=2, T''=0$  contribution corresponds to a quadrupole-quadrupole interaction

$$V_{QQ} = k r_1^2 r_2^2 P_2(\cos\theta_{12}) = k \mathbf{Q}_2(\mathbf{r}_1) \cdot \mathbf{Q}_2(\mathbf{r}_2), \quad (3.11a)$$

where the quadrupole tensor is defined in terms of spherical harmonics as

$$Q_{\lambda\mu}(\mathbf{r}) = \left[ \frac{4\pi}{2\lambda+1} \right]^{1/2} r^\lambda Y_{\lambda\mu}(\hat{\mathbf{r}}). \quad (3.11b)$$

There is indeed considerable evidence for a strong quadrupole component in the effective interaction (see,

TABLE I. Empirical and calculated values of the interaction parameters  $\alpha$  and  $\beta$  of Eqs. (3.8) and (3.9) for the  $0f_{7/2}$  shell. All parameter values are in MeV.

Parameter	Empirical <sup>a</sup>	Calculated <sup>b</sup>	
		$G$	$G+G_{3p-1h}$
$\alpha$	$0.23 \pm 0.01$	-0.21	0.15
$\beta$	$-3.33 \pm 0.12$	-0.66	-1.96

<sup>a</sup>Talmi, 1962.

<sup>b</sup>Brown and Kuo, 1967.

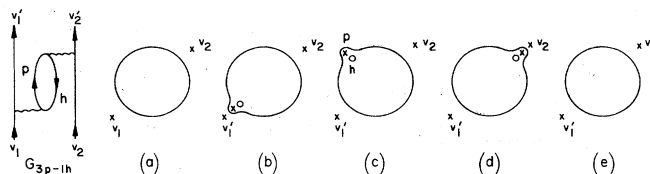


FIG. 32. Snapshots of the core-polarization process.

for example, Mottelson, 1959, 1962). In particular, very convincing evidence comes from the need for a nonzero  $E2$  effective charge for the valence neutron in  $^{17}\text{O}$ , since the  $E2$  operator picks out just the quadrupole component of the interaction between valence and core particles in the core-polarization diagram; see further discussion of the effective charge below. There is also an important  $J''=4, T''=0$  component in the core-polarization term, but the  $J''=2, T''=0$  component is the dominant one.

The large quadrupole component in the core-polarization term clearly gives rise to a long-range component in the effective interaction. The range of a given multipole component of the interaction is roughly inversely proportional to the multipole order, since the first node of the Legendre polynomial  $P_\lambda(\cos\theta_{12})$  comes at an angle  $\theta_{12} \approx \lambda^{-1}$ . Thus on the nuclear surface there will only be appreciable interaction between nucleons separated by less than  $R\lambda^{-1}$ , where  $R$  is the nuclear radius. Hence we conclude that the quadrupole component of the interaction has fairly long range. The origin of the long-range component of the core-polarization term may also be understood from the pictorial configuration-space representation of  $G_{3p-1h}$  given in Fig. 32. In order for two nucleons to interact via the bare interaction  $G$ , they must be fairly close to each other. [Indeed, for many purposes the bare  $G$  may be roughly represented by a  $\delta$ -function interaction; see, for example, Sharp and Zamick (1973).] Thus two valence nucleons on opposite sides of the core, as shown in Fig. 32(a), cannot interact directly via  $G$ . However, they may interact via the exchange of a particle-hole excitation as shown by the series of "snapshots" of the process depicted in Fig. 32(b)-(d). First, the valence particle  $v_1$  interacts—thus being left in a state  $v_1'$ —with a nearby core particle, creating a particle-hole pair [Fig. 32(b)], which then propagates over to the valence particle  $v_2$  [Fig. 32(c)] in a time interval  $\Delta t \approx \hbar/\Delta E$  where  $\Delta E$  is the excitation energy. When the particle-hole pair is close enough to  $v_2$  [Fig. 32(d)], it is annihilated via  $G$ , leaving  $v_2$  in a state  $v_2'$  [Fig. 32(e)]. Thus a long-range effective interaction is generated between a pair of valence particles in the states  $v_1$  and  $v_2$ , leaving them in the states  $v_1'$  and  $v_2'$ . There will also be some components of pairing type in  $G_{3p-1h}$ , since as shown in Table I the pairing parameter  $\beta$  of Eq. (3.8) is increased by the inclusion of  $G_{3p-1h}$ . This contribution is of short range and is generated by the higher multipole components of  $G_{3p-1h}$ .

Having observed the physically desirable and very reasonable effect of the second-order core-polarization correction  $G_{3p-1h}$ , one may tentatively draw the conclusion that all the other terms in the perturbation expansion of the effective interaction must essentially cancel each other, thus leaving to a good approximation

$$\mathcal{V}_v \approx G + G_{3p-1h} \quad (3.12)$$

This was the view generally held for the first six or seven years following the pioneering work of Kuo and Brown (1966). In the remaining part of this section we wish to check this hypothesis by considering other low-order terms in the expansion for  $\mathcal{V}_v$ .

First, we note that there are other second-order diagrams contributing to  $\mathcal{V}_v$ , as shown in Fig. 30(b). These are of two types, containing either insertions of closed loops representing the interaction with the core nucleons (so-called self-energy insertions) or the corresponding insertions of the negative of the one-body shell-model potential  $U_i$ . The former type is second order in  $G$ , whereas the latter has only one  $G$  vertex and arises because we defined the unperturbed Hamiltonian  $H_0$  by adding  $U = \sum U_i$  to the kinetic energy, and thus must subtract  $U$  from the two-body interaction  $\sum V_{ij}$  to obtain the perturbing potential [see Eqs. (2.2) and (2.3)]. Then, by introducing the  $G$  matrix as discussed in Sec. III.B, the perturbing potential becomes essentially  $G - U$ . Thus we also have to consider diagrams with  $(-U)$  vertices. Since  $U$  is a one-body operator, there are no contributions to the *two-body* effective interaction with only  $U$  vertices. Clearly, at least one  $G$  vertex is needed to link up the valence lines. Hence the lowest-order contribution with a  $U$  vertex comes in second order and is given by diagrams  $U_{pp}$  and  $U_{ph}$  in Fig. 30(b). Now, as we shall see in Sec. III.E, these diagrams would cancel exactly with the corresponding diagrams  $SE_{pp}$  and  $SE_{ph}$  with self-energy insertions if  $U$  were defined by the Hartree-Fock (HF) or more correctly by the Brueckner-Hartree-Fock approximation. We shall introduce the term HF insertion for the sum of corresponding self-energy and  $(-U)$  insertions and represent it by the diagrammatic notation shown in Fig. 33 (see also Fig. 50). Then, by definition, HF insertions are identically zero in a HF basis. However, for a different choice of  $U$ , such as the harmonic oscillator potential, the HF insertions will in general not be zero. In this case the HF insertions serve to modify the harmonic oscillator single-particle orbitals by mixing in oscillator orbitals of the same angular momentum, but with a different number of nodes. The inclusion of HF insertions to all orders would then restore the HF self-consistency of the single-particle orbitals. Thus the diagrams in Fig. 30(b) may be viewed as the lowest-order HF corrections to the bare  $G$  matrix elements.

In general diagrams with HF insertions have been ignored under the—more or less tacit—assumption that the harmonic oscillator single-particle wave functions

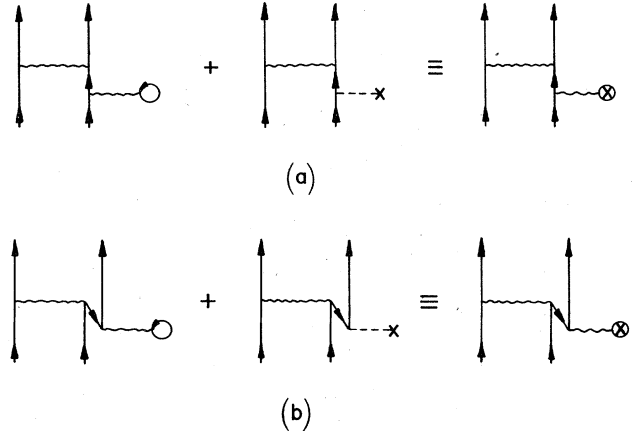


FIG. 33. Second-order diagrams with self-energy and  $(-U)$  insertions and convention for the sum (which is zero in a HF basis).

are sufficiently similar to the HF wave functions near the Fermi surface. Unfortunately, there appears to be no explicit calculation of the diagrams in Fig. 30(b) (or Fig. 33) using the  $G$  matrix elements of Kuo and Brown. There are, however, calculations by Ellis and Mavromatis (1971) using the Sussex matrix elements (Elliott *et al.*, 1968), which are fairly similar to the Kuo-Brown matrix elements. As expected, the HF corrections were found to be small for the  $(0d_{5/2})^2$  matrix elements. However, the  $(1s_{1/2})^2$  matrix elements were found to be reduced in magnitude—thus becoming less attractive—by about 1 MeV. This correction is indeed larger than any of the contributions from the core-polarization diagram  $G_{3p-1h}$ . Obviously, the reduction in the size of the  $(1s_{1/2})^2$  matrix elements is due to the fact that the HF wave function for the  $1s_{1/2}$  single-particle orbital extends further out than the harmonic oscillator wave function. Similarly, matrix elements involving the  $0d_{3/2}$  orbital were significantly weakened. Thus the HF corrections appear to be rather important, at least for the more weakly bound orbitals, indicating that the effective interaction ought to be expressed in a HF single-particle basis, as discussed in more detail in Sec. III.E.

In order to further examine the hypothesis (3.12) for the effective interaction it is clearly necessary to go beyond second order in the perturbation calculation. The third-order diagrams were evaluated by Barrett and Kirson (1970) for  $J=0, T=1$ , and by Goode (1974) for the other  $J$  and  $T$ . In both calculations diagrams with HF insertions were ignored. As shown in Table II,

TABLE II. Matrix elements  $\langle v_1^2 J=0, T=1 | \mathcal{V}_v | v_2^2 J=0, T=1 \rangle$  of the effective interaction in the  $(1s0d)$  shell, calculated in low-order perturbation theory. All matrix elements are in MeV.

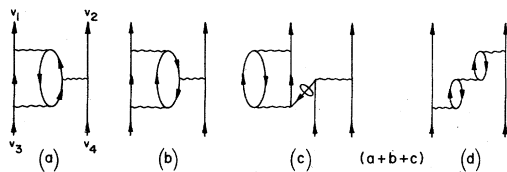
Valence orbits		1st order <sup>a</sup>	2nd order <sup>b</sup>	3rd order <sup>b</sup>	Total
$v_1$	$v_2$				1st+2nd+3rd
$d_{5/2}$	$d_{5/2}$	-1.24	-1.01	0.52	-1.73
$d_{5/2}$	$d_{3/2}$	-3.02	-0.73	1.10	-2.65
$s_{1/2}$	$s_{1/2}$	-2.05	0.04	0.15	-1.86

<sup>a</sup>Kuo, 1967.

<sup>b</sup>Barrett and Kirson, 1970, 1972.

Barrett and Kirson found that the total third-order contributions to the  $J=0, T=1$  matrix elements of the effective interaction were in many cases as large as the second-order ones, but of opposite sign, thus suggesting that the order-by-order perturbation expansion does not give reliable results for the effective interaction. For  $T=1, J \neq 0$  the effect of the third-order diagrams is smaller, as shown by the spectrum in column 4 of Fig. 31. However, for  $T=0$  there appears again to be a strong cancellation between second- and third-order contributions, particularly in the low-lying states.

An interesting aspect of Barrett and Kirson's work was their investigation of possible cancellations among third-order diagrams of similar structure. In particular, they examined the suggestion of Brandow (1967) that certain subsets of diagrams should cancel approximately according to the principle of number conservation (by analogy to charge conservation in the Ward identity in quantum electrodynamics). If valid to a reasonable approximation, this idea would be extremely useful, since it would reduce the number of higher-order diagrams which need to be calculated. As an example, consider diagrams (a), (b), and (c) in Fig. 34. If the middle vertex were the number operator, these diagrams would cancel exactly, as indicated. In physical terms these diagrams may be thought of as a correction to the bare interaction matrix element due to one valence particle exciting a particle-hole pair. The interaction of the remaining valence particle with the excited particle (a) is balanced against the interaction with the hole in the core (b) and the reduction in the bare matrix element due to the probability that one particle is no longer in a valence state (c). Barrett and Kirson (1970) reported that the cancellation was in fact fairly good for the  $J=0, T=1$  interaction; whereas an extended study by Ellis *et al.* (1972), in which all the  $(1s0d)$  shell matrix elements and a few  $(1p0f)$  shell matrix elements of the third-order number-conserving sets were calculated for a variety of forces, indicated that the cancellation is not sufficiently good to be really useful. In fact, in many cases the sum of the number-conserving diagrams is comparable in magnitude to the third-order core-polarization diagram (d), which is one of the largest third-order diagrams. The poor cancellation is mainly due to the folded diagram (c), which is proportional, but opposite in sign, to the bare interaction between the valence particles.



Number operator:	Z	$-\frac{1}{2}Z$	$-\frac{1}{2}Z$	0			
Kuo-Brown interaction:							
$v_1 = v_2$	$v_3 = v_4$	J					
Ods/2	Ods/2	0	-0.481	0.383	0.215	0.117	-0.241
Ods/2	Ods/2	0	-0.256	-0.029	0.631	0.346	-0.236
Ods/2	Ods/2	0	-0.442	0.434	0.018	0.010	-0.146

FIG. 34. Number-conserving set (a-c) and core-polarization diagram (d) in third order. The calculated values are taken from Barrett and Kirson, 1970, 1972.

Thus whenever the bare interaction is large, this diagram [together with diagram (b)] may easily overcancel diagram (a), which generally has the same sign as the bare interaction.

Other large third-order diagrams are shown in Fig. 30(c). These may be viewed as corrections to the second-order core-polarization diagram, since they modify the vertex which couples the valence particle to the particle-hole excitation of the core. Thus they are often referred to as vertex renormalizations. They are almost invariably repulsive for  $J=0, T=1$ , and together they more than cancel the second-order core-polarization contribution. Further discussion of these diagrams is deferred to Sec. III.D, where we deal with partial summations.

The third-order diagrams containing HF insertions have not been calculated, but Comins and Hewitt (1974) have carried out a related, although not strictly third-order, calculation. They first sum the diagonal HF insertions by using modified single-particle energies essentially as discussed in Sec. II.B.6 and Appendix B. They also include the effect of HF insertions in the intermediate states of the reaction matrix  $G$ . They then calculate all third-order diagrams which are not included in the above summation. These results are found to be qualitatively similar to those of Barrett and Kirson (1970). The individual diagrams are, however, reduced in size because larger energy denominators arise from the implicit inclusion of HF insertions.

In fourth order there are about a thousand diagrams contributing to the effective interaction. Thus a full fourth-order calculation, diagram by diagram, would seem to be intractable. However, the average fourth-order contribution to the effective interaction has been evaluated by Goode and Koltun (1975) using a special diagrammatic technique in which averages of valence-particle diagrams are expressed in terms of diagrams of closed-shell form. The average fourth-order contributions are found to be large. This is mainly due to poor cancellation in the number-conserving sets caused by large folded-diagram contributions. Clearly, averages cannot be large unless at least some of the individual terms are large. Thus it is concluded that the valence-linked expansion for the effective interaction is poorly behaved in low order.

One way to improve the convergence properties of the perturbation series for the effective interaction  $\mathcal{U}_v$  might be to remove the low-energy intermediate states from the reaction matrix  $G$  and include them explicitly in the perturbation calculation of  $\mathcal{U}_v$ . Thus the two-particle excitations of low energy would be treated on the same footing as the other low-energy excitations which lead to long-range correlations, while  $G$  would only include the high-energy excitations associated with the short-range correlations. This would make the bare  $G$  somewhat weaker, but would put the lost strength back into higher orders—in terms of diagrams containing two-particle intermediate states (of low energy) between successive  $G$  vertices. One would thus obtain a redistribution of strength over different orders which might serve to improve the convergence properties of the expansion for  $\mathcal{U}_v$ . This scheme, which is often referred to as double partitioning of the Hilbert space, was suggest-

ed by Brandow (1967) and has been strongly advocated by Brown (1971b). Calculations in this scheme, through third order in  $G$ , have been performed by Barrett (1974), who evaluated his  $G$  matrix from the Hamada–Johnston potential, but contrary to Kuo and Brown (1966, 1968; see also Kuo, 1967) used harmonic oscillator intermediate states (Barrett *et al.*, 1971). The convergence of the perturbation expansion for  $\mathcal{V}_v$  was improved in the double-partition approach, although the calculation was not conclusive, as both the HF corrections discussed above and other corrections to be discussed below were ignored. The results obtained for the third-order vertex corrections will be discussed in some detail in Sec. III.D. Similar effects were obtained (Barrett, 1972) using the  $G$  matrix elements of Kuo and Brown, although here there is a problem of double counting which has been the subject of heated debate in the literature (e.g., Barrett and Kirson, 1975; Krenciglowa *et al.*, 1976a, 1976b and references therein). We remark in passing that the new matrix elements of Kuo and collaborators (Krenciglowa *et al.*, 1976a, 1976b) are designed for double-partition calculations, but no systematic higher-order calculation has yet been made with these matrix elements.

Thus far we have attempted to describe the typical behavior of the effective interaction through the lowest few orders of perturbation theory, and a relatively simple picture has emerged. We have seen that quite good agreement with experiment is obtained through second order in  $G$ , provided that HF corrections be ignored. The large second-order contributions are, however, strongly cancelled by the third-order contributions, and thus the good agreement with experiment is destroyed. Furthermore, there is no evidence that the fourth-order contributions are small, and thus one is led to conclude that the perturbation expansion for  $\mathcal{V}_v$ , if not diverging, is poorly behaved in low order. Improved convergence properties may, however, be obtained if a double-partition approach is used which allows separate treatment of two-particle excitations of low and high energies. Unfortunately, this relatively simple picture is obscured not only by the HF corrections, which as discussed may be large, but also by other corrections and uncertainties which will now be discussed.

First, recall that all the higher-order terms discussed above (except the HF corrections) were evaluated using intermediate states of  $2\hbar\omega$  excitation energy. At first sight this truncation may seem reasonable, since the next higher intermediate states—of  $4\hbar\omega$  excitation energy—would have twice as large energy denominators as the  $2\hbar\omega$  excitations. However, the number of intermediate states increases strongly with the excitation energy. Furthermore, the  $G$  vertices involved may be large because of the strong tensor-force component in the  $G$  matrix, which may excite particles more than 100 MeV up in energy. Thus there is no reason to expect that the contributions from intermediate states beyond  $2\hbar\omega$  excitation energy should be negligible. This was confirmed by Vary *et al.* (1973), who showed that one has to include intermediate states up to about  $12\hbar\omega$  excitation in order to obtain reasonable convergence for the second-order core-polarization diagram  $G_{3p-1h}$ . For example, for the diagonal  $J=0, T=1$   $(0d_{5/2})^2$  matrix ele-

ment they obtained contributions of  $-0.710$ ,  $-0.379$ ,  $-0.114$ , and  $-0.085$  MeV by including intermediate states up to 2, 6, 12, and  $22\hbar\omega$  excitation, respectively. [These results were obtained using the  $G$  matrix elements calculated by Sauer (1970) from the Reid soft-core potential.] Thus the strong attractive contribution to  $G_{3p-1h}$  from  $2\hbar\omega$  particle-hole excitations is essentially wiped out by higher particle-hole excitations. On the average, the high intermediate states serve to make  $G_{3p-1h}$  considerably less attractive. On the other hand, the difference between the average  $T=1$  and  $T=0$  interactions appears to be increased, which is desirable from an experimental point of view. High intermediate-state contributions of similar magnitude have been obtained by Sandel *et al.* (1977) using the  $G$  matrix elements calculated by Barrett *et al.* (1971) from the Hamada–Johnston potential [see also Vary and Yang (1977)]. Thus the high intermediate states appear to be important for  $G_{3p-1h}$ , and one might have to give up the simple hypothesis (3.12) that  $\mathcal{V}_v$  is essentially given by  $G + G_{3p-1h}$ . Similarly, one would expect significant high intermediate-state contributions to other diagrams. The inclusion of high intermediate states in third order would be rather cumbersome, so one might have to design a simple method for doing this, for instance some partial summation similar to that used in calculating the reaction matrix  $G$ . Herbert and Barrett (1975) have evaluated third-order diagrams with intermediate states up to  $4\hbar\omega$  excitation (in a double-partition scheme) and found significant contributions from the  $4\hbar\omega$  intermediate states. In view of the above it is expected that one would have to include intermediate states of still higher energy in order to obtain convergence of the intermediate-state summation.

The need for a second correction arises from the neglect of the starting energy dependence of the  $G$  vertices in the early calculations of the higher-order diagrams. As pointed out above, the  $G$  matrix elements of Kuo and Brown (1966, 1968; see also Kuo, 1967) were independent of the starting energy  $\omega$ . This is an approximation which has been removed in more recent calculations of the  $G$  matrix (e.g., Barrett *et al.*, 1971; Sauer, 1970; Krenciglowa *et al.*, 1976b). Thus one should evaluate the higher-order diagrams using  $G$  vertices with the proper starting energy everywhere. As an example, consider the second-order core-polarization diagram  $G_{3p-1h}$  of Fig. 30(a), which is derived in detail in Appendix D. As shown in Eqs. (D5) and (D6), the lower and upper  $G$  vertices in  $G_{3p-1h}$  have starting energies  $\omega_L = e_{j_1} + e_{j_H}$  and  $\omega_U = e_{j_1} + e_{j_2} + e_{j_H} - e_{j_3}$ , respectively. These differ from the energy  $\omega_0 = e_{j_1} + e_{j_2}$  of the initial particles (which trivially is the starting energy of  $G$  in the first-order bare matrix element) and are hence said to be off the energy shell by the amounts  $\Delta\omega_L = e_{j_2} - e_{j_H}$  and  $\Delta\omega_U = e_{j_3} - e_{j_H}$ . In  $^{18}\text{O}$ ,  $\Delta\omega$  is 1 or  $2\hbar\omega$ , depending on whether the hole is in the  $(0s)$  or  $(0p)$  shell. The inclusion of off-energy-shell effects will make the  $G$  vertices smaller in magnitude, since the energy denominators in  $G$  are increased. The detailed  $\Delta\omega$  dependence of  $G$  is determined by the intermediate-state spectrum used in calculating the  $G$  matrix. If the plane-wave choice is made, the off-shell corrections are fairly small, although not negligible (Pradhan *et al.*, 1972).

Another choice which is frequently made for the intermediate-state spectrum is a harmonic oscillator shifted by a constant energy  $C$ . As we have remarked in Sec. III.B, this gives results similar to the plane-wave case if a suitable value of  $C$  is chosen ( $\approx 35$  MeV). However, if smaller values of  $C$  are employed the energy denominators are smaller, so the off-shell corrections are much more important (Sandel *et al.*, 1977; Vary and Yang, 1977). On a slightly different tack, we remark here that the dependence of the second- and third-order diagrams on the parameter  $C$  has been examined (Barrett, 1974; Herbert and Barrett, 1975; Sandel *et al.*, 1977; Vary and Yang, 1977). The behavior of the perturbation expansion appears somewhat improved for values of  $C$  smaller than 35 MeV. In our opinion, however, none of the calculations to date offer convincing evidence that low-order perturbation theory is adequate. Further, we feel that plane waves are the most reasonable choice for very high-lying states, although the question of the optimum choice for medium excitations remains open.

A third and more serious complication is that we do not really know what to expect from a low-order perturbation calculation of the effective interaction in  $^{18}\text{O}$ , since the order-by-order perturbation series will ultimately diverge because of the presence of so-called intruder states. It is seen from Fig. 31 that the calculations do not reproduce all the low-lying experimental levels shown. Phenomenological work, for instance by Engeland (1965), Benson and Flowers (1969), Ellis and Engeland (1970), Fortune and Headley (1974), Erikson and Brown (1977), and Lawson *et al.* (1976), indicates that the second  $0^+$  level and the third  $2^+$  level are mainly of  $(sd)^4p^{-2}$  structure; such low-lying particle-hole states are often referred to as deformed states. The  $0_2^+$  and  $2_3^+$  wave functions therefore have only small components in the  $(sd)^2$  valence space, and we would not expect to reproduce these levels in our calculation. Furthermore, since these  $(sd)^4p^{-2}$  states move down and intermingle with the  $(sd)^2$  states as the interaction is switched on, they must be classified as intruder states. This implies that the order-by-order perturbation expansion (in  $V$  strictly) must diverge, as discussed in Sec. II.E. This could be the reason for the large third- and fourth-order results; however, the intruder state problem does not arise for the effective charge, and as we shall see, the order-by-order results do not appear to be convergent. Also, Goode and Koltun (1975) find no evidence for convergence of the effective interaction in  $^9\text{Li}$ , where there are no intruder states. It seems reasonable to conclude that the basic reason for the poor behavior of the low-order perturbation expansion is that the  $G$  matrix elements are not sufficiently weak. The intruder state singularities are unlikely to influence low-order calculations strongly, although they probably make things worse (Pittel, 1976).

As discussed in Sec. II.E, reordering of the perturbation series can in principle yield a convergent expansion. A preliminary calculation in this vein was carried out by Krenciglowska *et al.* (1973), who extrapolated the sum of all the nonfolded diagrams (ignoring those with HF insertions) from the lowest three orders, using Padé approximants. The folded diagrams were then

evaluated from the sum of nonfolded diagrams (not all folded contributions were included), and apparent convergence was obtained. But this is clearly no longer an order-by-order summation of the perturbation expansion. From a purely practical point of view, it would be difficult to include the effects of low-lying deformed states via perturbation theory. It is probably most sensible to think of first calculating the  $(sd)^2$  effective interaction and then including a few low-lying deformed states explicitly in some (as yet to be determined) fashion before making very detailed comparisons with experiment. This is, in principle, the philosophy followed by Brown and collaborators in the so-called coexistence model (see Brown and Green, 1966; Gerace and Green, 1967; Erikson and Brown, 1977). One might then argue that in calculating the  $(sd)^2$  effective interaction one should not include diagrams with four-particle two-hole ( $4p - 2h$ ) intermediate states to avoid double counting. However, the majority of  $4p - 2h$  states are not intruder states, so one would probably make less error by including diagrams with  $4p - 2h$  intermediate states.

In conclusion, the perturbation expansion for the effective interaction does not appear to give reliable results when summed order by order in  $G$ . Although the results, as pointed out, are not conclusive because of the neglect of important corrections, one is eventually led to consider alternate ways of summing the perturbation expansion. Various such methods will be discussed in Sec. III.D.

## 2. Effective charge

We have pointed out previously that all the observable operators of interest in the shell model should be replaced by effective operators acting in the truncated valence space. Here we shall only discuss calculations of the effective electric quadrupole ( $E2$ ) operator for a single particle beyond the  $^{16}\text{O}$  closed-shell core. The necessary formalism has been discussed in Sec. II.D. It is customary to express the results in terms of an effective charge by dividing the matrix elements of the effective operator by the corresponding proton matrix elements of the bare operator, evaluated with harmonic oscillator wave functions  $\chi$ . Thus, in the notation of Eq. (2.70), the effective  $E2$  charge is given by

$$e_{fi}^{\text{eff}} = \frac{\langle f | \mathcal{E}_{2\mu} | i \rangle}{\langle \chi_f | \mathcal{E}_{2\mu} | \chi_i \rangle_{\text{proton}}} \equiv \frac{\langle \Psi_{Df} | \mathcal{E}_{2\mu}^{\text{eff}} | \Psi_{Di} \rangle}{\langle \chi_f | \mathcal{E}_{2\mu} | \chi_i \rangle_{\text{proton}}},$$

where

$$\mathcal{E}_{2\mu} = \sum_{\text{protons}} e r^2 Y_{2\mu}(\hat{\mathbf{r}}), \quad (3.13)$$

and we have  $e_{fi}^{\text{eff}} = e_{if}^{\text{eff}}$ .

As regards the experimental situation in mass 17, the data yield effective charges of about 0.5 for the odd neutron. For the odd proton the  $\gamma$  decay from the  $0.5$  MeV  $1/2^+$  level to the  $5/2^+$  ground state yields a value of 1.75 (with  $\hbar\omega = 14$  MeV). This large value is surely due to the fact that the  $1/2^+$  level is bound by only 0.1 MeV, and if one applies a simple correction for this effect, using wave functions calculated in a Woods-Saxon potential, one obtains a value of somewhat less than 1.5. So we need a proton effective charge of about 1.5, and a

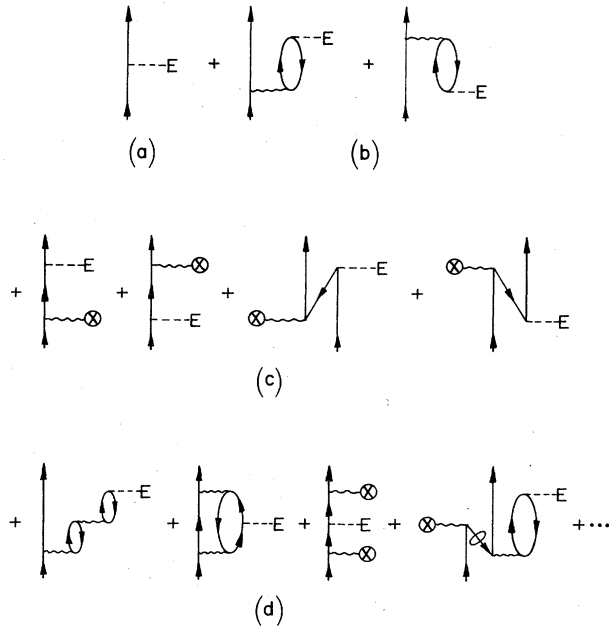


FIG. 35. Low-order contributions to the effective charge for a single valence nucleon. The electric multipole operator is represented by a dashed line with a letter  $E$ .

neutron effective charge of about 0.5, and this is consistent with shell-model studies in this region (see, for example, Halbert *et al.*, 1971). Values of this magnitude were obtained by Mottelson (1959), who evaluated the distortion of the closed shells due to the odd particle by filling particles in an anisotropic harmonic oscillator well and equating the shape of the density distribution with the shape of the potential. The first microscopic perturbation calculation of the effective  $E2$  operator was performed by Horie and Arima (1955), who evaluated static electric quadrupole moments for a number of nuclei to first order in the interaction  $V$ —which was taken to be of  $\delta$ -function form.

With the above experimental values in mind, let us turn to the calculation of the effective charge order by order in the reaction matrix  $G$ . The diagrammatic representation of low-order terms in the perturbation expansion for the effective operator is given in Fig. 35. Shown there are the zeroth-order diagram (a) represent-

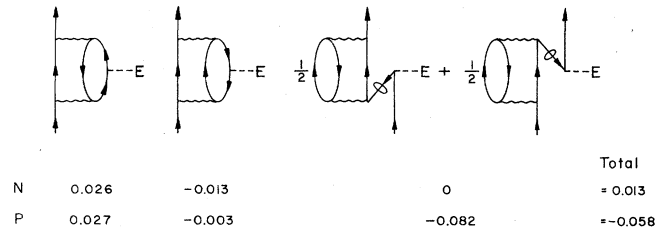


FIG. 36. Contributions from a number-conserving set to the  $d_{5/2}$ - $d_{5/2}$  effective charge. The calculated values are taken from Ellis and Siegel, 1971.

ing the bare operator, the first-order core-polarization (b) and Hartree-Fock (HF) insertion (c) diagrams, and a few of the many second-order diagrams (d), some of which are folded. Results are shown in Table III, where the notation  $d_{3/2}-s_{1/2}$  indicates the effective charge for a transition between the  $0d_{3/2}$  and  $1s_{1/2}$  single-particle states and  $N(P)$  refers to neutron (proton). Consider first the non-HF diagrams, which were evaluated through second order in  $G$  by Ellis and Siegel (1971), using the Kuo-Brown matrix elements (Kuo, 1967) and allowing intermediate states of  $2\hbar\omega$  excitation energy. The lowest-order core-polarization contribution is found to be important here, as with the effective interaction, although quantitatively insufficient. We have discussed the physical meaning of core polarization in the previous Sec. III.C.1, but it is worth noting that only quadrupole excitations of the core contribute here, in contrast to the effective interaction. Further, the particle and hole excited must both be protons, since the electric quadrupole operator only acts on protons. Since a valence proton can only excite protons via the  $T=1$  interaction, whereas a valence neutron can employ both the  $T=0$  and  $T=1$  interactions, we expect the core-polarization contribution to the effective charge for neutrons to be larger than that for protons, as seen in Table III.

As regards the total second-order results for the non-HF diagrams, we see from Table III that they are negative for protons, so there is very little evidence for convergence. Part of the reason for this is that the number-conserving sets cancel poorly. An example is shown in Fig. 36, where exact cancellation would follow if  $E$  were the number operator. Clearly, the folded diagram is too large for accurate cancellation, and we have remarked that this is often the case for the effective

TABLE III. Low-order results for the effective  $E2$  charge in the  $(1s0d)$  shell.

Order	Transition	$d_{5/2}-d_{5/2}$		$d_{3/2}-s_{1/2}$	
		N	P	N	P
0th order		0	1	0	1
1st order	Non-HF <sup>a</sup>	0.28	0.11	0.20	0.06
	HF <sup>b</sup>	0	0.08	0	0.34
	Total	0.28	0.19	0.20	0.40
2nd order	Non-HF <sup>a</sup>	0.06	-0.06	0.01	-0.16
	HF <sup>b</sup>	-0.18	-0.07	-0.08	0.11
	Total	-0.12	-0.13	-0.07	-0.05
0th+1st+2nd	Total	0.16	1.06	0.13	1.35

<sup>a</sup>Ellis and Siegel, 1971.

<sup>b</sup>Ellis and Mavromatis, 1971.

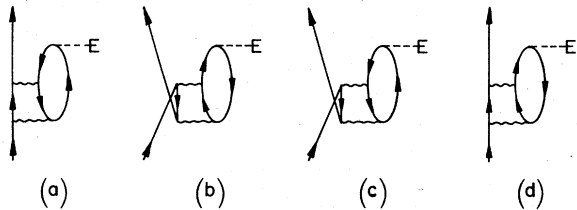


FIG. 37. Second-order vertex correction diagrams for the effective charge.

interaction too. In fact the qualitative behavior of corresponding diagrams for the effective charge and interaction is quite similar. Thus, the second-order (in  $G$ ) diagrams for the effective charge shown in Fig. 37 are analogous to the third-order diagrams for the effective interaction shown in Fig. 47 and give quite large contributions. We might remark that the second-order diagram in Fig. 37(d) has been omitted, since it is included in the first-order core-polarization diagram. One could, however, use a double-partition approach, as discussed for the effective interaction, and exclude from the intermediate states which go into the  $G$  matrix all  $2\hbar\omega$  excitations. In that case one would need to include the diagram of Fig. 37(d) in the second-order calculations, and one wonders whether this would improve the convergence. The answer is probably no, since, although it gives a significant contribution for neutrons of about 0.06, the contribution for protons is very small.

We now turn to the HF corrections. In Fig. 35 we have shown the first-order (c) and a few of the second-order (d) HF diagrams which arise. These were evaluated by Ellis and Mavromatis (1971), and their total contributions in each order are shown in Table III. [Note that the original Sussex interaction (Elliott *et al.*, 1968) was used and that some intermediate states of more than  $2\hbar\omega$  excitation energy were included—these features should, however, not be of importance for our qualitative considerations.] We see large HF effects for protons in first order, which arise because the infinite nature of the harmonic oscillator well serves to pull in the wave functions of these weakly bound valence orbitals too much. This results in too small a value for the matrix element of  $r^2$ , which is being corrected in lowest order by the HF insertions. In second order, many diagrams contribute, and the total value is usually negative. Adding non-HF and HF contributions, we find that the second-order total is very roughly  $-\frac{1}{3}$  of the first-order total. If we assume that we have a geometric series, this would imply that the full result is  $\frac{3}{4}$  of the first-order value. This would of course be too small. The only conclusion to be drawn from Table III is that there is no smooth order-by-order convergence in the perturbation expansion towards the desired values.

One might worry whether admixtures of low-lying deformed particle-hole states produce strong effects. In principle, of course, the perturbation formalism includes such effects, but in practice it would be very difficult to get accurate results, since the states in question have been so strongly shifted from their unperturbed positions. The evidence from phenomenological calculations (see Brown *et al.*, 1977) is that such effects are small, although not negligible. Incidentally, Brown

*et al.* (1977) analyze very carefully the empirical effective charges required by the data, but the reader is warned that they use a Woods-Saxon basis to evaluate the denominators of Eq. (3.13).

We would like to comment briefly on the effect of high-lying intermediate states in the non-HF diagrams. The first point to note is that the matrix elements of  $r^2$ , taken with harmonic oscillator wave functions, are nonzero only for single-particle states which differ by 0 or  $2\hbar\omega$  in energy. Thus the core-polarization diagrams of Fig. 35(b) only involve  $2\hbar\omega$  excitations for an oscillator basis. There are, however, other diagrams starting in second order which are not zero for more than  $2\hbar\omega$  excitations. For the two number-conserving sets of diagrams (one set is shown in Fig. 36), such effects have been found by Shimizu *et al.* (1974) to be small. They are, however, more significant in calculations of the effective magnetic dipole operator.

In conclusion, the perturbation expansion for the effective charge appears to show no clear evidence of convergence when summed order by order in  $G$ . Thus, just as for the effective interaction, one is led to consider alternate ways of summing the perturbation expansion, as discussed in the following Sec. III.D.

*Summary.* We have reviewed calculations of low-order contributions to the effective interaction and charge appropriate to masses 18 and 17, respectively. Although uncertainties exist, none of the calculations to date indicate smooth convergence to the results expected from the experimental energy spectra and electric quadrupole transition rates.

#### D. Calculation of effective operators by infinite partial summations

The apparent failure of the perturbation expansions for the effective interaction and charge to converge smoothly to the empirical values, when summed to successive powers in  $G$ , calls for alternate methods of summation. These involve regrouping the series into infinite sub-series of related diagrams which can be summed exactly or approximately. We shall refer to such methods as *infinite partial summations*. In fact, we have already used the idea of partial summation when we constructed the reaction matrix  $G$  by separate summation of all two-particle ladder diagrams in  $V_{12}$ . This is indeed a striking example of how partial summation may facilitate the convergence of the perturbation expansion when physically significant processes are included. In this section we shall consider other important processes which can be treated by partial summation.

##### 1. Effective interaction

In Sec. III.C we demonstrated that the effective interaction between two valence nucleons is strongly renormalized by core polarization. However, in the second- and third-order core-polarization diagrams considered above [see Figs. 30(a) and 34(d)] the core excitations were treated only to zeroth and first order, respectively. Since one knows that particle-hole states in closed-shell nuclei show strong collective properties, one would probably obtain a better approximation for the

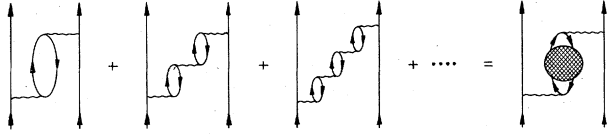


FIG. 38. Diagrams summed in the TDA treatment of core polarization. The contributions obtained by exchanging the external valence lines are implied; see discussion of Appendix D.

core excitations by iterating the particle-hole bubble to arbitrary order, as shown in Fig. 38. This series of diagrams can be expressed in terms of the two vertices  $\nu$  and  $f$  defined in Fig. 39. The vertex  $\nu$  couples a valence particle to an unperturbed core excitation (i.e., particle-hole pair), while the vertex  $f$  is the particle-hole interaction which "scatters" one unperturbed core excitation into another. Considering  $\nu$  and  $f$  as matrices, we can readily write the diagrammatic series of Fig. 38 in matrix notation as

$$G_{\text{TDA}} = \nu \frac{1}{\epsilon} \nu + \nu \frac{1}{\epsilon} f \frac{1}{\epsilon} \nu + \nu \frac{1}{\epsilon} f \frac{1}{\epsilon} f \frac{1}{\epsilon} \nu + \dots = \nu \frac{1}{\epsilon - f} \nu, \tag{3.14a}$$

or more explicitly

$$G_{\text{TDA}} = - \sum_{i,j} \nu |i\rangle \langle i| \frac{1}{\epsilon_i + f} |j\rangle \langle j| \nu, \tag{3.14b}$$

where we have introduced unperturbed particle-hole intermediate states  $i$  defined by

$$(-\epsilon) |i\rangle = \epsilon_i |i\rangle, \tag{3.15}$$

with  $\epsilon_i = (e_p - e_h)_i$ . Note that we have taken the valence-particle states to be degenerate, so that the valence-

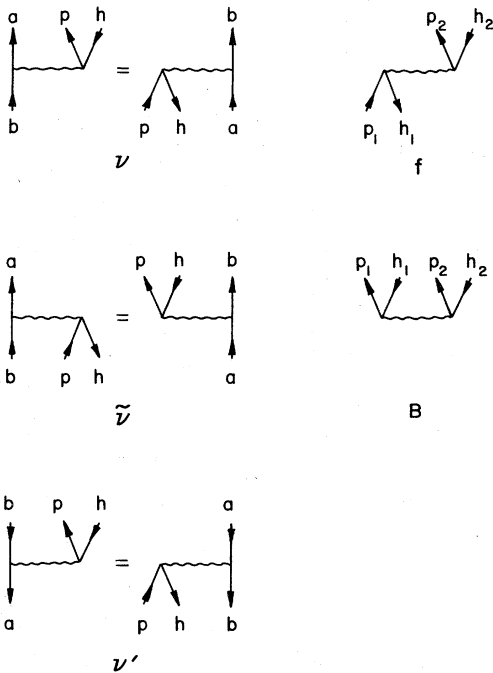


FIG. 39. Elementary vertices for various partial summations.

particle contribution to the energy denominator  $(\epsilon_p - H_0)$  cancels out. We further emphasize that Eq. (3.14b) has been written out in the particle-hole representation; this corresponds to calculating diagrams in the so-called cross channel (see, for example, Baranger, 1960; Lane, 1964).

It follows from Eq. (3.14) that the infinite subset of core-polarization diagrams shown in Fig. 38 can be summed simply by means of matrix inversion (Zamick, 1969). The series can also be summed by iteration (Ellis and Siegel, 1970), corresponding to explicit calculation of the individual terms on the right-hand side of Eq. (3.14a). An alternate method of calculation, which lends itself to direct physical interpretation, can be obtained from Eq. (3.14b) by expanding  $\langle i | (\epsilon_i + f)^{-1} | j \rangle$  in the basis diagonalizing  $(-\epsilon + f)$ . Denoting the particle-hole eigenstates of  $(-\epsilon + f)$  by  $\alpha$ , i.e.,

$$(-\epsilon + f) |\alpha\rangle = \epsilon_\alpha |\alpha\rangle$$

with

$$|\alpha\rangle = \sum_i X_{\alpha i} |i\rangle, \tag{3.16}$$

we have

$$\langle i | \frac{1}{(-\epsilon + f)} | j \rangle = \sum_\alpha \frac{X_{\alpha i} X_{\alpha j}}{\epsilon_\alpha}. \tag{3.17}$$

Substituting this back into Eq. (3.14b), we obtain

$$G_{\text{TDA}} = - \sum_{i,j} \nu |i\rangle \frac{X_{\alpha i} X_{\alpha j}}{\epsilon_\alpha} \langle j| \nu. \tag{3.18}$$

Thus in this approach, which was followed by Osnes and Warke (1969), the total core-polarization contribution to the effective interaction is given as the sum of the contributions from the individual eigenstates of the core, which are represented by the cross-hatched bubble on the right-hand side of the equation in Fig. 38. The calculation of core eigenstates in the basis of  $1p-1h$  states is often referred to as the Tamm-Dancoff approximation (TDA)—see, for example, Lane (1964)—hence the subscript on the left-hand side of Eqs. (3.14) and (3.18). It is instructive to compare the TDA result (3.18) with the lowest-order core-polarization term, which in the present notation takes the form

$$G_{3p-1h} = - \sum_i \nu |i\rangle \frac{1}{\epsilon_i} \langle i| \nu. \tag{3.19}$$

Thus, if there is a strong collective state with  $\epsilon_\alpha \ll \epsilon_i$ , the TDA result can be considerably enhanced over the lowest-order one. Clearly the TDA summation diverges for  $\epsilon_\alpha = 0$ ; however, it has a finite solution for  $\epsilon_\alpha < 0$  which must be rejected on physical grounds, since it corresponds to a  $1p-1h$  state below the  $0p-0h$  ground state (i.e., instability of the vacuum against  $1p-1h$  excitations). Such a situation is signaled by the divergence of the iterated solution of Eq. (3.14a).

Now, the particle-hole interaction across two oscillator shells (since the particle-hole states must have positive parity) has strong isoscalar monopole and quadrupole components which produce low-lying collective  $T''=0, J''=0$  and  $T''=0, J''=2$  states in TDA. For example, in  $^{16}\text{O}$  these states come at 10.4 and 15.3 MeV, respectively, compared to an unperturbed particle-hole

TABLE IV. Contributions from phonons of various  $T'', J''$  to the core-polarization matrix element  $\langle d_{5/2}^2 J=0, T=1 | \mathcal{U}_\nu | d_{5/2}^2 J=0, T=1 \rangle$  in various approximations. All energies in MeV.

$T''$	$J''$	$3p-1h^a$	TDA <sup>a</sup>	RPA <sup>a</sup>	Screened TDA <sup>a</sup>	Screened RPA <sup>a</sup>	SCCE(B) <sup>b</sup>
0	0	-0.048	-0.087	-0.409	-0.061	-0.068	-0.149
	1	0.071	0.064	0.068	0.059	0.055	0.078
	2	-0.629	-1.061	-1.458	-0.822	-0.912	-0.375
	3	0.072	0.074	0.076	0.075	0.073	0.072
	4	-0.213	-0.229	-0.239	-0.225	-0.229	-0.103
1	5	0.089	0.086	0.084	0.084	0.078	0.271
	0	-0.008	-0.007	-0.006	-0.007	-0.007	-0.007
	1	0.030	0.026	0.023	0.025	0.022	0.023
	2	-0.134	-0.111	-0.106	-0.114	-0.118	-0.127
	3	0.062	0.056	0.054	0.055	0.052	0.090
Total	4	-0.065	-0.060	-0.058	-0.062	-0.062	-0.112
	5	0.018	0.017	0.017	0.017	0.016	0.150
Total		-0.755	-1.232	-1.956	-0.975	-1.098	-0.190

<sup>a</sup>Kuo and Osnes, 1974.

<sup>b</sup>Kirson, 1974 and private communication.

energy  $\epsilon_i = 2\hbar\omega$  of 28 MeV. In <sup>40</sup>Ca the situation is even more dramatic, the corresponding energies being 3.1 and 9.4 MeV versus the unperturbed 21 MeV. Thus one would expect strong enhancement of the core polarization in TDA compared to lowest order. By and large the main contribution comes, as shown in Table IV, from the  $T''=0, J''=2$  state, which couples more strongly to the valence-particle states than does the more collective  $T''=0, J''=0$  state. This is due to the fact that the radial density distribution of the  $J''=0$  state has a node approximately where the valence-particle distribution is peaked, so there is a cancellation between the contributions from the interior and exterior regions. This cancellation is less effective when the valence-particle state has a node; in such cases there may be a substantial contribution from the collective  $T''=0, J''=0$  state. For other values of  $T'', J''$  the effect of summing the TDA series is fairly small, although Table IV does show a tendency for the  $T''=0$  contributions to increase and the  $T''=1$  contributions to decrease. This simply reflects the attractive (repulsive) nature of the particle-hole interaction in  $T''=0(1)$  states. Typical core-polarization matrix elements for two valence nucleons in the (1s0d) shell are shown in Table V, while the  $T=1$  spectra obtained with core-polarization corrections evaluated in lowest order and in TDA are compared in columns 5 and 6 of Fig. 31.

The mechanism behind the TDA enhancement of the core-polarization correction becomes particularly

transparent in the degenerate schematic model of Brown and Bolsterli (1959), where a *single* collective state is pushed far away from its unperturbed position and endowed with all of the transition strength. The schematic model (see Brown, 1971a) assumes a separable particle-hole interaction

$$f = \lambda |M\rangle\langle M| \tag{3.20a}$$

with matrix elements

$$\langle i | f | j \rangle = \lambda \langle i | M \rangle \langle M | j \rangle \equiv \lambda M_i M_j. \tag{3.20b}$$

Here,  $|M\rangle$  is to be interpreted as a multipole operator acting on the ground-state vacuum, so that  $M_i = \langle i | M | 0 \rangle$ . If one further assumes *degenerate* unperturbed particle-hole energies  $\epsilon_i = \epsilon_{ph}$ , one easily obtains for the collective state the following energy and transition amplitude to the ground state

$$\begin{aligned} \epsilon_\alpha &= \epsilon_{ph} + \lambda \sum_i M_i^2, \\ \langle M | \alpha \rangle &= \left( \sum_i M_i^2 \right)^{1/2}. \end{aligned} \tag{3.21a}$$

For the noncollective states we have

$$\epsilon_\beta = \epsilon_{ph}, \langle M | \beta \rangle = 0 \quad (\beta \neq \alpha). \tag{3.21b}$$

Inserting this into Eq. (3.18) and further assuming separable  $\nu$  vertices

$$\nu = \kappa |M\rangle\langle M|, \tag{3.22}$$

TABLE V. Core-polarization contributions to matrix elements  $\langle v_1^2 J=0, T=1 | \mathcal{U}_\nu | v_2^2 J=0, T=1 \rangle$  of the effective interaction in various approximations. All matrix elements are in MeV.

Valence orbits		$G^a$	$3p-1h^b$	TDA <sup>b</sup>	RPA <sup>b</sup>	Screened TDA <sup>b</sup>	Screened RPA <sup>b</sup>	SCCE(B) <sup>c</sup>
$v_1$	$v_2$							
$d_{5/2}$	$d_{5/2}$	-1.236	-0.755	-1.232	-1.956	-0.975	-1.098	-0.190
$d_{5/2}$	$d_{3/2}$	-3.025	-0.581	-0.915	-1.239	-0.786	-0.909	0.167
$s_{1/2}$	$s_{1/2}$	-2.049	0.046	-0.441	-4.604	-0.159	-0.280	-0.139

<sup>a</sup>Kuo, 1967.

<sup>b</sup>Kuo and Osnes, 1974.

<sup>c</sup>Kirson, 1974.

we obtain for the core-polarization correction in TDA

$$G_{\text{TDA}} = -\kappa^2 \frac{\sum_i M_i^2}{\epsilon_{\text{ph}} + \lambda \sum_i M_i^2} |M\rangle \langle M|. \quad (3.23)$$

For comparison, the lowest-order contribution (3.19) takes the form

$$G_{3p-1h} = -\kappa^2 \frac{\sum_i M_i^2}{\epsilon_{\text{ph}}} |M\rangle \langle M|. \quad (3.24)$$

Thus, in the schematic model, the TDA result for the core polarization is enhanced over the lowest-order estimate by a factor

$$\frac{G_{\text{TDA}}}{G_{3p-1h}} = \frac{\epsilon_{\text{ph}}}{\epsilon_{\text{ph}} + \lambda \sum_i M_i^2}. \quad (3.25)$$

Now, the separability condition (3.20) is roughly satisfied by the  $T''=0, J''=0$  particle-hole interaction of Kuo and Brown (Sprung and Jopko, 1972). For the  $T''=0, J''=2$  interaction the separability is not quite as good, but the TDA enhancement of the core polarization obtained in realistic calculations (Osnes *et al.*, 1971; Kuo and Osnes, 1974) is very roughly reproduced by the simple estimate (3.25) of the schematic model.

In the TDA the particle-hole excitations are defined relative to the unperturbed closed-shell ground state. However, the physical ground state of a closed-shell nucleus contains ground-state correlations or vacuum fluctuations, as shown in Fig. 40. If we allow for ground-state correlations of the type indicated, core polarization can take place via "backward-going" bubbles also, as shown in Fig. 41. The inclusion of such diagrams along with the TDA ones corresponds to calculating the core excitations in the random-phase approximation (RPA). This is known to increase the collectivity of the low-lying particle-hole states as compared to TDA, and thus we would expect further enhancement of the core polarization in RPA.

Using the schematic matrix notation introduced by Kirson (1971), it is easy to write down the RPA perturbation series for the core polarization. Defining additional vertices  $\bar{\nu}$  (which is essentially the transpose of  $\nu$ ) and  $B$  as shown in Fig. 39, we have

$$G_{\text{RPA}} = \nu \frac{1}{\epsilon - f} \nu + \bar{\nu} \frac{1}{\epsilon - f} B \frac{1}{\epsilon - f} \nu + \nu \frac{1}{\epsilon - f} B \frac{1}{\epsilon - f} B \frac{1}{\epsilon - f} \nu + \bar{\nu} \frac{1}{\epsilon - f} B \frac{1}{\epsilon - f} B \frac{1}{\epsilon - f} B \frac{1}{\epsilon - f} \nu + \dots \quad (3.26a)$$

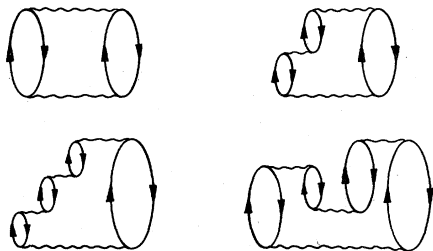


FIG. 40. Ground-state correlation diagrams contributing to the energy of a closed-shell nucleus. Note that if the first diagram is explicitly included, the  $G$  matrix must be defined in such a way that no double counting occurs.

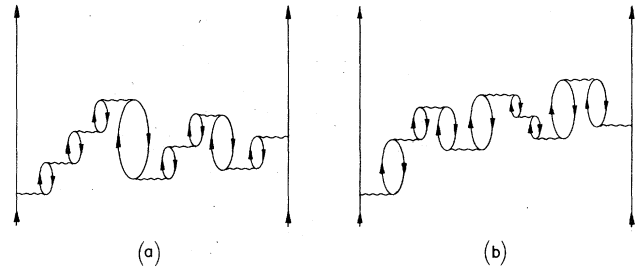


FIG. 41. Contributions to core polarization in the RPA.

Here, each energy denominator  $(\epsilon - f)^{-1}$  arises from a TDA string of bubbles [see Eq. (3.14a)]. Since we take all relative orderings of the particle-hole vertices in different strings, the factorization theorem (see Sec. II.B.5) can be applied, and hence the TDA strings can be treated independently of each other. Further, as seen from Fig. 41, terms with an even or odd number of  $B$  vertices terminate in  $\nu$  or  $\bar{\nu}$  vertices, respectively. Thus the series (3.26a) splits into two subseries which can easily be summed to give

$$G_{\text{RPA}} = \left[ \nu + \bar{\nu} \frac{1}{\epsilon - f} B \right] \frac{1}{\epsilon - f - B[1/(\epsilon - f)]B} \nu. \quad (3.26b)$$

This has been shown by Ellis and Siegel (1970) to be equivalent to

$$G_{\text{RPA}} = - \sum_{\alpha} \nu \frac{|\bar{\alpha}\rangle \langle \bar{\alpha}|}{\bar{\epsilon}_{\alpha}} \nu, \quad (3.27)$$

which was used by Osnes and Warke (1969). Here  $|\bar{\alpha}\rangle$  and  $\bar{\epsilon}_{\alpha}$  are the RPA eigenstates and eigenvalues [for a simple discussion of the RPA, the reader is referred to the monographs by Lane (1964) and Brown (1971a)]. Equation (3.26) is less transparent than Eq. (3.27), but can be evaluated by matrix inversion (Zamick, 1969) or iteration (Ellis and Siegel, 1970) without first having to solve the RPA equations.

The form of Eq. (3.27) is analogous to that of the TDA expression in Eq. (3.18), which can be rewritten as

$$G_{\text{TDA}} = - \sum_{\alpha} \nu \frac{|\alpha\rangle \langle \alpha|}{\epsilon_{\alpha}} \nu, \quad (3.18')$$

where  $|\alpha\rangle$  and  $\epsilon_{\alpha}$  are the TDA eigenstates and eigenvalues. Thus, if the core polarization is dominated by a single collective state (as is often the case in realistic calculations), the RPA result will be enhanced over the TDA result if  $\bar{\epsilon}_{\alpha} < \epsilon_{\alpha}$ . In fact, further enhancement comes from the RPA wave function in the numerator and is due to correlations between TDA bubbles induced by the  $B$  vertices. These features can be neatly illustrated in an extended version of the degenerate schematic model, discussed above, in which  $B$  vertices of separable form

$$B = \lambda |M\rangle \langle M| \quad (3.28)$$

are included. The energy of the collective state is now given by (Brown, 1971a)

$$\bar{\epsilon}_{\alpha} = \left[ \epsilon_{\text{ph}} \left( \epsilon_{\text{ph}} + 2\lambda \sum_i M_i^2 \right) \right]^{1/2}. \quad (3.29)$$

Comparison with the corresponding TDA energy  $\epsilon_{\alpha}$  of

Eq. (3.21a) shows that the ground-state correlations serve to lower the collective state. Furthermore, this effect can be quite dramatic. For example, if the energy of the TDA state is  $\frac{1}{2}\epsilon_{ph}$ , the RPA state will come at zero energy, corresponding to instability of the ground state. As remarked above, the ground-state correlations also affect the wave function of the collective state. Thus, in RPA, the transition amplitude to the ground state is

$$\langle M | \bar{\alpha} \rangle = \left[ \frac{\epsilon_{ph}}{\bar{\epsilon}_\alpha} \sum_i M_i^2 \right]^{1/2}, \quad (3.30)$$

compared to  $[\sum_i M_i^2]^{1/2}$  in TDA (Brown, 1971a). Hence, for an attractive force ( $\lambda < 0$ ), the transition strength is enhanced in RPA.

Then consider the RPA estimate of the core polarization in the schematic model. By simple algebra we obtain from Eq. (3.27)

$$G_{\text{RPA}} = -\kappa^2 \frac{\langle M | \bar{\alpha} \rangle^2}{\bar{\epsilon}_\alpha} |M\rangle \langle M| = -\kappa^2 \frac{\sum_i M_i^2}{\epsilon_{ph} + 2\lambda \sum_i M_i^2} |M\rangle \langle M|. \quad (3.31)$$

Thus the RPA result is enhanced over the lowest-order one [see Eq. (3.24)] by a factor

$$\frac{G_{\text{RPA}}}{G_{3p-1h}} = \frac{\epsilon_{ph}}{\epsilon_{ph} + 2\lambda \sum_i M_i^2}. \quad (3.32)$$

This can be compared with the corresponding TDA result of Eq. (3.25). We have thus demonstrated that the enhancement of the core polarization obtained in RPA for an attractive particle-hole interaction is due partly to correlations in the wave function (leading to increased transition strength) and partly to a decrease in the energy.

Again, the results of realistic calculations (Kuo and Osnes, 1974) are in qualitative agreement with the predictions of the schematic model. In  $^{16}\text{O}$  collective  $T'' = 0, J'' = 0$  and  $T'' = 0, J'' = 2$  particle-hole states are obtained in RPA at 5.4 and 14.5 MeV, respectively, compared to 10.4 and 15.3 MeV in TDA. In  $^{40}\text{Ca}$  the  $T'' = 0, J'' = 0$  state has an imaginary energy in RPA—indicating instability of the ground state—while the  $T'' = 0, J'' = 2$  state comes at 6.8 MeV, the corresponding energies in TDA being 3.1 and 9.4 MeV. The contributions to the diagonal  $T = 1, J = 0$  ( $d_{5/2}$ )<sup>2</sup> matrix element from these and other (less collective) core excitations are given in Table IV, and comparison with the corresponding contributions in lowest order and TDA shows that the enhancements of the  $T'' = 0, J'' = 0$  and  $T'' = 0, J'' = 2$  contributions are in rough agreement with the schematic model. Similar enhancements are reflected in the total core-polarization matrix elements shown in Table V. We further see from Fig. 31 (column 7) that evaluating the core-polarization correction in RPA leads to a dramatic increase in the binding energies of the low-lying states in  $^{18}\text{O}$ . In  $^{42}\text{Ca}$  the effect is still more pronounced, the calculated ground-state energy being about -7 MeV (excluding of course the effect of the collective monopole state, which has an imaginary energy), compared to an experimental value of about -3 MeV.

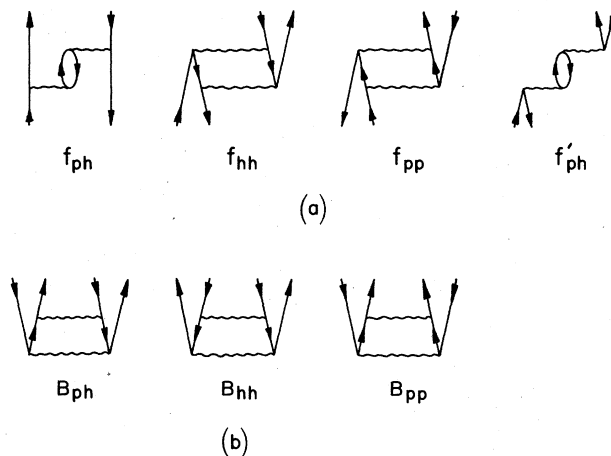


FIG. 42. Second-order corrections to the particle-hole (a) and ground-state correlation (b) vertices.

This strong enhancement of the core polarization is clearly not physical. This is also obvious from the calculated energies of the collective isoscalar monopole and quadrupole states. Experimentally, there are simply no such states at these low energies. From inelastic scattering data there is, however, evidence for a broad resonance at approximately  $60\text{--}70 A^{-1/3}$  MeV (corresponding to 24–28 MeV in  $^{16}\text{O}$  and 18–20 MeV in  $^{40}\text{Ca}$ ) which could be the isoscalar monopole or quadrupole state, but most likely the quadrupole one (Satchler, 1972).<sup>3</sup> Reasonable estimates of these positions have been obtained by introducing a phenomenological density dependence in the particle-hole interaction (Sharp and Zamick, 1973, 1974). However, to our knowledge, no density-independent realistic interaction has succeeded in reproducing the positions of the isoscalar monopole and quadrupole states.

In view of this, one was led to consider corrections to the particle-hole interaction similar to those introduced in Fig. 30a for the particle-particle interaction. Various such corrections are shown in Fig. 42(a). Here the term  $f_{ph}$  is a core-polarization correction—but now in the particle-hole interaction. In physical terms it may be interpreted just as  $G_{3p-1h}$  in Fig. 32—with the valence particle  $v_2$  replaced by a hole. However, contrary to  $G_{3p-1h}$ ,  $f_{ph}$  is mainly repulsive, thus making the  $T'' = 0$  particle-hole interaction less attractive. The effect of  $f_{ph}$  on the TDA bubbles is illustrated in Fig. 43. First, we note that diagram (a), which is obtained using the bare particle-hole interaction  $f$ , is equivalent to diagram (a'), since antisymmetrized particle-hole vertices are used. It is easy to see that inclusion of the correction  $f_{ph}$  gives rise to diagrams of the form (b). In electron gas theory,  $f_{ph}$  is referred to as the self-screening of the exchange term, and we shall adopt this terminology here. We emphasize that the screening—by the exchange of a particle-hole bubble—must take place in the exchange term. In the direct term, bubbles are automatically generated by diagonalization (or iteration) of the bare particle-hole interaction, and thus cor-

<sup>3</sup>Experimental data for  $^{16}\text{O}$  indicate a very broad resonance centered at 21 MeV (Knöpfle *et al.*, 1975).

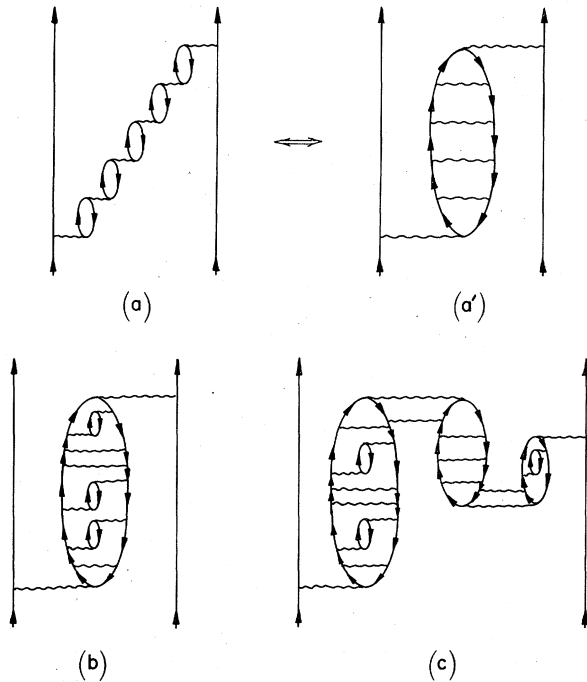


FIG. 43. Comparison of TDA diagram (a, a') obtained with bare particle-hole vertices, and TDA (b) and RPA (c) diagrams obtained with vertices including screening corrections to second order.

rection terms like  $f'_{ph}$  in Fig. 42(a) are not included to avoid double counting. The other corrections shown in Fig. 42(a) are less important than  $f_{ph}$  (Osnes *et al.*, 1971) and will not be further discussed here, except that it should be pointed out that  $f_{pp}$  is only allowed if a doubly partitioned Hilbert space is used, as discussed in the previous Sec. III.C.

Corrections of the type discussed above may also be introduced for the ground-state correlation vertex  $B$ , as shown in Fig. 42(b). Here  $B_{ph}$  is analogous to  $f_{ph}$  for the particle-hole interaction and serves to make  $B$  less attractive. The effect of  $B_{ph}$  (and  $f_{ph}$ ) on the RPA is shown diagrammatically in Fig. 43(c). As discussed in some detail by Kirson (1971), these corrections serve to prevent ground-state correlations from building up in the core, thus reducing the difference between the RPA and TDA. Furthermore, the TDA phonons will be pushed up in energy, since  $f_{ph}$  is predominantly repulsive. Both these features are observed in realistic calculations of the  $2\hbar\omega$  core excitations of interest here (Osnes *et al.*, 1971; Kuo and Osnes, 1973, 1974). In  $^{16}\text{O}$  the inclusion of all the second-order corrections shown in Fig. 42 (except of course  $f'_{ph}$ ) served to increase the energies of the  $T''=0, J''=0$  and  $T''=0, J''=2$  phonons from, respectively, 10.4 and 15.3 MeV to 18.5 and 20.2 MeV in TDA, and from 5.4 and 14.5 MeV to 18.1 and 20.0 MeV in RPA. Furthermore, the RPA transition strengths were reduced by factors of 2.9 and 1.1 for the monopole and quadrupole states, respectively. In  $^{40}\text{Ca}$  the effect of screening was found to be spectacular, raising the monopole state from 3.1 to 13.3 MeV in TDA and from an imaginary energy to 12.7 MeV in RPA. The quadrupole state was raised from 9.2 to 15.7 MeV

in TDA and from 6.8 to 15.5 MeV in RPA. Also, the quadrupole transition strength was reduced by a factor of 1.9 in RPA. It is interesting to note that the positions of the monopole and quadrupole states obtained in the screened TDA and RPA are not too far from those given by Satchler (1972). In passing we remark that similar screening effects have been found for the  $1\hbar\omega$  particle-hole states in various closed-shell nuclei by de Takacsy (1967), Sartoris and Zamick (1967), Barrett (1968), Dieperink *et al.* (1968), Kuo (1968), and Blomqvist and Kuo (1969).

Now, the effect of screening on the core polarization of the effective interaction is easily obtained by substituting the screened phonons into Eqs. (3.18') and (3.27) for the TDA and RPA, respectively. As shown in Table V, the matrix elements are strongly reduced in magnitude compared to the ordinary TDA and RPA. This reduction is, as expected, mainly due to the reduced size of the  $T''=0, J''=2$  contributions, as shown in Table IV. The corresponding energy spectra for  $^{18}\text{O}$  are displayed in columns 8 and 9 of Fig. 31 and show very good agreement with the experimental energy spectrum—probably too good, in view of all the contributions still left out.

The above procedure, in which the particle-hole interaction was corrected by screening (and other processes) to second order, was generalized by Kirson (1971, 1974) to include screening to arbitrary order. Thus a renormalized particle-hole interaction  $f_\infty$  was obtained by summing the series

$$f_\infty = f + \nu' \frac{1}{\epsilon} \nu + \nu' \frac{1}{\epsilon} f_\infty \frac{1}{\epsilon} \nu + \nu' \frac{1}{\epsilon} f_\infty \frac{1}{\epsilon} f_\infty \frac{1}{\epsilon} \nu + \dots$$

$$= f + \nu' [1/(\epsilon - f_\infty)] \nu, \quad (3.33)$$

where the vertices  $f$ ,  $\nu$ , and  $\nu'$  are all defined in Fig. 39. Consider the iterative solution of Eq. (3.33). The first iteration will replace  $f_\infty$  by  $f$  on the right-hand side, thus generating the TDA series shown in Fig. 44(a). The next iteration will use this set of diagrams for  $f_\infty$  on the right-hand side, producing the additional diagrams indicated in Fig. 44(b), where the particle-hole bubbles are nested inside one another. The next iteration will nest the bubbles one step more deeply, as shown in Fig. 44(c), and so on. This requires some care with the energy denominators, which are only schematically treated in Eq. (3.33). It is also worth realizing that while Eq. (3.33) explicitly shows first an interaction with the particle line ( $\nu$ ) and then an interaction with the hole line ( $\nu'$ ), terms with this ordering reversed are also to be included. This corresponds to exchange of the external particle and hole lines.

The physical meaning of Eq. (3.33) should be clear. One obtains the screened particle-hole interaction  $f_\infty$  by renormalizing the bare interaction  $f$  by the same particle-hole excitations which are generated by the screened interaction  $f_\infty$ . In a similar fashion, the ground-state correlation vertex  $B$  may be screened to arbitrary order by

$$B_\infty = B + f_\infty \frac{1}{\epsilon} B + f_\infty \frac{1}{\epsilon} f_\infty \frac{1}{\epsilon} B + \dots$$

$$= B + f_\infty \frac{1}{\epsilon - f_\infty} B. \quad (3.34)$$

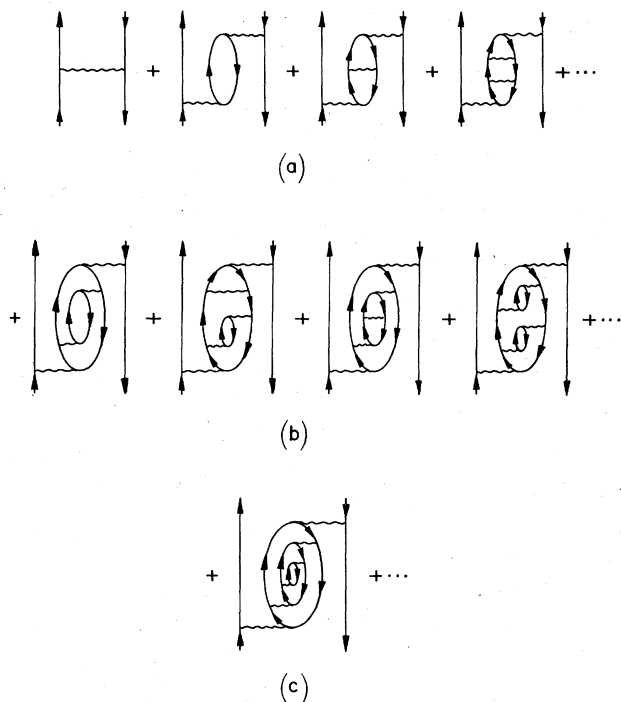


FIG. 44. Diagrams included in the particle-hole interaction when it is screened to all orders.

The reader is again warned that this is a schematic equation. It is understood that the interaction  $f_\infty$  here acts between all particles and holes which lie in *different* propagating particle-hole pairs (compare Fig. 41 with Figs. 43 and 46), since Eq. (3.33) already allows for interactions within a given propagating particle-hole pair. Now we can obtain the fully screened TDA and RPA core-polarization corrections from Eqs. (3.14) and (3.26) by replacing  $f$  and  $B$  by  $f_\infty$  and  $B_\infty$ , and they are found to be very similar to those obtained for the second-order screening corrections.

The renormalization processes discussed above all serve to modify the propagation of a particle-hole pair, and have thus been termed *propagator* renormalizations by Kirson and Zamick (1970). Other important processes which affect the core polarization of the effective interaction are the so-called *vertex* renormalizations, which modify the coupling of a valence particle or hole to a particle-hole pair. These processes can be quite important and were found to give rise to large third-order diagrams [see Fig. 30(c)] as discussed in the previous Sec. III.C. Thus Kirson and Zamick (1970) were led to renormalize the  $\nu$  vertex by the second-order corrections  $\nu_{ph}$ ,  $\nu_{hp}$ , and  $\nu_{hh}$  shown in Fig. 45 and obtained large reductions of the core polarization in the ordinary RPA. In

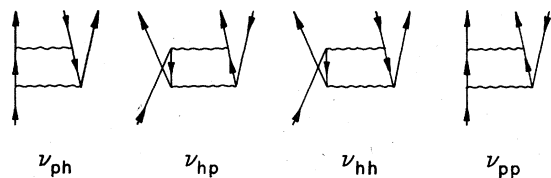


FIG. 45. Second-order corrections to the  $\nu$  vertex of Fig. 39.

particular, the contributions from the  $T''=0, J''=2$  particle-hole states are reduced in magnitude by a factor of about 2. Kirson (1971, 1974) then went on to generalize the vertex corrections  $\nu_{ph}$  and  $\nu_{hp}$  with particle-hole intermediate states to all orders by

$$\begin{aligned} \nu_\infty &= \nu + f \frac{1}{\epsilon - f} \nu + \bar{\nu} \frac{1}{\epsilon - f} B, \\ \nu'_\infty &= \nu' + f \frac{1}{\epsilon - f} \nu' + \bar{\nu}' \frac{1}{\epsilon - f} B. \end{aligned} \tag{3.35}$$

A further generalization was obtained by replacing here the bare particle-hole and ground-state correlation vertices by the fully screened ones of Eqs. (3.33) and (3.34). But then, in order to obtain a completely self-consistent treatment of the particle-hole interaction, one needs to use the renormalized  $\nu$  and  $\nu'$  vertices of Eq. (3.35) in evaluating the screened  $f_\infty$  and  $B_\infty$  vertices of Eqs. (3.33) and (3.34). Thus one finally arrives at the self-consistent coupled equations [SCCE(B)] of Kirson (1974)

$$\begin{aligned} f_\infty &= f + \nu'_\infty \frac{1}{\epsilon - f_\infty} \nu_\infty, \\ \nu_\infty &= \nu + f_\infty \frac{1}{\epsilon - f_\infty} \nu_\infty + \bar{\nu}_\infty \frac{1}{\epsilon - f_\infty} B_\infty, \\ \nu'_\infty &= \nu' + f_\infty \frac{1}{\epsilon - f_\infty} \nu'_\infty + \bar{\nu}'_\infty \frac{1}{\epsilon - f_\infty} B_\infty, \\ B_\infty &= B + f_\infty \frac{1}{\epsilon - f_\infty} B_\infty. \end{aligned} \tag{3.36}$$

[In Kirson's early version (1971) of SCCE, the screening of the  $B$  vertices was not included.] The above equations may be solved by iteration and the resulting vertices used in Eq. (3.26) to evaluate the core polarization of the effective interaction. This way all core-polarization diagrams are included which contain particle-hole propagation, screening, and vertex renormalizations to arbitrary order, as illustrated by the example in Fig. 46. This method has been applied to the degenerate schematic model by Sprung and Jopko (1972), and realistic calculations have been carried out for mass 18 by Kirson (1971, 1974) and for mass 42 by Jopko and Sprung (1973). Very small core-polarization corrections were obtained (see Tables IV and V), and the resulting spectra were not very different from those calculated with the bare  $G$  matrix (see Fig. 31, column 10).

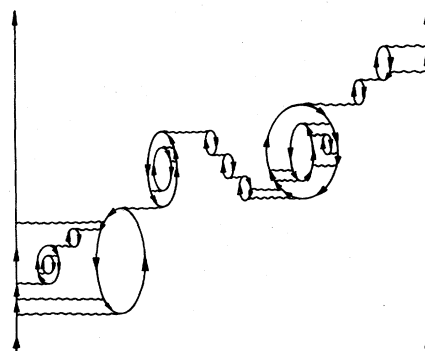


FIG. 46. Typical diagram arising in the self-consistent coupled equations (3.36).

This result is rather perplexing, since it appears to be in strong disagreement with experiment—and hence with the simple and physically appealing second-order result of Kuo and Brown (1966) shown in Eq. (3.12). Thus it is necessary to consider processes which were neglected in the SCCE. Although, as pointed out by Kirson and Zamick (1970), the processes included in the SCCE account for almost all of the third-order contribution (however, the screening corrections do not come in until fourth order), processes with particle-particle intermediate states were consistently left out by Kirson to avoid double counting of excitations already included in the  $G$  matrix. Such processes are, however, legitimate in a double-partition approach, as discussed in the previous Sec. III.C. For instance, one would obtain an additional second-order vertex correction  $\nu_{pp}$  with particle-particle intermediate states, as shown in Fig. 45. This term is expected to have opposite sign to the corresponding terms  $\nu_{ph}$  and  $\nu_{hp}$  with particle-hole intermediate states and hence to reduce somewhat the strong vertex corrections observed above. To get some estimate of this effect, consider the lowest-order vertex corrections to the core-polarization diagram shown in Fig. 47. As found by Barrett (1974), the introduction of particle-particle intermediate states [diagram (e)] in a double-partition approach serves to reduce the sum of diagrams (b) and (c) (with particle-hole intermediate states) by roughly one quarter. A similar result is obtained by assuming that a double-partition approach can be applied to the  $G$  matrix elements of Kuo and Brown (Barrett, 1972). In addition, there is a contribution from the hole-hole interaction [diagram (d)] which is small, but also serves to reduce the vertex corrections. Thus the second-order vertex corrections are reduced by approximately one third due to particle-particle and hole-hole intermediate states. Similarly, there are particle-particle and hole-hole contributions to the second-order screening corrections, as shown in Fig. 42. These were included in the calculations of Osnes *et al.* (1971) and Kuo and Osnes (1974) and thus explain why a slightly larger screening effect was obtained there, compared to Kirson's work (1971, 1974). In view of the above, it might be interesting to include such effects with more recent  $G$  matrices designed for a double-partition approach, to see if the SCCE result of Kirson is significantly changed. However, as discussed in the previous Sec. III.C, there are further neglected effects such as contributions from high intermediate states, off-shell effects in the  $G$  vertices, and HF corrections. As all of these effects tend to make the low-

order contributions smaller in magnitude, it is at the present stage difficult to see how we can get enough core polarization from partial summations to satisfy Eq. (3.12).

In passing we mention that schemes similar to the SCCE of Kirson have been used in Landau theory to calculate the phonon-induced part of the quasiparticle interaction in liquid  $^3\text{He}$  (Babu and Brown, 1973) and nuclear matter (Sjöberg, 1973). Relatively poor results were obtained for liquid  $^3\text{He}$ , where "soft" phonons (spin fluctuations) give rise to very large contributions so that multiple phonon exchange cannot be neglected. The method appears to be more adequate for nuclear matter, where there are no soft modes. Further, it has been noted by Bäckman (see Sjöberg, 1973) that the SCCE is a conserving approximation in the sense that it conserves the Pauli principle sum rule in Landau theory.

A somewhat different description of the intermediate states has been examined by Goode and Kirson (1974; see also Goode, 1971). Rather than using screened TDA phonons, they take the states obtained from a diagonalization of the  $2\hbar\omega$   $1p$ - $1h$  and  $2p$ - $2h$  excitations of the  $^{16}\text{O}$  core (these states couple to the valence particles only through their  $1p$ - $1h$  components). This procedure includes the TDA diagrams, some screening diagrams, and also some new types of diagrams. Some enhancement over TDA is obtained, but the efficacy of the vertex corrections is such that, when they are included, the results become close to the original SCCE values obtained by Kirson (1971).

Finally, a set of diagrams with  $4p$ - $2h$  intermediate states has been summed by Rajewski and Kirson (1972), following an approach similar to the SCCE used by Kirson (1971). Only a small (and attractive) effect was obtained, which is reasonable since the correlations—especially among the four particles—responsible for building up deformed states (see Sec. III.C.) were not included.

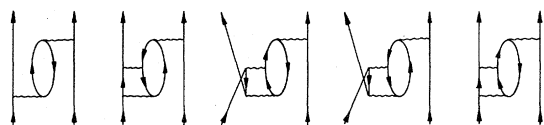
## 2. Effective charge

As seen in Sec. III.C, the calculation of the effective charge is closely parallel to the calculation of the effective interaction. Thus partial summations similar to those discussed above for the effective interaction have been carried out for the effective charge. In fact, the TDA and RPA summations were first carried out for the effective charge by Siegel and Zamick (1969, 1970).

In TDA we sum the diagrams shown in Fig. 48(a). Their contributions to the effective  $E2$  operator of Eq. (3.13) is easily found to be

$$g_{2\mu}^{\text{eff}} = - \sum_{j,k} \langle 0 | g_{2\mu} | j \rangle \frac{X_{\alpha j} X_{\alpha k}}{\epsilon_{\alpha}} | k \rangle \nu + \text{h.c.}, \quad (3.37)$$

where  $\alpha$  and  $j, k$  label TDA eigenstates and unperturbed particle-hole states, respectively. Expression (3.37) is closely similar to Eq. (3.18) for the effective interaction, and a similar notation is used. In particular, the vertices are expressed in the particle-hole channel and the external lines should be coupled accordingly. The results of calculations for the TDA are shown in Table VI. We see that both proton and neutron effective charges are enhanced. We can understand this in the



	(a)	(b)	(c)	(d)	(e)
Kuo-Brown	-0.755	0.478	0.293	-0.069	-0.185
Barrett DP	-0.504	0.288	0.166	-0.047	-0.102

FIG. 47. Core polarization with bare (a) and corrected (b-e)  $\nu$  vertices. The calculated values are taken from Barrett, 1972, 1974; the Barrett DP results are quoted for a starting energy of  $-3$  MeV.

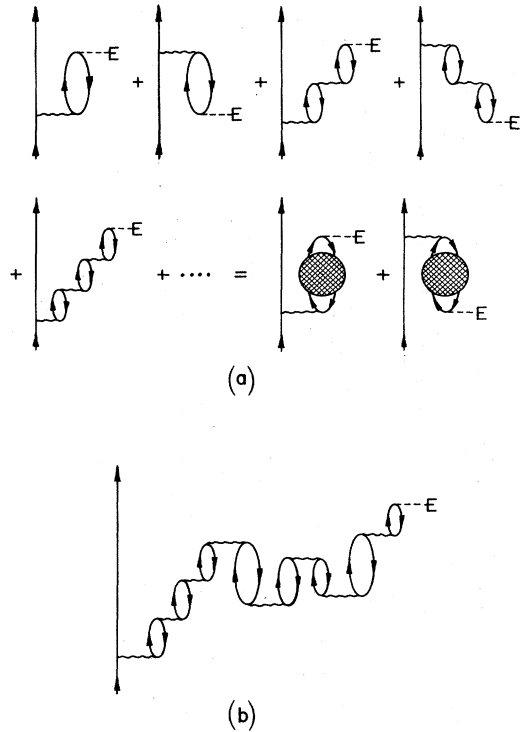


FIG. 48. TDA series for the effective charge (a) and diagram contributing to the RPA series (b).

same way as for the effective interaction by separating the contributions to the effective charge from the isoscalar and isovector parts of the quadrupole operator. The isospin separation of the operator is obtained by writing

$$\begin{aligned} \mathcal{G}_{2\mu} &= \sum_{\text{protons}} e r^2 Y_{2\mu}(\hat{\mathbf{r}}) \\ &= \sum_i \frac{e}{2} (1 - \tau_z(i)) r_i^2 Y_{2\mu}(\hat{\mathbf{r}}_i) = \mathcal{G}_{2\mu}(\tau=0) + \mathcal{G}_{2\mu}(\tau=1) \end{aligned}$$

with

$$\begin{aligned} \mathcal{G}_{2\mu}(\tau=0) &= \sum_i \frac{e}{2} r_i^2 Y_{2\mu}(\hat{\mathbf{r}}_i), \\ \mathcal{G}_{2\mu}(\tau=1) &= - \sum_i \frac{e}{2} \tau_z(i) r_i^2 Y_{2\mu}(\hat{\mathbf{r}}_i). \end{aligned} \quad (3.38)$$

Here we have used  $\tau_z = -1$  and  $+1$  for a proton and neutron, respectively. Calculating effective charges for the

TABLE VI. The effective charge for various approximations to the core polarization.

Approximation	Transition	$d_{5/2} - d_{5/2}$		$d_{3/2} - s_{1/2}$	
		N	P	N	P
1st order <sup>a</sup>		0.33	1.10	0.24	1.05
TDA <sup>a</sup>		0.50	1.32	0.32	1.17
RPA <sup>a</sup>		0.66	1.48	0.38	1.23
Screened TDA <sup>a</sup>		0.40	1.21	0.28	1.12
Screened RPA <sup>a</sup>		0.44	1.25	0.30	1.14
SCCE(B) <sup>b</sup>		0.32	1.13	0.20	1.03

<sup>a</sup>Kuo and Osnes, 1973.

<sup>b</sup>Kirson, 1974 and private communication.

isoscalar and isovector parts of the operator separately, we can relate these to the proton and neutron effective charges by

$$e_{\text{fi}}^{\text{eff}}(\text{proton}) = \frac{1}{2} [e_{\text{fi}}^{\text{eff}}(\tau=0) + e_{\text{fi}}^{\text{eff}}(\tau=1)]. \quad (3.39)$$

Now the isoscalar effective charge will involve quadrupole  $T''=0$  states and must therefore be enhanced over the lowest-order values, since a collective state is pushed down. In fact, in the schematic model it is straightforward to show that identical enhancements are obtained for the effective charge and the quadrupole contribution to the effective interaction; however, this is only roughly borne out by the actual calculations. As regards the isovector case, the general tendency is for the  $T''=1$  particle-hole states to be pushed up, as the interaction is mainly repulsive, and further there is little collectivity. Thus the isovector contributions are not very different from those obtained in first order.

If we now include the diagrams with "backward-going" bubbles, such as that shown in Fig. 48(b), we obtain the RPA estimate of the effective charge. The results are given in Table VI and show significant enhancement. However, the effect is much more dramatic (and unphysical) in <sup>41</sup>Ca because, as we have previously mentioned, the  $T''=0, J''=2$  collective state is unstable and drops towards zero energy. Fortunately, the phonons can be stabilized by screening, as discussed for the effective interaction. Thus the results in Table VI are similar to those obtained for the effective interaction in Table V, namely the screened RPA is close to the screened TDA and there is not too much difference between TDA and the screened TDA. It is also worth pointing out that when screening is included, very similar enhancements are found in mass 17 and mass 41. Furthermore, the mass 41 effective charges produce reasonable transition rates in mass 42 and mass 43 nuclei when used together with wave functions calculated with the corresponding effective interaction (Kuo and Osnes, 1975); in masses 18 and 19 the results are not quite as good (Kuo and Osnes, 1977).

Just as for the effective interaction, Kirson (1974) went on to include both screening and vertex renormalizations to all orders in his SCCE. The results in Table VI show values close to those obtained in first order. The quenching obtained here is smaller than for the effective interaction. This is partly because we only have quadrupole states here, whereas for the effective interaction the other multipoles add some repulsion. Further, there is here only a single valence-particle to core-phonon vertex which can suffer renormalization, whereas for the effective interaction there are two such vertices.

*Summary.* We have discussed various exact summations of infinite subsets of diagrams. Firstly, the TDA series can be generated by using the eigenstates of the particle-hole interaction, instead of unperturbed states in the core-polarization diagram. This results in enhancement of the effective operators, due mainly to the collective isoscalar quadrupole state which is strongly pushed down. The RPA gives additional enhancement and often tends to be unstable. However, by screening the particle-hole interaction, the TDA result is essen-

tially regained. The screened result can in turn be cut down by a class of vertex renormalization effects; the effective interaction is reduced to roughly the bare result, whereas the effective charge is reduced to the first-order result.

### E. Calculations in a Hartree-Fock basis

All the calculations we have discussed so far have been concerned with various methods of treating the perturbation  $V$ , while the unperturbed Hamiltonian  $H_0$  has always been chosen to be a harmonic oscillator Hamiltonian. This is convenient, but the choice of  $H_0$  is at our disposal. Recall from Sec. II.A that  $H_0$  is defined by adding a one-body potential  $U$  to the kinetic energy operator; the perturbation  $V$  then contains  $-U$ . Since we are not able to carry out an exact calculation, the results we obtain will certainly depend on the choice of  $H_0$ . Intuitively one would expect that the best results would be obtained, with a minimum of calculation, if  $U$  were chosen to be the average potential experienced by an individual nucleon. This is not known exactly, of course. At a phenomenological level one might choose  $U$  to be a Woods-Saxon rather than a harmonic oscillator potential—the two are compared in Fig. 49. A more fundamental microscopic choice for  $U$  is the Hartree-Fock (HF) potential, with which we shall be principally concerned in this section.

We define our unperturbed single-particle wave functions and energies by carrying out a HF calculation in the closed-shell system—in our example  $^{16}\text{O}$ . This has the advantage that it yields a potential with spherical symmetry, so that the single-particle states have a definite angular momentum. Hence we are just modifying the harmonic oscillator radial wave functions and energies. It should be reasonable to use these results for a system with two nucleons outside the closed shell— $^{18}\text{O}$  in the present case. Now the HF single-particle equation reads

$$\langle \alpha | T | \beta \rangle + \sum_{\rho \text{ occupied}} \langle \alpha \rho | V_{12} | \beta \rho \rangle = e_{\alpha} \delta_{\alpha\beta}, \quad (3.40)$$

where the matrix elements of  $V_{12}$  are understood to be antisymmetrized. The first and second terms in Eq. (3.40) give, respectively, the matrix elements of the

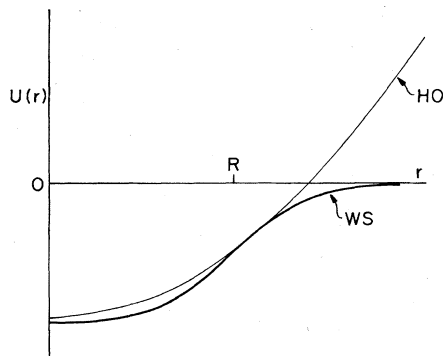


FIG. 49. Comparison of Woods-Saxon and harmonic oscillator potentials for a light nucleus such as  $^{16}\text{O}$ . The radius of the Woods-Saxon well is indicated and the zero of the oscillator well is arbitrarily adjusted.

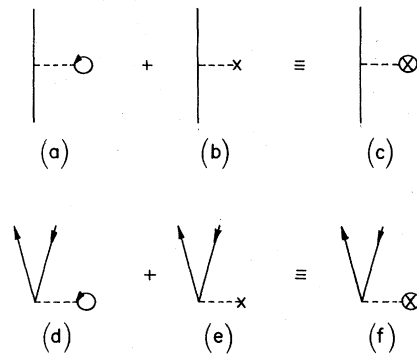


FIG. 50. Self-energy and  $(-U)$  insertions and convention for the sum, which is identically zero in a HF basis.

kinetic energy operator and of the HF one-body potential which arises from the interaction with the particles occupying the states  $\rho$  of the closed-shell ground state (e.g.,  $\rho$  would run over the four  $0s$  and  $12\ 0p$  states for  $^{16}\text{O}$ , c.f. Fig. 1). We can represent this one-body interaction by diagrams (a) and (d) of Fig. 50. Diagram (a) will be applicable if  $\alpha$  and  $\beta$  both refer to filled shells (vertical line is then a downgoing hole line) or empty shells (particle line), while (d) arises if one of  $\alpha, \beta$  refers to a filled shell and the other to an empty one. Now, since diagram (a) by definition represents the one-body potential  $U$ , while the cross in diagram (b) stands for  $-U$ , the sum of diagrams (a) and (b), i.e., diagram (c), is identically zero. Similarly, diagram (f) is zero. Thus, when the HF choice is made for  $H_0$ , we can ignore any diagrams in our perturbation expansion which have diagrams (a), (b), (d), or (e), or equivalently (c) or (f), inserted in them.

We can also view the above in terms of a partial summation. Suppose we take  $H_0$  to be a harmonic oscillator Hamiltonian, so that the insertions (c) and (f) of Fig. 50 are nonzero in general. Now take, say, the core-polarization diagram and sum up these insertions to all orders, thus including complicated diagrams such as that of Fig. 51(a). This is equivalent to evaluating the core-polarization diagram in a HF basis. The correspondence is rather clear for the energy denominator, which is obtained by summing the diagonal insertions as discussed in Sec. II.B.6 and Appendix B. The off-diagonal insertions will replace each pure harmonic oscillator wave function by a linear combination of oscillator wave functions, which diagonalizes Eq. (3.40). An expansion in harmonic oscillator wave functions is, in fact, the usual method of solving this equation.

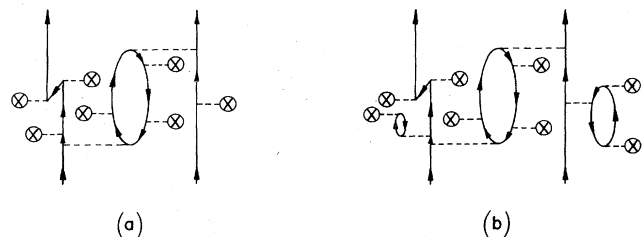


FIG. 51. Typical diagrams in an oscillator basis which are implicitly summed when the second-order core-polarization diagram is evaluated in a Hartree-Fock basis.

We have not yet touched on the self-consistency requirement of Eq. (3.40), namely that the wave functions of the filled states  $\rho$  which are used in setting up the one-body HF potential should be the same as those obtained by solving the single-particle eigenvalue problem. This self-consistency requirement is usually met by an iterative procedure. Starting with an initial guess for the wave functions  $\rho$ , the HF potential can be calculated and the eigenvalue problem of Eq. (3.40) solved. This yields new wave functions for the occupied states, which yield a new HF potential, for which the eigenvalue problem can be solved again. And so on, until self-consistency is achieved. From a diagrammatic point of view, the self-consistency condition means that additional diagrams are being summed. Thus in Fig. 51(a) the HF insertions all have pure oscillator wave functions for the filled core states [labeled  $\rho$  in Eq. (3.40)]. This restriction is removed by including diagrams of the type shown in Fig. 51(b), leading to self-consistency for the core orbitals.

We refer to standard quantum mechanics texts for a more thoroughgoing discussion of HF theory. It is shown there that the HF choice for the single-particle orbits is the optimum one, in the sense that the energy of the ground state is minimized.

There is a final point to be made, namely, that we must replace the potential  $V_{12}$  by a  $G$  matrix which is a function of the starting energy. This involves the single-particle energies for which the HF choice should be made. Thus there is an additional self-consistency requirement and we need a so-called Brueckner-Hartree-Fock calculation. This additional self-consistency requirement is often ignored in calculations of effective operators, and we shall not discuss it further here, but simply refer to the work of Davies and Baranger (1970) and Becker *et al.* (1974) on closed-shell systems.

With a HF unperturbed Hamiltonian the effective interaction between two valence nucleons in the  $(1s0d)$  shell was calculated to second order by Ellis and Mavromatis (1971), using the Sussex matrix elements (Elliott *et al.*, 1968). The spectra obtained in  $^{18}\text{O}$  for the bare interaction and the bare interaction plus core polarization, are shown in Fig. 52. The rather strong differences from the corresponding oscillator results may be qualitatively understood by reference to Fig. 49, assuming that the Woods-Saxon well is a reasonable approximation to the HF potential. The region where the Woods-Saxon and oscillator potentials are similar will be important for those orbitals which are strongly bound (in our case the  $0s$  and  $0p$  states), so the radial wave functions should differ little. However, for the weakly bound  $0d_{5/2}$  and  $1s_{1/2}$  valence orbitals, the finite nature of the Woods-Saxon potential will allow the wave functions to leak further out than in the oscillator case. A similar effect is seen for the  $0d_{3/2}$  valence orbital and the  $(1p0f)$  orbitals, although it should be understood here that we are dealing with unbound states. The tails of the wave functions should therefore oscillate, whereas they will decay to zero in the HF calculation, since we expand in a finite oscillator basis. We nevertheless hope to represent reasonably well the important interior region of the resonant continuum wave functions. In summary, the HF wave functions for the  $(1s0d)$  and  $(1p0f)$  orbitals

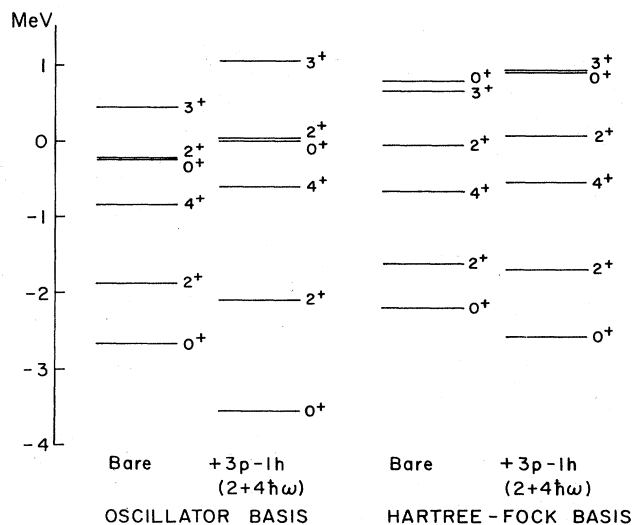


FIG. 52. Comparison of oscillator and HF spectra for  $^{18}\text{O}$ . Results are shown for the bare interaction and for the bare interaction plus the second-order core-polarization diagram (from Ellis and Mavromatis, 1971).

are more spread out than their oscillator counterparts. Thus interaction matrix elements involving these states will be weakened, and this is reflected in the results of Fig. 52. We may remark that the bare spectrum shows a strong shift in the second  $0^+$  state due to a 1 MeV change in the diagonal  $(1s_{1/2})^2$  matrix element. This appears desirable as we have pointed out that it is the third, rather than the second, experimental  $0^+$  level which is predominantly of  $(sd)^2$  structure.

On the basis of the above remarks it would be expected that the second-order diagram with  $4p-2h$  intermediate states [see Fig. 30(a)] and the TDA and RPA series would be weakened in a HF basis; this is found to be the case (Ellis and Mavromatis, 1971; Ellis and Osnes, 1972a). Including these effects gives little change in the results shown in Fig. 52 for the bare interaction plus the lowest-order core-polarization term.

In Table VII we show the results for the effective charge (Ellis and Mavromatis, 1971; Ellis and Osnes, 1972b). Since we still normalize by dividing by the pure oscillator matrix elements [see Eq. (3.13)], the bare, zeroth-order values for protons are just given by  $\langle r^2 \rangle_{\text{HF}} / \langle r^2 \rangle_{\text{HO}}$ . The above remarks indicate that this ratio will be greater than unity. The values are quite state dependent, as the  $0d_{5/2}$  valence wave function is least affected by the finite nature of the Woods-Saxon well. This is

TABLE VII. Comparison of oscillator and HF effective charges.

Order	Transition	$d_{5/2}-d_{5/2}$		$d_{3/2}-s_{1/2}$	
		N	P	N	P
0th order <sup>a</sup>	Osc.	0	1	0	1
	HF	0	1.10	0	1.63
RPA <sup>b</sup>	Osc.	0.63	1.48	0.31	1.19
	HF	0.16	1.19	0.14	1.70

<sup>a</sup>Ellis and Mavromatis, 1971.

<sup>b</sup>Ellis and Osnes, 1972b.

reasonable since this state is the most strongly bound and its wave function is nodeless. The enhancement seen here for protons seems to be needed if the effective charge is to be boosted towards the experimental value. The results of an RPA calculation are also shown in Table VII; intermediate states corresponding to 2 and  $4\hbar\omega$  excitations in an oscillator basis were included here. Clearly, the RPA diagrams are strongly reduced when we switch from an oscillator to a HF basis.

Thus we have seen for both the effective interaction and the effective charge that, by changing from an oscillator to a HF basis, rather large effects are obtained which, on the whole, lead to poorer agreement with the experimental data. At least the qualitative trends in the calculations should be reliable. Indeed, Köhler (1974) has pointed out that since core-polarization effects correspond physically to disturbing the closed-shell core, they will be smaller if the core is initially in a state of equilibrium. A HF calculation minimizes the total energy of the core, which of course corresponds to an equilibrium condition. A related point is the improved convergence often obtained in model calculations when one switches to a HF basis (Anastasio *et al.*, 1976; Leinaas and Kuo, 1976a; Starkand and Kirson, 1976). The detailed quantitative results, on the other hand, will be sensitive to the particular HF calculation carried out, since they depend strongly on the wave functions. The bare results seem to be quite well established, since they compare nicely with calculations performed with Woods-Saxon wave functions (Kahana *et al.*, 1969; Siegel, 1970). On the other hand, the size of the core-polarization effects, discussed above, is less certain. Thus Malta (1972) has used *modified* Sussex matrix elements in a HF calculation, and the results available show a smaller reduction with respect to the pure oscillator values. This appears to be mainly due to the occupied orbitals of the  $^{16}\text{O}$  core, which have larger and more realistic radii in her calculations. Model simulations of HF wave functions tend to confirm her results (Goodin *et al.*, 1977). It seems that on switching from an oscillator to a HF basis, it is reasonable to associate a reduction factor of 0.7 with each vertex entering the diagram. This is only a rough, over-all characterization of course; see Goodin *et al.* (1977) for more details. Further study of HF effects, and indeed of the whole question of the choice of unperturbed basis, is certainly needed.

We have here discussed the HF choice for the spherical one-body potential. It is well known, however, that quadrupole deformations of the single-particle potential play an important role in nuclear structure. It would seem important to try to include both spherical (monopole) and quadrupole effects consistently *ab initio*. Some interesting model calculations in this spirit have been made (Harvey, 1975; Harvey *et al.*, 1976), and applications to the actual problem at hand are in progress.

**Summary.** By choosing an oscillator single-particle potential so that the wave functions of the filled shells overlap well with those obtained in a Hartree-Fock calculation, one finds that the wave functions of the valence and empty shells extend much further out in the HF

case. This is responsible for the reduction in the magnitude of the core-polarization diagram and the TDA and RPA series when the unperturbed harmonic oscillator Hamiltonian is replaced by a HF Hamiltonian. The bare interaction is also weakened, while the bare proton effective charge is increased, since the matrix element of  $r^2$  is involved.

## F. Matrix diagonalization methods

At first sight, it might seem that the simplest approach to effective operators would be to set up and diagonalize a large matrix, thus solving the Schrödinger equation exactly in a large, but truncated, Hilbert space. An effective interaction which reproduces  $d$  of the large-matrix eigenvalues  $E_i$  could then be obtained in the following way. Take, as usual, the projections  $|\psi_D^i\rangle$  of the large-matrix eigenvectors on the smaller valence space. Now, as we have remarked, these will not be orthogonal, but we can always find a second set of vectors  $|\bar{\psi}_D^i\rangle$  such that

$$\langle \bar{\psi}_D^j | \psi_D^i \rangle = \langle \psi_D^j | \bar{\psi}_D^i \rangle = \delta_{ij}. \quad (3.41)$$

These two sets of vectors are said to be biorthogonal. Then, the effective Hamiltonian operator is clearly

$$H_{\text{eff}} = \sum_{i=1}^d |\psi_D^i\rangle E_i \langle \bar{\psi}_D^i|, \quad (3.42)$$

since

$$H_{\text{eff}} |\psi_D^i\rangle = E_i |\psi_D^i\rangle. \quad (3.43)$$

Of course, further work would be needed to extract the purely two-body effective interaction  $U_V$  from  $H_{\text{eff}}$  since, for instance, one-body single-particle energy terms will be present as well. We could also obtain, say, an effective  $E2$  operator by using the full eigenvectors and the valence space projections.

While this is apparently straightforward, there are, in fact, disadvantages to the matrix approach. Firstly, only a very limited number of configurations can be treated, albeit exactly, if the size of the matrices is to remain tractable. For instance, the prototype calculation of  $^{18}\text{O}$  includes, in addition to the  $(sd)^2$  valence states, all  $3p-1h$  states of  $2\hbar\omega$  unperturbed excitation energy. There are 213 such states for  $J=0$ , and for  $J>0$  the figure is much larger. [The few states which involve the  $(2s1d0g)$  orbitals are normally ignored.] This is already a big calculation, so it becomes difficult to investigate the effect of including additional configurations. Perturbation theory is, in principle, more flexible here in allowing the important physical processes to be isolated without arbitrary space truncations.

A second difficulty with the matrix approach lies in the extraction of the two-body effective interaction from Eq. (3.42). This can be done in the case of a 0 plus  $2\hbar\omega$  space (Ellis, 1975), but no completely general technique is available. Let us confine our attention to the simplest case, namely the prototype calculation mentioned above, with the assumption that the coupling between the  $1p-1h$  states and the  $^{16}\text{O}$  closed-shell ground state vanishes [i.e., HF insertions of the type shown in Fig. 50(f) are zero]. We mentioned above that the single-particle energy terms are present in Eq. (3.42).

TABLE VIII. Comparison of matrix elements  $\langle v_1^2 J=0, T=1 | \mathcal{U}_v | v_2^2 J=0, T=1 \rangle$  of the effective interaction derived from order-by-order perturbation calculations, TDA, and matrix diagonalization. All matrix elements are in MeV.

Approximation	Valence orbits			
	$v_1 = d_{5/2}$	$v_2 = d_{5/2}$	$v_1 = d_{5/2}$	$v_2 = d_{3/2}$
Non-HF	1st order <sup>a</sup>		-1.236	-3.025
	1st+ 2nd order <sup>a</sup>		-1.991	-3.605
	1st+ 2nd+ 3rd order <sup>a</sup>		-1.720	-3.065
	TDA <sup>b</sup>		-2.469	-3.939
	Matrix diag. <sup>a</sup>		-1.613	-2.975
HF	1st+ 2nd+ 3rd order <sup>a</sup>		-1.376	-2.914
	Matrix diag. <sup>a</sup>		-1.595	-2.727

<sup>a</sup> Starkand and Kirson, 1975, 1976.

<sup>b</sup> Kuo and Osnes, 1974

They can be evaluated by carrying out the analogous calculation in  $^{17}\text{O}$  [i.e., (*sd*) valence state plus  $2\hbar\omega$   $2p-1h$  states]. This is not the whole story, however, since Eq. (3.42) also contains contributions from unlinked diagrams (Mavromatis, 1973; Goode, 1975). To see that this is so, recall from the discussion of Sec. II.C that the unlinked diagrams of Figs. 11(c) and 12(a) canceled. Now the folded diagram of Fig. 12(a) will be included in the matrix calculation since it is essentially the product of two diagrams, each involving a  $3p-1h$  intermediate state. The nonfolded diagrams of Fig. 11(c), on the other hand, will not be included, since they involve a  $4p-2h$  intermediate state and this is not present in the matrix. Thus contributions from unlinked, folded diagrams will be present in Eq. (3.42) and these can be evaluated by the technique of Starkand and Kirson (1975) and Ellis (1975). Then, at last, a linked two-body effective interaction can be obtained.

A third and final difficulty arises from the starting energy dependence of the *G* matrix. It is not possible to take this properly into account with the matrix method. It is also worth remarking that the matrix results will include ladder diagrams, so the *G* matrix must be defined in such a way that there is no double counting.

We shall discuss first the results obtained for the effective interaction in the prototype calculation outlined above. These are exact within the truncated space, i.e., perturbation theory diagrams with  $3p-1h$  intermediate states are included to all orders, so they can be compared with results obtained in approximate perturbation calculations. Such comparisons were marred in the early work (Lo Iudice *et al.* 1971, 1974, 1975; Goode, 1975) by the presence of unlinked diagrams. It was left to Starkand and Kirson (1975, 1976) to obtain a fully linked effective interaction, showing in the process that the unlinked contributions are large—several hundred keV in diagonal matrix elements. We quote in Table VIII some of their results obtained with the *G* matrix elements of Kuo (1967) and a harmonic oscillator unperturbed Hamiltonian. Two different types of calculations are shown. In the first, labeled non-HF, the HF insertions are taken to be zero, and in the second, labeled HF, these insertions are properly included. To allow a fair comparison with the matrix results, only  $3p-1h$  intermediate states are allowed in the perturbation series, and ladder diagrams are included regardless

of double counting. The perturbation results through third order are seen to be in rather good agreement with the matrix results in the non-HF case. In contrast, the TDA results are much too attractive. The TDA series is summed in the matrix method, but some vertex correction effects are included too. These are known to be large and repulsive (see, for example, Table X and Fig. 47) and are mainly responsible for the difference. The HF case shows less good agreement between third-order and exact matrix results. It is probably fair to say that the third-order result cannot be relied upon to be accurate, even if, as here, the order-by-order series does in fact converge (Hofmann *et al.*, 1976).

For the analogous effective charge calculation in mass 17—(*sd*) valence particle plus all  $2\hbar\omega$   $2p-1h$  states and HF insertions ignored—we do not have to worry about the complication of unlinked diagrams. We do have a problem, however, since the results obtained by Goode and Siegel (1970) differ from those of Lo Iudice *et al.* (1974). This is probably due to approximations made in the earlier study, so we take results from the latter reference for Table IX. These results are reasonably concordant with the work of Andō *et al.* (1977), in which a multiple scattering approach is used which is, in principle, equivalent to the matrix method. Table IX shows good agreement between second-order perturbation theory and the matrix results. The TDA results are also reasonable for neutrons, whereas the proton results are too large. These features and the differences from the effective interaction results can be qualitatively

TABLE IX. Comparison of effective charges derived from order-by-order perturbation calculations, TDA, and matrix diagonalization.

Approximation	Transition	$d_{5/2}-d_{5/2}$		$d_{3/2}-s_{1/2}$	
		N	P	N	P
0th order <sup>a</sup>		0	1	0	1
0th+ 1st order <sup>a</sup>		0.33	1.10	0.24	1.05
0th+ 1st+ 2nd order <sup>a</sup>		0.44	1.12	0.33	1.01
TDA <sup>b</sup>		0.50	1.32	0.32	1.17
Matrix diag. <sup>c</sup>		0.43	1.14	0.29	0.94

<sup>a</sup> Ellis and Siegel, 1971 and unpublished work.

<sup>b</sup> Kuo and Osnes, 1973.

<sup>c</sup> Lo Iudice *et al.*, 1974.

TABLE X. Comparison of important second-order effective charge diagrams with the corresponding third-order effective interaction diagrams.

Class of diagrams	Effective charge <sup>a</sup>		Effective interaction <sup>b</sup> (in MeV)
	$d_{5/2}^2 - d_{3/2}^2$	$P$	
Vertex	-0.038	-0.060	0.478
TDA	0.081	0.129	-0.241
Ladder	0.056	0.012	-0.185
Number conserving	0.012	-0.060	0.118
Total	0.111	0.021	0.170

<sup>a</sup>Ellis and Siegel, 1971 and unpublished work.

<sup>b</sup>Barrett and Kirson, 1970, 1972; Barrett, 1972.

understood by reference to Table X. Here we compare second-order diagrams for the effective charge with the corresponding third-order diagrams for the effective interaction. The vertex correction diagram is seen to be relatively much bigger for the effective interaction than for the neutron effective charge, and thus in the former case the TDA is much too large, whereas it is fairly reasonable in the latter. Now comparing neutron and proton effective charges from the matrix calculation with the first-order results, we find an increase in magnitude for neutrons, whereas the proton case shows a much smaller increase or even a reduction. From Table X we see that this behavior arises firstly from the ladder diagram, which is much smaller for protons. Secondly, the number-conserving sets give a large negative value for protons. Much of this comes from the folded diagrams which normalize the initial and final wave functions (see Sec. II.D.). The importance of normalization effects has been stressed by Goode *et al.* (1972). Incidentally, this reference contains an interesting decomposition of the matrix approach, which shows the sequence of approximations needed to obtain the TDA.

It should be noted that the  $2p-1h$  and  $3p-2h$  bases used here will contain spurious components which involve excitations of the center-of-mass of the whole nucleus, as well as the intrinsic excitations that are physically relevant. Andō *et al.* (1977) have found that the approximate elimination of spurious states leads to a more attractive effective interaction, although the effective charge is little changed. Perhaps more attention should be paid to this difficult question of spurious effects in truncated bases, but we shall not discuss it further here.

Finally we mention that a matrix calculation has been performed with a basis consisting of the  $(sd)^2$  valence states plus all  $2\hbar\omega$  excitations (Watt *et al.*, 1974). This enormous calculation is only possible using the powerful Glasgow shell-model technique. Unfortunately, there is no known way to obtain just the linked two-body effective interaction with this technique. It is therefore difficult to know what weight to attach to the results, which suggest that the correction to the bare effective interaction is somewhat overestimated by second-order perturbation theory. Note, however, that this is in agreement with the trend shown in Table VIII.

**Summary.** In making comparison between perturbation calculations and the "exact" results from matrix

diagonalizations, great care is needed to eliminate extraneous effects, in particular, unlinked diagrams. Third-(second-)order perturbation theory for the effective interaction (charge) often gives good results, but its accuracy cannot be relied on. The TDA approximation is fairly reasonable for the neutron effective charge, but is strongly cut back by vertex corrections for the effective interaction and proton effective charge. In the latter case normalization effects are also important.

### G. Many-body effective operators

We have in this review restricted our attention to the calculation of the two-body effective interaction and the one-body effective charge appropriate to the nuclear shell model. These quantities are frequently applied to studies of nuclei involving many particles. However, we have pointed out in Sec. II that in many-particle systems the effective operators in question will have many-body components. Note that we are not talking here about many-body nuclear forces. Even if we start from a basic two-nucleon interaction, many-body effective forces will arise from using a truncated valence space. Examples of three-body effective forces are shown in Fig. 53. Diagram (a) arises as one particle is excited

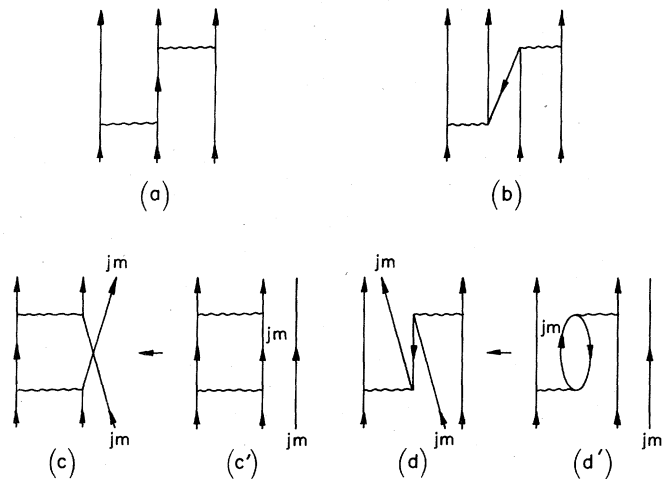


FIG. 53. Second-order contributions to the three-body effective interaction. Diagrams (c) and (d) are particular cases of diagrams (a) and (b) and arise from corrections for violation of the Pauli exclusion principle, as shown.

by another and then de-excited by the third, whereas in diagram (b) one particle excites a particle-hole pair and the hole is subsequently filled as a result of the interaction between the remaining two particles. Part of diagrams (a) and (b) is needed to correct for violations of the Pauli exclusion principle. For example, diagrams (c) and (d), which have the external labels restricted as shown, serve to correct for the violation of the exclusion principle in the two-body diagrams (c') and (d'), respectively, where intermediate excitations are blocked by the noninteracting third particle. (A little thought should convince the reader that diagrams of type (c) should be included regardless of whether the  $G$  matrix is calculated by double partition or the standard procedure.) In general, violation of the exclusion principle by using  $n$ -body effective forces in an  $(n+1)$ -particle system is corrected for by  $(n+1)$ -body exclusion-violating diagrams. This effect is in fact already present in the two-particle system since, as shown in Fig. 63 of Appendix D, part of the much celebrated core-polarization diagram corrects for blocking of intermediate states in the second-order contribution to the single-particle energy. Now, if attractive contributions to the effective interaction are blocked, the corresponding Pauli corrections will be repulsive. This may in part explain why it has been necessary to add repulsion to two-body effective forces in order to obtain reasonable results for nuclei with several valence nucleons (Bertsch, 1968; Preedom and Wildenthal, 1972). It should be stressed, however, that Pauli corrections only represent a small part of the many-body diagrams; the major part is there in its own right.

Second-order three-body diagrams have been calculated in the  $(0p)$  shell by Singh (1974) and Dirim *et al.* (1975), using, respectively, the original and modified Sussex matrix elements, and in the  $(0f_{7/2})$  shell by Osnes (1968), Yariv (1974), and Andreozzi and Sartoris (1976), using the Kuo-Brown matrix elements. In most cases rather small matrix elements were found. However, in a system of  $n$  valence particles there are  $\binom{n}{3}$  three-body interactions compared to  $\binom{n}{2}$  two-body interactions, so appreciable three-body effects may still be obtained towards the end of the valence shell. On the other hand, rather large three-body matrix elements have been found in various model calculations employing highly truncated shell-model spaces (Bertsch, 1968; Quesne, 1970; Eisenstein and Kirson, 1973; Barrett *et al.*, 1975; Andreozzi and Sartoris, 1976).

Similarly, one may consider many-body contributions to the effective charge. For two valence nucleons there will be two-body contributions, as shown in Fig. 54. In general these are neglected, since phenomenological calculations indicate that the measured transition rates

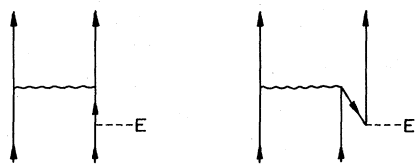


FIG. 54. Lowest-order contributions to the two-body effective charge.

can be well described by one-body effective charges. However, explicit calculations in mass 18 by Harvey and Khanna (1970), using a phenomenological quadrupole-quadrupole interaction, gave two-body effective charges as large as 5–20% of the one-body values. Since the number of pairs increases strongly as valence particles are added, substantial two-body contributions would be obtained for systems of several valence particles. However, Lo Iudice *et al.* (1974) used a diagonalization technique and found a much smaller value, 1% or less. The situation is thus unclear, but one hopes that such effects are small; empirically this appears to be the case.

*Summary.* Three-body contributions to the effective interaction and two-body contributions to the effective charge are considered. Calculations of these quantities are scarce, but indicate relatively modest values. Still, such effects may be strongly felt in systems of many valence particles. Empirically, there seems to be little need for explicit inclusion of many-body effects. In most cases it is adequate to include them in an average way by small modifications in the two-body effective interaction (and perhaps the one-body effective charge).

#### IV. CONCLUSIONS

We have outlined in Sec. II the linked, folded-diagram perturbation expansion needed for the calculation of the effective interaction and other effective operators appropriate to the nuclear shell model. From a physical point of view the folded-diagram expansion is both appealing and convenient, as it allows us to identify and evaluate important physical processes diagrammatically. Only in the case of effective operators (other than the effective interaction) in many-particle systems is there left some room for improvement (see, for example, Kirson, 1975).

In Sec. III we have discussed actual calculations of the effective interaction between two valence nucleons in the  $(1s0d)$  shell outside an  $^{16}\text{O}$  core, and also of the effective electric quadrupole operator (or effective charge) for a single  $(1s0d)$  nucleon beyond the  $^{16}\text{O}$  core. Such calculations are commonly carried out in a harmonic oscillator basis. However, the matrix elements of the nucleon-nucleon interaction would be enormous in an oscillator basis because of the strong short-range repulsion. A necessary first step is therefore to achieve reasonably sized matrix elements by going to a  $G$  matrix, where one allows the particles in question to interact an arbitrary number of times. This corresponds to the summation of ladder diagrams. In physical terms these serve to induce small admixtures in the relative wave function, allowing it to become very small at short distances where the strong repulsion acts. The perturbation series must therefore be rewritten in terms of  $G$  matrix interactions in spite of the fact that this leads to additional complications, such as those associated with the energy dependence of  $G$ .

The bare (i.e., first-order)  $G$  matrix elements give a large part of the effective interaction. However, the core-polarization diagram, which is of second order in  $G$  (see Fig. 30), is needed to bring the calculations into

substantial agreement with the experimental spectrum of  $^{18}\text{O}$ . On the other hand, the corresponding calculations for the effective charge (through first order in  $G$ ) yield results which are too small. It is, of course, natural to investigate corrections of higher order in  $G$  and to hope that they are negligible. This hope has not been realized, so that, at present, it is difficult to have confidence in low-order calculations. A similar conclusion is reached when "exact" matrix diagonalization results are compared to perturbation theory. Finally, it should be mentioned that the presence of intruder states in the  $^{18}\text{O}$  spectrum means that the order-by-order series must ultimately diverge, although it is unlikely that this mathematical property is the dominant feature in the low-order results. Nevertheless, the intruder state problem gives cause for concern, since we do not yet have techniques adequate for dealing with it.

In the core-polarization diagram we consider unperturbed particle-hole states, although it is well known that particle-hole states in closed-shell nuclei show strong collective properties. To take this into account we allow the particle and hole to interact in the Tamm-Dancoff or random-phase approximations, thus summing a particular class of diagrams. This produces strong enhancements in the calculated effective operators, but these can be damped by including additional processes. Two damping mechanisms are known. The first allows self-screening of the particle-hole interaction, together with corrections at the vertex connecting the valence particle to the particle-hole pair. The second mechanism involves using a Hartree-Fock unperturbed basis rather than a harmonic oscillator one. This should be more realistic, since it allows the wave functions of weakly bound and unbound orbitals to extend out further, with the effect that the matrix elements are weakened. Either of these damping mechanisms yields effective interaction matrix elements which resemble the bare oscillator values and neutron effective charges close to the first-order results. Agreement with experiment is therefore poor. For protons the core-polarization effects are also strongly damped, but because of the presence of

$r^2$  in the operator, the zeroth-order values are enhanced in a Hartree-Fock basis and this is certainly desirable.

One further complication should be mentioned. If for the core-polarization diagram intermediate states of rather high excitation energy are included, a significantly less attractive effective interaction is obtained. This arises from the strong tensor force components in  $G$ .

At present we do not know how to fit all of the results summarized above into a coherent picture. Thus the fundamental problem of calculating effective operators for the nuclear shell model is not yet resolved. It should not be surprising that this question is a difficult one, given the many-body nature of the problem. However, it is possible to get reasonable magnitudes for both the effective interaction and charge by adopting *ad hoc* procedures based on physical intuition and prejudice. This should encourage us to direct further efforts and resources to the important problem of deriving effective operators from first principles.

## V. ACKNOWLEDGMENTS

We should like to thank collectively a number of our colleagues for reading various parts of the manuscript and for commenting thereon. One of us (P. J. E.) would like to thank NORDITA for summer support at the University of Oslo in 1971, where the outline of some of this work was developed. Further, he is grateful for hospitality at Stony Brook during a visit in the summer of 1975. We also are grateful for hospitality at the Nuclear Physics Laboratory of the University of Oxford during the early stages of this work.

## APPENDIX A. GOLDSTONE DIAGRAMS VERSUS FOLDED DIAGRAMS

It is clear that for the nondegenerate problem one could use either the standard Goldstone (1957) treatment with the unperturbed state as vacuum or the linked, folded expansion of Brandow (1967), using the true vacuum  $| \rangle$ . Both approaches yield a completely linked expansion with Rayleigh-Schrödinger denominators. They must be equivalent order-by-order in the perturbation, but the correspondence is not at all obvious.

We feel an illustration is useful. Specifically, we shall take the diagrams of Fig. 55 and show that the sum of the Goldstone diagrams (a) and (b) is equal to the sum of the folded diagrams (c) and (d). These are not the only third-order diagrams, but they are the only third-order diagrams with matrix elements of this "particle-hole structure"; the equivalence must therefore hold for this subset of the third-order diagrams alone. By use of the diagram rules in Appendix C or by explicit evaluation we find for diagram (a)

$$D_a = -\frac{1}{2} \sum_{\alpha\beta\gamma\delta} \frac{\langle \alpha\delta | V_{12} | ab \rangle \langle \beta\gamma | V_{12} | \delta\gamma \rangle \langle ab | V_{12} | \alpha\beta \rangle}{(e_\alpha + e_\beta - e_a - e_b)(e_\alpha + e_\delta - e_a - e_b)}. \quad (\text{A1})$$

The Greek letters are summed over occupied and the Latin letters over unoccupied orbitals. The factor of  $\frac{1}{2}$  follows, since we are using antisymmetrized matrix

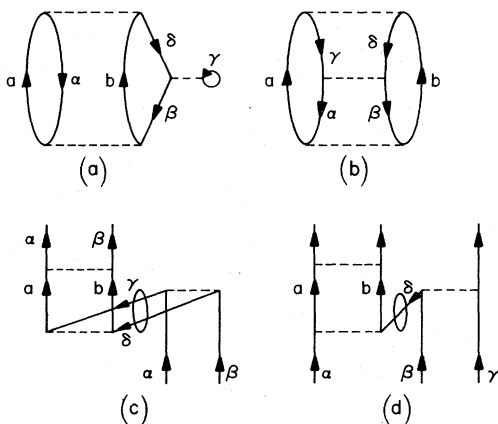


FIG. 55. Equivalent ways of representing the energy of a closed-shell nucleus. The Goldstone diagrams (a) and (b) are only equal to the folded diagrams (c) and (d) in the sum. (Note that the external legs of the folded diagrams must be summed over the filled orbitals).

elements while we sum over all  $a, b$ .

Diagram (b) has the value

$$D_b = \frac{1}{8} \sum_{\substack{ab \\ \alpha\beta\gamma\delta}} \frac{\langle \gamma\delta | V_{12} | ab \rangle \langle \alpha\beta | V_{12} | \gamma\delta \rangle \langle ab | V_{12} | \alpha\beta \rangle}{(e_\alpha + e_\beta - e_a - e_b)(e_\gamma + e_\delta - e_a - e_b)}. \quad (\text{A2})$$

For the folded diagram (c) we should in principle have a number of noninteracting lines representing the occupied states other than  $\alpha$  and  $\beta$ —these have been erased, but we must clearly return to the same pair of states  $\alpha, \beta$  as we started with. Now the diagram, summed over all occupied orbitals  $\alpha, \beta$  so as to obtain the total energy, has the value

$$D_c = -\frac{1}{8} \sum_{\substack{ab \\ \alpha\beta\gamma\delta}} \frac{\langle \alpha\beta | V_{12} | ab \rangle \langle ab | V_{12} | \gamma\delta \rangle \langle \gamma\delta | V_{12} | \alpha\beta \rangle}{(e_\gamma + e_\delta - e_a - e_b)(e_\alpha + e_\beta - e_a - e_b)}. \quad (\text{A3})$$

Three factors of  $\frac{1}{2}$  are needed—one each for the  $ab$  and  $\gamma\delta$  pairs, and the third factor because the interchange of  $\alpha$  and  $\beta$  is included by the exchange diagrams while we sum over all  $\alpha, \beta$ . Note that we sum over all  $\gamma, \delta$  for the folded lines.

Diagram (d) is more complicated. We start with initial states  $\alpha\beta\gamma$  ( $\alpha \neq \beta \neq \gamma$ ). Clearly the unlabeled final states leaving the top of the diagram must be  $\alpha\beta\gamma$  in some order. We need to count each possible permutation just once. Consider

$$D_{d1} = -\frac{1}{2} \sum_{\substack{ab \\ \alpha\beta\gamma\delta \\ (\alpha \neq \beta, \alpha \neq \gamma)}} \frac{\langle \alpha\beta | V_{12} | ab \rangle \langle ab | V_{12} | \alpha\delta \rangle \langle \delta\gamma | V_{12} | \beta\gamma \rangle}{(e_\alpha + e_\delta - e_a - e_b)(e_\beta + e_\gamma - e_a - e_b)}. \quad (\text{A4})$$

This corresponds to the final permutation, from left to right,  $\alpha\beta\gamma$  and also, because of the use of antisymmetrized matrix elements, the permutations  $\beta\alpha\gamma$ ,  $\alpha\gamma\beta$ , and  $\gamma\alpha\beta$ . [Note that the restrictions  $\alpha \neq \beta$  and  $\beta \neq \gamma$  are automatically included in Eq. (A4).] The remaining permutations  $\beta\gamma\alpha$  and  $\gamma\beta\alpha$  must be written separately, and since each permutation arises twice when we sum over all  $\alpha\beta\gamma$  with antisymmetrized matrix elements, we require an additional factor of  $\frac{1}{2}$ . We obtain

$$\begin{aligned} D_{d2} &= -\frac{1}{4} \sum_{\substack{ab \\ \alpha\beta\gamma\delta \\ (\alpha \neq \beta, \alpha \neq \gamma)}} \frac{\langle \beta\gamma | V_{12} | ab \rangle \langle ab | V_{12} | \alpha\delta \rangle \langle \beta\gamma | V_{12} | \delta\alpha \rangle}{(e_\alpha + e_\delta - e_a - e_b)(e_\beta + e_\gamma - e_a - e_b)} \\ &= \frac{1}{4} \sum_{\substack{ab \\ \alpha\beta\gamma\delta \\ (\gamma \neq \beta, \gamma \neq \alpha)}} \frac{\langle \alpha\beta | V_{12} | ab \rangle \langle ab | V_{12} | \gamma\delta \rangle \langle \alpha\beta | V_{12} | \gamma\delta \rangle}{(e_\gamma + e_\delta - e_a - e_b)(e_\beta + e_\alpha - e_a - e_b)}, \end{aligned} \quad (\text{A5})$$

and in the last step we have interchanged dummy summation labels  $\alpha$  and  $\gamma$  and reordered some of the matrix elements.

Now we observe that  $D_{d1}$  is the same as  $D_a$ , apart from the restriction  $\alpha \neq \gamma$ —the exclusion principle is obeyed for incoming lines of the folded diagram, but is ignored in the Goldstone case. Now we can remove the restrictions  $\alpha \neq \gamma$  in Eq. (A4) and  $\gamma \neq \beta, \gamma \neq \alpha$  in Eq. (A5) because the contributions of the additional terms exactly cancel. With these restrictions removed we have

$$D_a = D_{d1}; \quad D_b = D_c + D_{d2}. \quad (\text{A6})$$

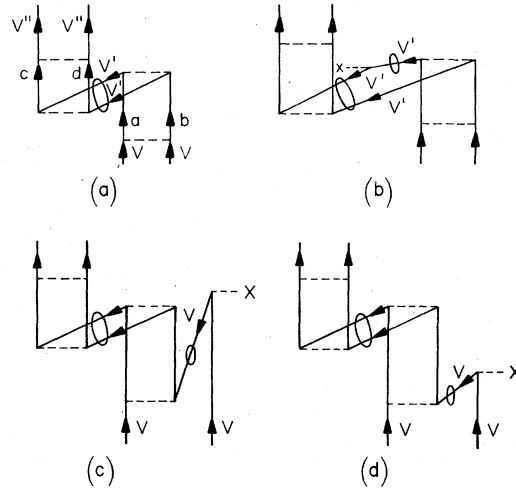


FIG. 56. Diagrams (b), (c), and (d) show the lowest order corrections to diagram (a) which remove the degeneracy of the valence energies.

### APPENDIX B. NONDEGENERATE VALENCE ENERGIES

We have remarked in Sec. II.C that the use of degenerate valence energies simplifies the formalism, but that this restriction can be removed afterwards by summing up the degeneracy-breaking terms in the perturbation, as at the end of Sec. II.B.6. Here we discuss this in more detail for the diagram of Fig. 12(b), which gave rise to the two folded diagrams of Fig. 12(c). One of these is shown again in Fig. 56, diagram (a), the other is to be understood. In this diagram the labels  $a, b, c$ , and  $d$  represent excitations out of the valence orbitals, while  $v, v'$  and  $v''$  represent valence states. The labeling here is taken to refer to the angular momentum of the state. The corresponding  $z$  components of angular momentum are suppressed for the purposes of our schematic argument. Thus the Pauli exclusion principle is not violated when, for simplicity, we give both valence states the same label. The valence states are degenerate with unperturbed single-particle energies  $e$ .

Now let us consider the degeneracy-breaking terms in the perturbation

$$\xi_v |v\rangle \langle v| + \xi_{v'} |v'\rangle \langle v'| \quad (\text{B1})$$

which will convert the single-particle energies  $e$  to

$$e_v = e + \xi_v; \quad e_{v'} = e + \xi_{v'}. \quad (\text{B2})$$

To first order in these terms we shall obtain diagrams (b), (c), and (d), each of which, in fact, represents several diagrams. Firstly the  $\xi$  insertion, represented by the cross, can occur on either of the valence lines—this gives a factor of 2. Secondly all orderings of the interactions consistent with the folded structure are to be taken, i.e., we shall factorize. In diagrams (b) and (c) we have folded twice out of the “main” part of the diagram (the sequence is different), while in diagram (d) we fold out of the “main” part a piece which is itself folded [see the discussion of Eqs. (2.65) and (2.66)]. The unlabeled lines in diagrams (b)–(d) correspond to those in diagram (a).

Only the energy denominator and  $\zeta$  insertions are important for the argument, so we write for the sum of diagrams (a)–(d)

$$\frac{1}{(2e - e_a - e_b)(2e - e_c - e_d)^2} \left\{ 1 - \frac{2\zeta_{v'}}{2e - e_c - e_d} - \frac{2\zeta_v}{2e - e_c - e_d} - \frac{2\zeta_v}{2e - e_a - e_b} \right\}. \quad (\text{B3})$$

These are simply the lowest-order terms which convert the energy denominators of diagram (a) to

$$\frac{1}{(2e_v - e_a - e_b)(2e_{v'} - e_c - e_d)(2e_v - e_c - e_d)} \equiv \frac{1}{(2e_v - e_c - e_d)(2e_v + 2e_{v'} - e_a - e_b - e_c - e_d)} \left\{ \frac{1}{2e_v - e_a - e_b} + \frac{1}{2e_{v'} - e_c - e_d} \right\}. \quad (\text{B4})$$

The latter result follows from the factorization theorem. If we now incorporate the degeneracy-breaking terms (B1) in the unperturbed Hamiltonian  $H_0$ , the first of the two terms follows by operating with  $(2e_v - H_0)^{-1}$  between each interaction in diagram (a) alone. The second term is given similarly by operating on the companion diagram shown explicitly in Fig. 12(c).

Notice that in the above discussion the energies  $e_{v'}$  of the outgoing lines do not enter. A consequence of this is that even diagrams without any folds give rise to a non-Hermitian effective interaction if the valence energies are not degenerate.

### APPENDIX C. DIAGRAM RULES

We give here the diagram rules to be followed for the linked, folded effective interaction discussed in Sec. II.C; these are based on the work of Brandow (1967). Simplifications of the diagram series are possible when projecting core excitations are present; this was mentioned briefly in Sec. II.D, and we refer to Brandow (1967, 1975) for further details. The present rules can also be applied to the case of zero valence particles, i.e., the nondegenerate closed-shell system, in the Goldstone hole representation (see Day, 1967). Alternatively one could use the folded series here; see the discussion of Appendix A. As regards effective operators (other than the interaction), the additional rules have been indicated in Sec. II.D.

#### A. General structure of the diagrams

A general nonfolded diagram will consist of a set of lines entering the bottom of the diagram, representing

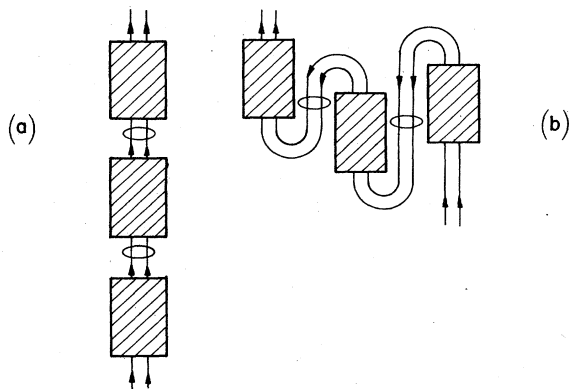


FIG. 57. General structure of the diagrams in unfolded (a) and folded (b) form.

the initial valence state, a number of interactions, and a set of lines leaving the top of the diagram which denote the final valence state. Apart from the case of a single interaction between the initial and final states, there will be one or more intermediate states which must all lie outside the valence space.

A general folded diagram is obtained by joining together a sequence of nonfolded diagrams. An example is given in Fig. 57(a). Here the diagram is said to be drawn in unfolded form. The loops are used to indicate valence states between the nonfolded shaded blocks. Fig. 57(a) is redrawn in folded form in Fig. 57(b). As usual, all dashed interaction lines must occur at different horizontal levels. Further, the topmost interaction of a given folded block must lie above the lowest interaction of the preceding block. In addition the topmost interaction of the folded diagram must be the same as the topmost interaction of the unfolded form of the diagram. These are the only restrictions on the ordering of the interactions in one shaded block with respect to the interactions in another. A number of examples of the folding procedure have been given in Sec. II.

Only linked diagrams need to be considered. Note that it is not necessary for each of the shaded blocks in Fig. 57(a) to be separately linked; we only require the whole diagram to be linked, e.g., Fig. 58 should be included. Within the definition of linked we include diagrams with one or more completely noninteracting valences lines; these noninteracting valence lines should be erased. If all valence lines are noninteracting we are dealing with a diagram which contributes to the energy of the nondegenerate core, rather than the effective interaction.

Note that although we choose a standard ordering for the labels on the incoming valence lines at the bottom of a diagram, we must allow all permutations of the labels on the outgoing valence lines at the top. Each of these contributions must be counted. See, for example, Appendix D.

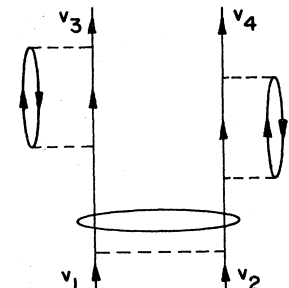


FIG. 58. A diagram which contributes to the linked, folded series for the two-body effective interaction.

**B. Evaluation of the diagrams**

**1. Matrix elements**

Each one-body interaction  $-U$  of Eq. (2.3) contributes

$$\langle \text{particle out} | -U | \text{particle in} \rangle, \tag{C1}$$

where in (out) refers to lines with arrows pointing toward (away from) the vertex.

Each two-body interaction  $V_{12}$  gives a matrix element

$$\langle \text{particle out left, particle out right} | V_{12} | \text{particle in left, particle in right} \rangle. \tag{C2}$$

Here left and right refer to the appropriate ends of the vertex. Each two-body matrix element is antisymmetrized, i.e., it contains both direct and exchange terms, explicitly,

$$\langle ij | V_{12} | kl \rangle \equiv \langle i(1)j(2) | V_{12} | k(1)l(2) - k(2)l(1) \rangle \tag{C3}$$

$$\equiv \frac{1}{2} \langle i(1)j(2) - i(2)j(1) | V_{12} | k(1)l(2) - k(2)l(1) \rangle. \tag{C4}$$

This automatically includes exchange diagrams where a direct matrix element is replaced by an exchange matrix element at one or more vertices. These exchange diagrams must therefore not be counted separately. Also, we should not include separately topologically equivalent diagrams which only differ by an interchange of the left and right ends of one or more vertices. Thus we need to evaluate one diagram from the set of exchange and topologically equivalent diagrams which can be drawn. Equivalent diagrams are most easily identified by contracting the dashed line to a dot [Hugenholtz (1957) notation], since they all take the same form in this notation. Further discussion of equivalent diagrams is given in Sec. C of Appendix C below.

**2. Summations**

We refer to Fig. 57. Within each shaded block, downgoing (upgoing) lines are to be summed over all orbitals which are (are not) filled in the unperturbed closed-shell core. Between blocks, each of the looped, folded lines is to be summed over all valence orbitals. In all cases the Pauli exclusion principle is to be ignored.

**3. Energy denominators**

Energy denominators may be evaluated by operating with  $(\epsilon_v - H_0)^{-1}$  between the interactions, giving

$$\left[ \epsilon_v + \sum (\text{hole-particle}) \text{ energies} \right]^{-1}.$$

Here  $\epsilon_v$  is the unperturbed energy of the initial valence state entering the bottom of the diagram. It is essential to treat the downgoing folded valence lines as hole lines in evaluating the denominator.

**4. Factors and phases**

A factor of  $\frac{1}{2}$  is to be included for each equivalent pair of lines. An equivalent pair of lines is defined to be two lines which start at the same interaction, end at the same interaction and go in the same direction. Notice that two folded lines can satisfy the equivalent pair definition.

As regards phases, it is necessary first of all to

choose a standard ordering for the products of single-particle wave functions which make up our valence states. Secondly the diagram in question should be drawn in such a way that the first, second, ... line from the left entering the bottom of the diagram traces through a series of interactions and remains the first, second, ... line from the left on emerging at the top of the diagram. Thus the diagram in Fig. 59 should be drawn in the form (b), rather than (a). Then the sign of the diagram is given by

$$(-1)^{n_{SO} + n_F + n_H + n_L + n_{VH}},$$

where  $n_{SO}$  is the total number of interchanges of pairs of labels on the valence lines leaving the top of the diagram needed to achieve standard ordering (the incoming valence lines at the bottom of the diagram are assumed to be in standard order),  $n_F$  is the number of folds,  $n_H$  is the number of hole lines (in the nonfolded shaded blocks of Fig. 57),  $n_L$  is the number of closed loops, and  $n_{VH}$  is the number of valence hole lines at the bottom of the diagram plus the number of folded valence hole lines. This quantity is needed if our valence states consist of a number of holes in the core, or if both particles and holes are present. (Such cases have not been explicitly discussed, but the effective interaction formalism can be applied here too.)

**C. Further discussion and examples**

We first elaborate on the question of exchange and topologically equivalent diagrams using the core-polarization diagram as an example (see the following Appendix D for a detailed evaluation of this diagram). Consider diagrams (a) and (b) of Fig. 60. For the present discussion we shall use direct matrix elements only at each vertex, so using Eq. (C2) for the matrix elements and Sec. B.4 for the phase, we obtain for diagram (a)

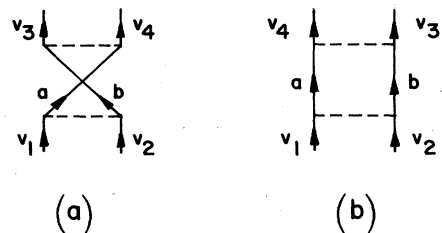


FIG. 59. An illustration, for the purposes of the phase rule of Appendix C (Sec. B.4), of a diagram which is drawn in non-allowed form (a) and allowed form (b).

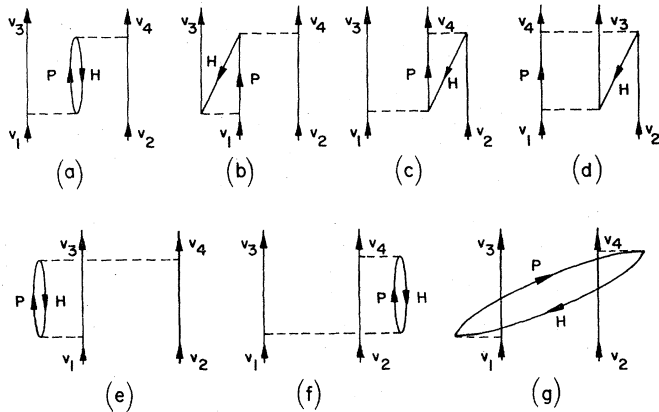


FIG. 60 Exchange and topologically equivalent versions of the core-polarization diagram (not all possibilities are shown).

$$\langle v_3(1)P(2) | V_{12} | v_1(1)H(2) \rangle \langle H(1)v_4(2) | V_{12} | P(1)v_2(2) \rangle. \quad (\text{C5})$$

Diagram (b) gives

$$-\langle v_3(1)P(2) | V_{12} | H(1)v_1(2) \rangle \langle H(1)v_4(2) | V_{12} | P(1)v_2(2) \rangle. \quad (\text{C6})$$

The change in sign arises since  $n_L = 1$  for diagram (a) and 0 for diagram (b). Diagram (b) can be called an exchange diagram, since it differs from diagram (a) just in the interchange of  $H$  and  $v_1$  at the lower vertex, i.e., we have taken the exchange matrix element here. In similar fashion exchange diagrams (c) and (d) are obtained from diagram (a) by taking the exchange matrix element at the upper vertex and at both vertices, respectively. Clearly all these diagrams can be included by evaluating just one of them using the antisymmetrized matrix elements of Eq. (C3). Now consider diagrams (e), (f), and (g) of Fig. 60, which are obtained from diagram (a) by interchanging the left and right ends of one or both interaction vertices, i.e., interchanging the labels 1 and 2 in one or both matrix elements of Eq. (C5). These four diagrams, (a), (e), (f), and (g), are said to be topologically equivalent, since they obviously all have the same value and represent the same physical process. If we count them all, a factor of  $\frac{1}{4}$  is required. Similarly Fig. 60(b) is one member of a group of four topologically equivalent diagrams (not shown), and the same remark applies to Figs. 60(c) and (d). In all we have 16 diagrams and a factor of  $\frac{1}{4}$ . This just corresponds to writing out all the terms when Eq. (C4) is used for the matrix elements entering, say, diagram (a). Obviously the simplest procedure is to select one member of the set of exchange and topologically equivalent diagrams and use Eq. (C3) or (C4) for the matrix element at each vertex. We mentioned above that a

FIG. 61. The core polarization diagram in Hugenholtz notation. Note that in this notation all the diagrams of Fig. 60 take the form shown here.

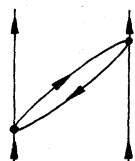


TABLE CI. Illustration of the phase rule for various diagrams.

Diagram	$n_{SO}$	$n_F$	$n_H$	$n_L$	$n_{VH}$	Phase
Fig. 58	0	1	2	2	0	-1
Fig. 59(b)	1	0	0	0	0	-1
Fig. 60(a)	0	0	1	1	0	+1
Fig. 60(d)	1	0	1	0	0	+1
Fig. 62(a)	0	0	1	1	1	-1
Fig. 62(b)	0	1	3	1	3	+1

simple test for the equivalence of diagrams is to contract the dashed interaction line to a dot. If this is done for the diagrams of Fig. 60 they all yield Fig. 61, thus demonstrating their equivalence.

The need for the equivalent pair rule of Sec. B.4 is easily seen by reference to the ladder diagram, Fig. 59(b). To count each intermediate state we should sum over state labels  $a > b$ . This can be replaced by a sum over all  $a, b$ , as required by Sec. B.2 above, if a factor of  $\frac{1}{2}$  is introduced. (The case  $a = b$  gives zero, since antisymmetrized matrix elements are used.) Note that the case where both  $a$  and  $b$  refer to valence orbitals must be omitted from the summation, since the intermediate states must lie outside the valence space.

Several examples of the application of the phase rule, Sec. B.4, are given in Table CI; standard orderings for our valence states have been chosen to be  $v_1v_2$  and  $v_3v_4$ . Notice that the Hartree-Fock bubble insertion of Fig. 62 gives one hole line and one closed loop. It is often worthwhile to check the phase by writing down the appropriate creation and annihilation operators and working out the contractions explicitly.

#### APPENDIX D. EXPLICIT EVALUATION OF THE CORE-POLARIZATION DIAGRAM

Firstly, it is worth pointing out that part of the core-polarization diagram arises as a correction for Pauli exclusion principle violations. Thus in Fig. 63(a) the presence of the noninteracting valence line causes the one-body diagram to violate the Pauli exclusion principle. The correction for this is given by Fig. 63(b) and, as we see by reference to Fig. 60(d), this is an exchange form of the core-polarization diagram. Notice that the labels on the final state are restricted, so this gives only part of the total core-polarization contribution.

Turning to the evaluation of the core-polarization diagram, we need to consider the contribution of all the diagrams of Fig. 64. These diagrams differ by exchanges of the valence particle labels on the external legs and, since they are not automatically included by

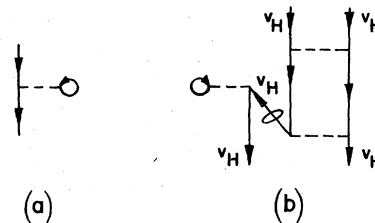


FIG. 62. Diagrams contributing to the one- and two-body effective interaction for valence holes.

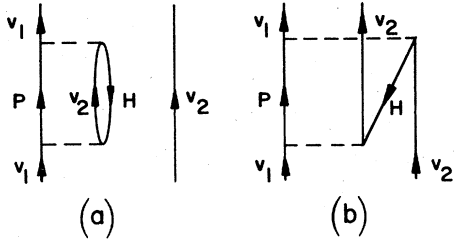


FIG. 63. Illustration of the fact that the core-polarization diagram, (b), corrects for violation of the Pauli exclusion principle in diagram (a).

using antisymmetrized matrix elements, they must be put in explicitly. In Fig. 64 the label  $v_1$  implies angular momentum  $j_1$ ,  $z$ -component  $m_1$ , and isospin  $z$ -component  $\tau_1$ ; the label  $P$  implies angular momentum  $j_P$ ,  $z$ -component  $m_P$ , and isospin  $z$ -component  $\tau_P$ , etc. Using the diagram rules, with  $v_1v_2$  and  $v_3v_4$  as standard ordering, we obtain for Fig. 64(a)

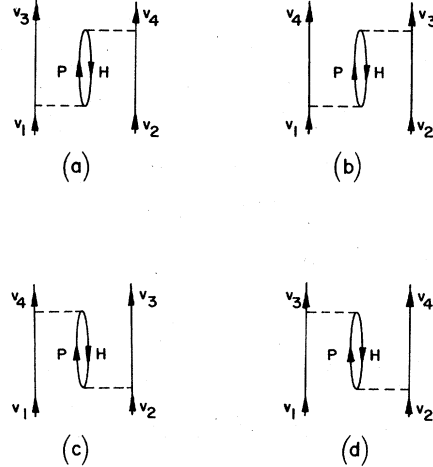


FIG. 64. The four independent core-polarization contributions to the effective interaction. They must all be included.

$$\begin{aligned}
 & [(1 + \delta_{j_1j_2})(1 + \delta_{j_3j_4})]^{-1/2} \sum_{\substack{j_P, j_H \\ z\text{-components} \\ (M, M_T \text{ fixed})}} C(j_1 m_1 j_2 m_2; JM) C(\frac{1}{2} \tau_1 \frac{1}{2} \tau_2; TM_T) C(j_3 m_3 j_4 m_4; JM) C(\frac{1}{2} \tau_3 \frac{1}{2} \tau_4; TM_T) \\
 & \times \frac{\langle j_3 m_3 \tau_3 j_P m_P \tau_P | V_{12} | j_1 m_1 \tau_1 j_H m_H \tau_H \rangle \langle j_4 m_4 \tau_4 j_H m_H \tau_H | V_{12} | j_2 m_2 \tau_2 j_P m_P \tau_P \rangle}{e_{j_1} - e_{j_3} + e_{j_H} - e_{j_P}}. \quad (D1)
 \end{aligned}$$

Here we have normalized our valence states and coupled them to total angular momentum  $J$ , isospin  $T$ , with corresponding  $z$ -components  $M$  and  $M_T$ . The labels  $J$ ,  $M$ ,  $T$ , and  $M_T$  must be the same for our initial and final valence states because of the invariance of the interaction  $V_{12}$  under rotations in space and also under rota-

tions in isospin space. This property of  $V_{12}$  makes it useful to couple the two particle states in the matrix elements to a definite angular momentum and isospin, as these labels are diagonal and the matrix element is independent of the corresponding  $z$ -components. We then obtain for Eq. (D1)

$$\begin{aligned}
 & [(1 + \delta_{j_1j_2})(1 + \delta_{j_3j_4})]^{-1/2} \sum_{\substack{j_P, j_H \\ j_1, T_1, j_2, T_2}} R(j_1, j_2, j_3, j_4, j_P, j_H, J_1, J_2) R(\frac{1}{2}, \frac{1}{2}, \frac{1}{2}, \frac{1}{2}, \frac{1}{2}, \frac{1}{2}, T_1, T_2) \\
 & \times \frac{\langle (j_3 j_P) J_1 T_1 | V_{12} | (j_1 j_H) J_1 T_1 \rangle \langle (j_4 j_H) J_2 T_2 | V_{12} | (j_2 j_P) J_2 T_2 \rangle}{e_{j_1} - e_{j_3} + e_{j_H} - e_{j_P}}. \quad (D2)
 \end{aligned}$$

Here the states involved in the antisymmetrized twobody matrix elements are normalized according to

$$\langle (j_a j_b) J_\alpha T_\alpha | (j_a j_b) J_\alpha T_\alpha \rangle = 1 + (-1)^{J_\alpha + T_\alpha + 1} \delta_{j_a j_b}$$

and

$$\begin{aligned}
 R(j_1, j_2, j_3, j_4, j_P, j_H, J_1, J_2) &= \sum_{\substack{z\text{-components} \\ (M \text{ fixed})}} C(j_3 m_3 j_P m_P; J_1 M_1) C(j_1 m_1 j_H m_H; J_1 M_1) \\
 &\times C(j_4 m_4 j_H m_H; J_2 M_2) C(j_2 m_2 j_P m_P; J_2 M_2) C(j_1 m_1 j_2 m_2; JM) C(j_3 m_3 j_4 m_4; JM) \\
 &= \sum_{J''} (-1)^{j_2 + j_4 + J_1 + J_2 + J} (2J_1 + 1)(2J_2 + 1)(2J'' + 1) \\
 &\times \begin{Bmatrix} j_1 & j_2 & J \\ j_4 & j_3 & J'' \end{Bmatrix} \begin{Bmatrix} j_1 & j_3 & J'' \\ j_P & j_H & J_1 \end{Bmatrix} \begin{Bmatrix} j_2 & j_4 & J'' \\ j_H & j_P & J_2 \end{Bmatrix}. \quad (D3)
 \end{aligned}$$

The latter step follows after some straightforward, though tedious, Racah algebra. The summation over the three 6- $j$  symbols can be written as a 9- $j$  symbol; however, it is often more useful to keep the above form since  $J''$  is the result of coupling the angular momenta of the particle  $j_P$  and the hole  $j_H$ . The analogous isospin recoupling expression provides the corresponding label  $T''$ . It is useful to decompose the diagram according to the  $J''T''$  of the particle-hole pair, as we have seen in Sec. III.

The contribution of Fig. 64(a) to the matrix element of the effective interaction  $\langle(j_3 j_4)JT | \mathcal{V}_V | (j_1 j_2)JT \rangle$  is thus

$$\begin{aligned} &\text{for diagram (b) } j_3 \leftrightarrow j_4 \text{ additional phase } (-1)^{j_3+j_4-J-T} \\ &\text{for diagram (c) } j_1 \leftrightarrow j_2 \text{ additional phase } (-1)^{j_1+j_2-J-T} \\ &\text{for diagram (d) } j_1 \leftrightarrow j_2, j_3 \leftrightarrow j_4 \text{ additional phase } (-1)^{j_1+j_2+j_3+j_4}. \end{aligned}$$

To see the origin of the extra phase needed, consider diagram (b). Firstly we need  $(-1)^j$ , due to the nonstandard ordering of the final valence state, and secondly we need a phase  $(-1)^{j_3+j_4-J+\frac{1}{2}+\frac{1}{2}-T}$  so that  $v_3$  and  $v_4$  are coupled in the standard order, as in the Clebsch-Gordan coefficients of Eq. (D1). If  $j_1=j_2=j_3=j_4$ , then diagrams (a), (b), (c), and (d) clearly all have the same value.

So far we have used the interaction  $V_{12}$  but, as we have discussed in Sec. III.B, this must be replaced by the reaction matrix  $G(\omega)$ . In other words each single interaction is generalized to allow an infinite series of ladder interactions, so that in the present case we shall include diagrams of the type indicated in Fig. 65. The replacement of the matrix elements of  $V_{12}$  by those of  $G(\omega)$  in Eq. (D2) is complicated by the need to choose the correct starting energy  $\omega$ . For the lower vertex this can be determined by looking at the lowest two interactions in Fig. 65, which give

$$\frac{\langle v_3 P | V_{12} | ab \rangle \langle ab | V_{12} | v_1 H \rangle}{e_{j_1} + e_{j_H} - e_{j_a} - e_{j_b}}. \quad (\text{D4})$$

Recall from Sec. III.B that the energy denominator of the  $G$  matrix is given by  $(\omega - H_0)$  with  $H_0$  acting on the intermediate two-particle state. This gives  $(\omega - e_{j_a} - e_{j_b})$  in the present case, so in order to obtain the denominator of expression (D4) we require

$$\begin{aligned} \omega &= e_{j_1} + e_{j_H} \\ &= (e_{j_1} + e_{j_2}) + (e_{j_H} - e_{j_2}). \end{aligned} \quad (\text{D5})$$

The latter form emphasizes that this value of  $\omega$  differs from that required for the bare matrix element, namely  $\omega = e_{j_1} + e_{j_2}$ . In similar fashion it can be shown that at the upper vertex

$$\omega = (e_{j_1} + e_{j_2}) + (e_{j_H} - e_{j_3}) \quad (\text{D6})$$

is required.

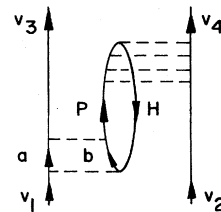


FIG. 65. Typical diagram arising when particle-particle ladders are summed to replace the matrix elements of  $V_{12}$  by those of the reaction matrix  $G$  in the core-polarization diagram.

given by expressions (D2) and (D3). These expressions may also be used for diagrams (b), (c), and (d) of Fig. 64 by suitable interchange of the labels. Explicitly

## REFERENCES

- Ajzenberg-Selove, F., 1972, Nucl. Phys. A **190**, 1.  
 Anastasio, M. R., J. W. Hockert, and T. T. S. Kuo, 1974, Phys. Lett. B **53**, 221.  
 Anastasio, M. R., and T. T. S. Kuo, 1975, Nucl. Phys. A **238**, 79.  
 Anastasio, M. R., T. T. S. Kuo, T. Engeland, and E. Osnes, 1976, Nucl. Phys. A **271**, 109.  
 Anastasio, M. R., T. T. S. Kuo, and J. B. McGrory, 1975, Phys. Lett. B **57**, 1.  
 Andō, K., H. Bandō, and S. Nagata, 1977, Prog. Theor. Phys. **57**, 1303 and 1584.  
 Andreozzi, F., and G. Sartoris, 1976, Nucl. Phys. A **270**, 388.  
 Babu, S., and G. E. Brown, 1973, Ann. Phys. (N.Y.) **78**, 1.  
 Baranger, M., 1960, Phys. Rev. **120**, 957.  
 Baranger, M., 1969, in *Proceedings of the International School of Physics "Enrico Fermi"*, Course XL, Varenna, 1967, edited by M. Jean (Academic, New York), p. 511.  
 Barrett, B. R., 1968, Nucl. Phys. A **109**, 129.  
 Barrett, B. R., 1972, Phys. Lett. B **38**, 371.  
 Barrett, B. R., 1974, Nucl. Phys. A **221**, 299.  
 Barrett, B. R., E. C. Halbert, and J. B. McGrory, 1975, Ann. Phys. (N.Y.) **90**, 321.  
 Barrett, B. R., R. G. L. Hewitt, and R. J. McCarthy, 1971, Phys. Rev. C **3**, 1137.  
 Barrett, B. R., and M. W. Kirson, 1970, Nucl. Phys. A **148**, 145.  
 Barrett, B. R., and M. W. Kirson, 1972, Nucl. Phys. A **196**, 638.  
 Barrett, B. R., and M. W. Kirson, 1973, in *Advances in Nuclear Physics*, edited by M. Baranger and E. Vogt (Plenum, New York), Vol. 6, p. 219.  
 Barrett, B. R., and M. W. Kirson, 1975, Phys. Lett. B **55**, 129.  
 Becker, R. L., K. T. R. Davies, and M. R. Patterson, 1974, Phys. Rev. C **9**, 1221.  
 Benson, H. G., and B. H. Flowers, 1969, Nucl. Phys. A **126**, 332.  
 Bertsch, G. F., 1965, Nucl. Phys. **74**, 234.  
 Bertsch, G. F., 1968, Phys. Rev. Lett. **21**, 1694.  
 Bethe, H. A., 1956, Phys. Rev. **103**, 1353.  
 Bethe, H. A., 1965, Phys. Rev. **138**, 804B.  
 Bethe, H. A., 1971, Ann. Rev. Nucl. Sci. **21**, 93.  
 Bethe, H. A., B. H. Brandow, and A. G. Petschek, 1963, Phys. Rev. **129**, 225.  
 Bethe, H. A., and J. Goldstone, 1957, Proc. R. Soc. Lond. A **238**, 551.

- Bloch, C., and J. Horowitz, 1958, Nucl. Phys. **8**, 91.
- Blomqvist, J., and T. T. S. Kuo, 1969, Phys. Lett. B **29**, 544.
- Brandow, B. H., 1966, Phys. Rev. **152**, 863.
- Brandow, B. H., 1967, Rev. Mod. Phys. **39**, 771; see also *Lectures in Theoretical Physics XI-B*, edited by K. T. Mahanthappa and W. E. Brittin (Gordon and Breach, New York, 1969), p. 55; and *Advances in Quantum Chemistry*, edited by P.-O. Löwdin (Academic, New York) Vol. 10, to be published.
- Brandow, B. H., 1975, in *Proceedings of the International Topical Conference on Effective Interactions and Operators in Nuclei*, Tucson, 1975, edited by B. R. Barrett, Lecture Notes in Physics **40**, 1 (Springer-Verlag, Berlin).
- Brown, B. A., A. Arima, and J. B. McGrory, 1977, Nucl. Phys. A **277**, 77.
- Brown, G. E., 1971a, *Unified Theory of Nuclear Models and Forces* (North-Holland, Amsterdam).
- Brown, G. E., 1971b, Rev. Mod. Phys. **43**, 1.
- Brown, G. E., and M. Bolsterli, 1959, Phys. Rev. Lett. **3**, 472.
- Brown, G. E., and A. M. Green, 1966, Nucl. Phys. **85**, 87.
- Brown, G. E., and A. D. Jackson, 1975, *The Nucleon-Nucleon Interaction* (North-Holland, Amsterdam).
- Brown, G. E., and T. T. S. Kuo, 1967, Nucl. Phys. A **92**, 481.
- Brueckner, K. A., 1955, Phys. Rev. **100**, 36.
- Brueckner, K. A., C. A. Levinson, and H. M. Mahmoud, 1954, Phys. Rev. **95**, 217.
- Comins, H. N., and R. G. L. Hewitt, 1974, Nucl. Phys. A **228**, 141 and 153.
- Dahll, G., E. Østgaard, and B. Brandow, 1969, Nucl. Phys. A **124**, 481.
- Davies, K. T. R., and M. Baranger, 1970, Phys. Rev. C **1**, 1640.
- Dawson, J. F., I. Talmi, and J. D. Walecka, 1962, Ann. Phys. (N.Y.) **18**, 339.
- Day, B. D., 1964, Ph.D. Thesis, Cornell University, unpublished.
- Day, B. D., 1967, Rev. Mod. Phys. **39**, 719.
- de-Shalit, A., and I. Talmi, 1963, *Nuclear Shell Theory* (Academic, New York).
- de Takacsy, N., 1967, Nucl. Phys. A **95**, 505.
- des Cloizeaux, J., 1960, Nucl. Phys. **20**, 321.
- Dieperink, A. E. L., H. P. Leenhouts, and P. J. Brussaard, 1968, Nucl. Phys. A **116**, 556.
- Dirim, H., J. P. Elliott, and J. A. Evans, 1975, Nucl. Phys. A **244**, 301.
- Eden, R. J., and N. C. Francis, 1955, Phys. Rev. **97**, 1366.
- Eisenstein, I., and M. W. Kirson, 1973, Phys. Lett. B **47**, 315.
- Elliott, J. P., A. D. Jackson, H. A. Mavromatis, E. A. Sander-son, and B. Singh, 1968, Nucl. Phys. A **121**, 241.
- Elliott, J. P., and A. M. Lane, 1957, in *Encyclopedia of Physics*, edited by S. Flügge (Springer, Berlin), Vol. 39, p. 241.
- Ellis, P. J., 1975, Phys. Lett. B **56**, 232.
- Ellis, P. J., and T. Engeland, 1970, Nucl. Phys. A **144**, 161; see also Engeland, T., and P. J. Ellis, 1972, Nucl. Phys. A **181**, 368.
- Ellis, P. J., A. D. Jackson, and E. Osnes, 1972, Nucl. Phys. A **196**, 161.
- Ellis, P. J., and H. A. Mavromatis, 1971, Nucl. Phys. A **175**, 309.
- Ellis, P. J., and E. Osnes, 1972a, Phys. Lett. B **41**, 97.
- Ellis, P. J., and E. Osnes, 1972b, Phys. Lett. B **42**, 335.
- Ellis, P. J., and E. Osnes, 1973, Phys. Lett. B **45**, 425.
- Ellis, P. J., and S. Siegel, 1970, Nucl. Phys. A **152**, 547.
- Ellis, P. J., and S. Siegel, 1971, Phys. Lett. B **34**, 177.
- Engeland, T., 1965, Nucl. Phys. **72**, 68.
- Erikson, T., and G. E. Brown, 1977, Nucl. Phys. A **277**, 1.
- Feshbach, H., 1962, Ann. Phys. (N.Y.) **19**, 287.
- Fortune, H. T., and S. C. Headley, 1974, Phys. Lett. B **51**, 136.
- Frantz, L. M., and R. L. Mills, 1960, Nucl. Phys. **15**, 16.
- Gerace, W. J., and A. M. Green, 1967, Nucl. Phys. A **93**, 110.
- Goldstone, J., 1957, Proc. R. Soc. Lond. A **239**, 267.
- Goode, P., 1971, Nucl. Phys. A **172**, 66.
- Goode, P., 1974, Phys. Lett. **51B**, 429.
- Goode, P., 1975, Nucl. Phys. A **241**, 311.
- Goode, P., and M. W. Kirson, 1974, Phys. Lett. **51B**, 221.
- Goode, P., and D. S. Koltun, 1975, Nucl. Phys. A **243**, 44.
- Goode, P., and S. Siegel, 1970, Phys. Lett. **31B**, 418.
- Goode, P., B. J. West, and S. Siegel, 1972, Nucl. Phys. A **187**, 249.
- Goodin, F. L., P. J. Ellis, and P. R. Goode, 1977, Phys. Rev. C **16**, 784.
- Halbert, E. C., J. B. McGrory, B. H. Wildenthal, and S. P. Pandya, 1971, in *Advances in Nuclear Physics*, edited by M. Baranger and E. Vogt (Plenum, New York), Vol. 4, p. 315.
- Hamada, T., and I. D. Johnston, 1962, Nucl. Phys. **34**, 382.
- Harvey, M., 1975, Ann. Phys. (N.Y.) **94**, 47.
- Harvey, M., and F. C. Khanna, 1970, Nucl. Phys. A **155**, 337.
- Harvey, M., H. C. Lee, and P. Amiot, 1976, "Renormalization for Collective Motion within a Truncated Space of the Spherical Shell Model, II. Projected Frame in a Schematic Model," preprint.
- Herbert, F., and B. R. Barrett, 1975, Nucl. Phys. A **254**, 13.
- Hofmann, H. M., S. Y. Lee, J. Richert, H. A. Weidenmüller, and T. H. Schucan, 1973, Phys. Lett. B **45**, 421.
- Hofmann, H. M., S. Y. Lee, J. Richert, H. A. Weidenmüller, and T. H. Schucan, 1974a, Ann. Phys. (N.Y.) **85**, 410.
- Hofmann, H. M., J. Richert, and T. H. Schucan, 1974b, Z. Phys. **268**, 293.
- Hofmann, H. M., Y. Starkand, and M. W. Kirson, 1976, Nucl. Phys. A **266**, 138.
- Horie, H., and A. Arima, 1955, Phys. Rev. **99**, 778.
- Hughenoltz, N. M., 1957, Physica **23**, 481.
- Johnson, M. B., and M. Baranger, 1971, Ann. Phys. (N.Y.) **62**, 172.
- Jopko, A. M., and D. W. L. Sprung, 1973, Can. J. Phys. **51**, 2275.
- Kahana, S., H. C. Lee, and C. K. Scott, 1969, Phys. Rev. **180**, 956.
- Katz, A., 1960, Nucl. Phys. **20**, 663.
- Kirson, M. W., 1971, Ann. Phys. (N.Y.) **66**, 624 and **68**, 556.
- Kirson, M. W., 1974, Ann. Phys. (N.Y.) **82**, 345.
- Kirson, M. W., 1975, in *Proceedings of the International Topical Conference on Effective Interactions and Operators in Nuclei*, Tucson, 1975, edited by B. R. Barrett, Lecture Notes in Physics (Springer, Berlin), Vol. 40, p. 330.
- Kirson, M. W., and L. Zamick, 1970, Ann. Phys. (N.Y.) **60**, 188.
- Knöpfle, K. T., G. J. Wagner, H. Breuer, M. Rogge, and C. Mayer-Böricke, 1975, Phys. Rev. Lett. **35**, 779.
- Köhler, H. S., 1974, "The Selfconsistent Field and the Convergence of Rearrangement and Core-Polarization Diagrams," unpublished.
- Krenciglowa, E. M., C. L. Kung, T. T. S. Kuo, and E. Osnes, 1976a, Phys. Lett. B **63**, 141.
- Krenciglowa, E. M., C. L. Kung, T. T. S. Kuo, and E. Osnes, 1976b, Ann. Phys. (N.Y.) **101**, 154.
- Krenciglowa, E. M., and T. T. S. Kuo, 1974, Nucl. Phys. A **235**, 171.
- Krenciglowa, E. M., and T. T. S. Kuo, 1975, Nucl. Phys. A **240**, 195.
- Krenciglowa, E. M., T. T. S. Kuo, E. Osnes, and B. Giraud, 1973, Phys. Lett. B **47**, 322.
- Kuo, T. T. S., 1967, Nucl. Phys. A **103**, 71.
- Kuo, T. T. S., 1968, Nucl. Phys. A **122**, 325.
- Kuo, T. T. S., 1974, Ann. Rev. Nucl. Sci. **24**, 101.
- Kuo, T. T. S., and G. E. Brown, 1966, Nucl. Phys. **85**, 40.
- Kuo, T. T. S., and G. E. Brown, 1968, Nucl. Phys. A **114**, 241.
- Kuo, T. T. S., S. Y. Lee, and K. F. Ratcliff, 1971, Nucl. Phys. A **176**, 65.
- Kuo, T. T. S., and E. Osnes, 1973, Nucl. Phys. A **205**, 1.
- Kuo, T. T. S., and E. Osnes, 1974, Nucl. Phys. A **226**, 204.
- Kuo, T. T. S., and E. Osnes, 1975, Phys. Rev. C **12**, 309.

- Kuo, T. T. S and E. Osnes, 1977, in *Contributions to the Topical Conference on the Physics of Medium-Light Nuclei*, Florence, 1977 (University of Florence, Florence, Italy) p. 22.
- Lane, A. M., 1964, *Nuclear Theory* (Benjamin, New York).
- Lawson, R. D., F. J. D. Serduke, and H. T. Fortune, 1976, *Phys. Rev. C* **14**, 1245.
- Lee, T.-S. H., and S. Pittel, 1975, *Phys. Lett. B* **53**, 409.
- Leinaas, J. M., and T. T. S. Kuo, 1976a, *Phys. Lett. B* **62**, 275.
- Leinaas, J. M., and T. T. S. Kuo, 1976b, *Ann. Phys. (N.Y.)* **98**, 177.
- Lo Iudice, N., D. J. Rowe, and S. S. M. Wong, 1971, *Phys. Lett. B* **37**, 44.
- Lo Iudice, N., D. J. Rowe, and S. S. M. Wong, 1974, *Nucl. Phys. A* **219**, 171.
- Lo Iudice, N., D. J. Rowe, and S. S. M. Wong, 1975, *Nucl. Phys. A* **245**, 479.
- Löwdin, P.-O., 1962, *J. Math. Phys.* **3**, 969.
- Maçfarlane, M. H., 1969, in *Proceedings of the International School of Physics "Enrico Fermi"*, Course XL, Varenna, 1967, edited by M. Jean (Academic, New York), p. 457.
- Malta, C., 1972, D. Phil. Thesis, University of Sussex, unpublished; see also Malta, C. P., and E. A. Sanderson, 1974, *Nucl. Phys. A* **225**, 189.
- Mavromatis, H. A., 1973, *Nucl. Phys. A* **206**, 477.
- Mayer, M. G., and J. H. D. Jensen, 1955, *Elementary Theory of Nuclear Shell Structure* (Wiley, New York).
- Morita, T., 1963, *Prog. Theor. Phys.* **29**, 351.
- Moszkowski, S. A., and B. L. Scott, 1960, *Ann. Phys. (N.Y.)* **11**, 65.
- Mottelson, B. R., 1959, in *The Many-Body Problem*, Summer School of Theoretical Physics, Les Houches, 1958, edited by C. DeWitt and P. Nozières (Wiley, New York), p. 283.
- Mottelson, B. R., 1962, in *Proceedings of the International School of Physics "Enrico Fermi"*, Course XV, Varenna, 1960, edited by G. Racah (Academic, New York), p. 44.
- Oberlechner, G., F. Owono-N'-Guema, and J. Richert, 1970, *Nuovo Cimento B* **68**, 23.
- Osnes, E., 1968, *Phys. Lett. B* **26**, 274.
- Osnes, E., T. T. S. Kuo, and C. S. Warke, 1971, *Nucl. Phys. A* **168**, 190.
- Osnes, E., and C. S. Warke, 1969, *Phys. Lett. B* **30**, 306.
- Pandharipande, V. R., and R. B. Wiringa, 1976, *Nucl. Phys. A* **266**, 269.
- Pittel, S., 1976, *Nucl. Phys. A* **271**, 62.
- Pittel, S., C. M. Vincent, and J. D. Vergados, 1976, *Phys. Rev. C* **13**, 412.
- Pradhan, H. C., P. U. Sauer, and J. P. Vary, 1972, *Phys. Rev. C* **6**, 407.
- Preedom, B. M., and B. H. Wildenthal, 1972, *Phys. Rev. C* **6**, 1633.
- Quesne, C., 1970, *Phys. Lett. B* **31**, 7.
- Rajaraman, R., and H. A. Bethe, 1967, *Rev. Mod. Phys.* **39**, 745.
- Rajewski, J., and M. W. Kirson, 1972, *Nucl. Phys. A* **181**, 409.
- Reid, R. V., 1968, *Ann. Phys. (N.Y.)* **50**, 411.
- Richert, J., T. H. Schucan, M. H. Simbel, and H. A. Weidenmüller, 1976, *Ann. Phys. (N.Y.)* **96**, 139.
- Sandel, M. S., R. J. McCarthy, and B. R. Barrett, 1977, *Z. Phys. A* **280**, 259.
- Sartoris, G., and L. Zamick, 1967, *Phys. Lett. B* **25**, 5.
- Satchler, G. R., 1972, *Nucl. Phys. A* **195**, 1; see also *Comments Nucl. Part. Phys.* **5**, 145.
- Sauer, P. U., 1970, *Nucl. Phys. A* **150**, 467.
- Schaefer, P. A., 1974, *Ann. Phys. (N.Y.)* **87**, 375.
- Schiffer, J. P., and W. W. True, 1976, *Rev. Mod. Phys.* **48**, 191.
- Schucan, T. H., 1975, in *Proceedings of the International Topical Conference on Effective Interactions and Operators in Nuclei*, Tucson, 1975, edited by B. R. Barrett, *Lecture Notes in Physics* (Springer, Berlin), Vol. 40, p. 228.
- Schucan, T. H., and H. A. Weidenmüller, 1972, *Ann. Phys. (N.Y.)* **73**, 108.
- Schucan, T. H., and H. A. Weidenmüller, 1973, *Ann. Phys. (N.Y.)* **76**, 483.
- Sharp, R. W., and L. Zamick, 1973, *Nucl. Phys. A* **208**, 130.
- Sharp, R. W., and L. Zamick, 1974, *Nucl. Phys. A* **223**, 333.
- Shimizu, K., M. Ichimura, and A. Arima, 1974, *Nucl. Phys. A* **226**, 282 and private communication.
- Siegel, S., 1970, Ph.D. Thesis, Rutgers University, unpublished.
- Siegel, S., and L. Zamick, 1969, *Phys. Lett. B* **28**, 453.
- Siegel, S., and L. Zamick, 1970, *Nucl. Phys. A* **145**, 89 and **A** **155**, 674.
- Singh, B., 1974, *Nucl. Phys. A* **219**, 621.
- Sjöberg, O., 1973, *Ann. Phys. (N.Y.)* **78**, 39.
- Sprung, D. W. L., and A. M. Jopko, 1972, *Can. J. Phys.* **50**, 2768.
- Starkand, Y., and M. W. Kirson, 1975, *Phys. Lett. B* **55**, 125.
- Starkand, Y., and M. W. Kirson, 1976, *Nucl. Phys. A* **261**, 453.
- Talmi, I., 1962, *Rev. Mod. Phys.* **34**, 704.
- Tsai, S. F., 1973, Ph.D. Thesis, State University of New York at Stony Brook, unpublished.
- Vary, J. P., P. U. Sauer, and C. W. Wong, 1973, *Phys. Rev. C* **7**, 1776.
- Vary, J. P., and S. N. Yang, 1977, *Phys. Rev. C* **15**, 1545.
- Vincent, C. M., 1976, *Phys. Rev. C* **14**, 660.
- Vincent, C. M., and S. Pittel, 1973, *Phys. Lett. B* **47**, 327.
- Watson, K. M., 1953, *Phys. Rev.* **89**, 575.
- Watt, A., B. J. Cole, and R. R. Whitehead, 1974, *Phys. Lett. B* **51**, 435.
- Weidenmüller, H. A., 1974, in *Proceedings of the International Conference on Nuclear Structure and Spectroscopy*, edited by H. P. Blok and A. E. L. Dieperink (Scholar's Press, Amsterdam), Vol. II, p. 1.
- Yariv, Y., 1974, *Nucl. Phys. A* **225**, 382.
- Yukawa, H., 1935, *Proc. Math. Soc. Japan* **17**, 48.
- Zabolitzky, J. G., 1974, *Nucl. Phys. A* **228**, 285.
- Zamick, L., 1969, *Phys. Rev. Lett.* **23**, 1406.